
**UNIVERSITA' POLITECNICA DELLE MARCHE**

**SCUOLA DI DOTTORATO IN MEDICINA E CHIRURGIA**

**CURRICULUM "SALUTE DELL'UOMO"**

**Ph.D. Thesis**

# *In vitro* strategies and development of bioengineered approaches for studying age-related osteochondral diseases

***Tutor***
**Prof. Monica Mattioli-Belmonte Cima**

***Ph.D. candidate***
**Dr. Giorgia Cerqueni**

**XXXIII cycle**

**Table of Contents**


1. Introduction ..... 3
1.1 Articular Cartilage ..... 3
1.1.1 Cartilage ECM ..... 4
1.1.2 Cartilage zones ..... 5
1.1.3 Cartilage Cells ..... 8
1.2 Synovial membrane ..... 9
1.3 Bone tissue ..... 10
1.3.1 Bone Extracellular Matrix ..... 12
1.3.2 Bone vascularisation ..... 13
1.3.3 Bone innervation ..... 15
1.3.4 Bone cells ..... 15
1.3.5 Bone remodelling ..... 19
1.4 Osteoarthritis ..... 24
1.4.1 Pathogenesis of osteoarthritis ..... 25
1.5 Models of osteoarthritis ..... 30
2 Thesis aim ..... 34
3 2D model system: Synovium-Derived Stem Cells and osteoclasts activity. ..... 35
3.1 Draft of the study ..... 36
3.2 Materials and methods ..... 36
3.2.1 SDSCs isolation ..... 36
3.2.2 SDSCs characterization ..... 37
3.2.3 SDSCs *in-vitro* differentiation ..... 38
3.2.4 Osteoclastogenesis assessment ..... 39
3.2.5 qRT-PCR ..... 40
3.2.6 Statistical analysis ..... 41
3.3 Results ..... 42
3.3.1 SDSCs characterization ..... 42
3.3.2 SDSCs differentiation ability ..... 42
3.3.3 Evaluation of Osteoclasts-like cells formation ..... 43
3.3.4 qRT-PCR ..... 45
3.4 Discussion ..... 45
3.5 Conclusion ..... 48

4 3D model system: An engineered *in-vitro* model to reproduce OA. ..... 49
4.1 Draft of the study ..... 51
4.2 Materials and methods ..... 51
4.2.1 Gellan Gum Methacrylate synthesis (GGMA) ..... 51
4.2.2 Chondroitin sulfate (CSDP) synthesis ..... 52
4.2.3 GG hydrogel preparation ..... 52
4.2.4 CSDP hydrogel preparation ..... 53
4.2.5 PLA 3D printing and functionalisation ..... 54
4.2.6 Cell culture ..... 54
4.2.7 Manufacturing of the PLA/GG/CSDP ..... 55
4.2.8 Statistical analysis ..... 60
4.3 Results ..... 60
4.3.1 Hydrogels characterisation ..... 60
4.3.2 PLA/GEL/nHA characterization ..... 61
4.3.3 Cell viability ..... 62
4.3.4 Assessment of healthy and OA conditions ..... 64
4.4 Discussion ..... 67
4.5 Conclusions ..... 72
4.6 Limitation and perspectives of this research ..... 73
References ..... 74

## 1. Introduction

The skeletal system is composed of skeletal muscles, bone and cartilage that together perform several functions such as support, posture, protection of the internal organs, movement, blood cell production and storage of minerals.

Articular cartilage and bone derived from mesoderm and, for their proper characteristics and functions are classified in highly specialized connective tissues. The connective tissues are constituted of cells within an extracellular matrix (ECM) and provide structural and metabolic support to other tissues. The connective tissue local cells can be categorized into two classes: resident cells, which develop within the tissue remaining inside for all their life, and roaming cells that migrate from the bloodstream in response to several stimuli like inflammation and/or damage.

In the connective tissue, the ECM component prevails, assuming distinctive features concerning the specific functions it has to perform: it could be fluid to let cells easily pass, or solid but loose to lodge vascular vessels and transport substances, or calcified to build extremely hard structures. The differences in the ECM's nature are due to ratio variations of its main components that are protein fibers and the amorphous ground substance: a stiff ECM contains a large number of protein fibers, while a loose ECM is mainly composed of amorphous ground substance. However, intermediate forms that differently balance these two components are highly represented.

### 1.1 Articular Cartilage

Different types of cartilage are present in the body and hyaline cartilage, the most copious type of cartilage in the human body[1], forms the articular cartilage (AC) covering with a thickness of 2-4 $mm^2$ the epiphyses end of the bone. AC is a robust and viscoelastic highly specialized connective tissue located in the diarthrodial joints. The functions of AC are providing a smooth

and lubricated surface for the articulation with a low frictional coefficient, absorbing the shock cushioning and facilitating the load propagation avoiding the inhomogeneous subchondral bone overload[3]. Differently from bone, AC lacks vascular and lymphatic vessels as well as neurons[4]. These features do not make it a prone tissue to repair. Moreover, AC must continuously sustain the phenomena of mechanical stress to radiate the load into the bone. Therefore, the preservation of the health state of the AC is of utmost importance.

### 1.1.1 Cartilage ECM

Cartilage ECM protects chondrocytes from mechanical loads, thus maintaining their phenotype, stores growth factors and cytokines essential for chondrocytes to manage the inner nutrient diffusion and let the mechanical signal transduction to the cells[4]. Collagen, proteoglycans, and other non-collagenous proteins compose the ECM and together help to preserve water inside the ECM, crucial to maintaining cartilage mechanical proprieties[4]. Inside the AC, it is possible to distinguish three zones: the tangential (or superficial), the transitional (or middle) and the deep zone followed by the calcified zone (Figure 1). In each zone, the ECM is organized in pericellular, territorial and interterritorial regions.

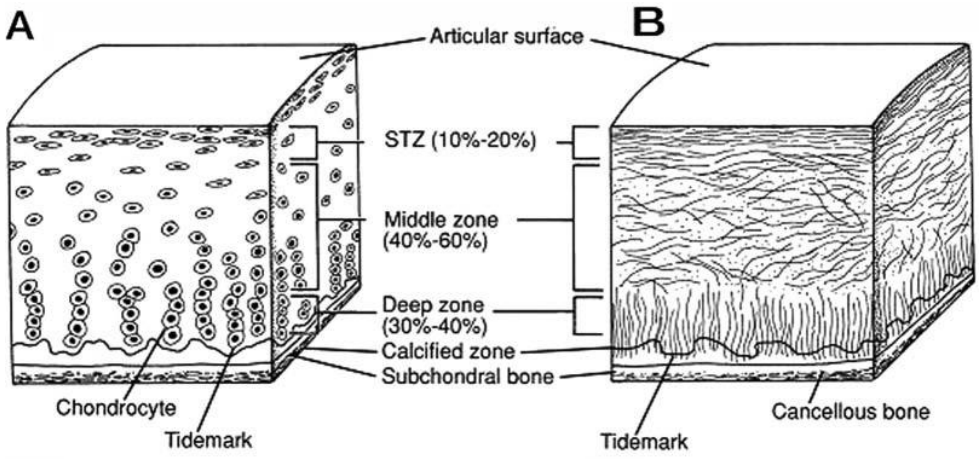


*Figure 1: Schematic, cross-sectional diagram of healthy articular cartilage: (A) cell organization in the zones of articular cartilage; (B) collagen fiber architecture. Image from [5].*

### 1.1.2 Cartilage zones

The tangential zone composes approximately 10% to 20% of AC and represents a thin layer. Collagen II and IX are the main types in this zone and are align parallel to the surface. A high number of flattened chondrocytes are present in this zone. The tangential zone supports several functions like AC nutrient diffusion, for its proximity to the synovial fluid, and the resistance to shear, tensile and compressive stress for the maintenance of the deeper layers.

The 40%-60% of AC is represented by the transitional zone that is localized immediately under the superficial one. The collagen fibrils, thicker than those in the superficial zone are combined diagonally and the chondrocytes are spherical and at low density. This zone is resistant to compressive forces.

The last 30% of AC is the deep zone and its ECM composition is suitable for opposing enormous compressive forces. The collagen fibrils are distributed perpendicularly to the articular surface and large diameter fibrils have radial disposition. The proteoglycans are represented in the largest amount while water is present in the lowest concentration. The arrangement of the chondrocytes is dictated by the collagen fibers and they organize themselves to form columns parallel to each other but perpendicular to the surface of the cartilage[2].

Under the deep zone, the tidemark distinguishes subchondral bone (SB) from the calcified cartilage zone, where chondrocytes are few and hypertrophic, which sealing the AC to SB. The SB includes the compact bone plate, in contact with the calcified cartilage, and, below, the trabecular bone [6].

#### *1.1.2.1 Cartilage ECM regions*

Cartilage ECM regions depend on chondrocytes' proximity, ECM composition and collagen organization.

The matrix that completely envelopes chondrocytes forms the pericellular matrix and contains proteoglycans, glycoproteins, and other non-collagenous molecules. This area is involved in the transduction of the mechanical signal to the chondrocytes[7].

The pericellular matrix is surrounded by a territorial matrix composed of fine collagen fibrils forming a woven net around the cells[8,9]. This network protects chondrocytes against mechanical stresses and gives them the ability to resist significant loads.

The largest region is the interterritorial one, where collagen fibrils are oriented according to the zone in which they are located, and proteoglycans are extensively expressed. This region massively contributes to the AC biomechanical properties[10].

#### *1.1.2.2 Components of cartilage ECM*

Water comprises 80% of cartilage wet weight. The most quantity is included inside the ECM pores[11,12], while the less amount takes place into the intrafibrillar space of collagen. The water content decreases with deep, passing from 80% at the transitional zone to 65% in the deep layer[4]. The water associated with fibrillar collagen can be moved through ECM by employing a pressure gradient or compressing the solid matrix[13,14]. Moreover, water is essential for lubrification, and to distribute nutrients to chondrocytes and ions essential for signaling[15–17].

The most abundant structural macromolecule in ECM is collagen that comprises 60% of cartilage dry weight. The 90-95% of collagen is type II and form fibrils and fibers interconnected with proteoglycans. Less represent collagen types are I, IV, V, VI, IX, and XI.

Proteoglycans are molecules composed of a linear peptide core where one or more glycosaminoglycan chains, formed by more than 100 monosaccharides, are covalently attached, and extend out of the core. Glycosaminoglycans remain separated from each other due to charge repulsions. Different proteoglycans molecules are represented in AC including aggrecan, biglycan and fibromodulin, and this class of molecules accounts for 10%-15% of AC wet weight. Aggrecan is the most copious and biggest proteoglycan and possesses more than one

hundred chondroitin sulfate and keratin sulfate chains. Moreover, aggrecan can complex with hyaluronan to form large aggregates[4] (Figure 2). Aggrecan occupies the interfibrillar space and, thanks to its osmotic properties, it is the main responsible for the compressive loads' resistance by the AC.

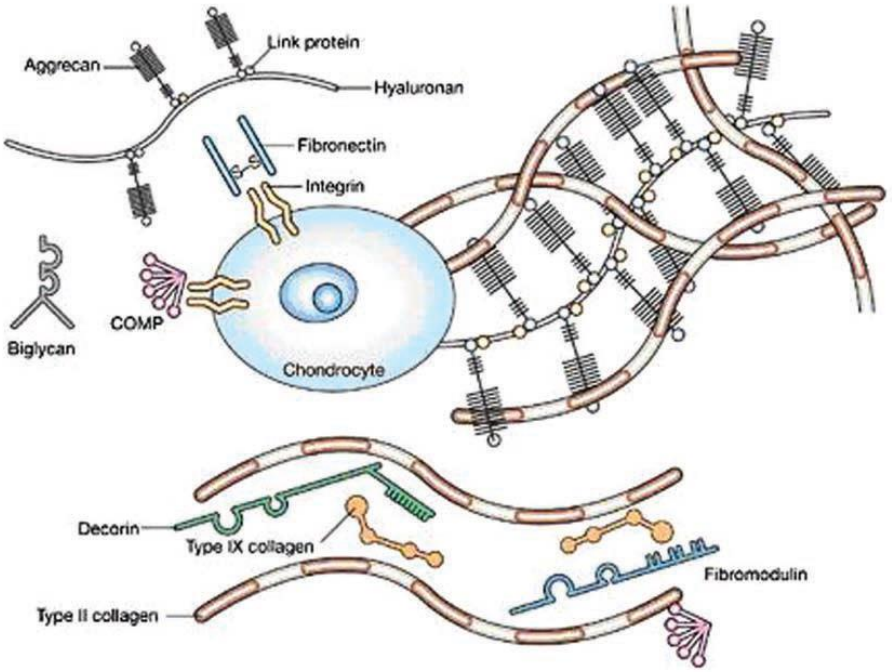


*Figure 2: Articular Cartilage extracellular matrix. Type II collagen and proteoglycans (notably, aggrecan) are the two major load-bearing macromolecules present in AC. Non-collageneous molecules and small proteoglycans are present in smaller amount. The interaction between the highly negatively charged cartilage proteoglycans and type II collagen provides the compressive and tensile strength of the tissue. From Ref. 18.*

### 1.1.3 Cartilage Cells

The solely specialized cells that reside in cartilage are chondrocytes, which are dispersed in cartilage ECM and are cytoplasmically isolated from the neighbouring cells, establishing a direct cell-to-cell signal transduction only rarely. Chondrocytes are derived from mesoderm and occupy only 1-5% of the entire AC[3]. The chondrocytes are trapped within their own produced matrix which abolishes cell migration. For the avascular characteristic of this tissue, the passage of nutrients and the elimination of waste products occurs by diffusion passing through the cartilage surface[19]. Moreover, chondrocytes can work in a low oxygen environment exhibiting a low metabolic turnover and containing low mitochondrial numbers[20]. Morphologically chondrocytes appear normally rounded or polygonal apart from those localized at AC surface that can be flattened or discoid[20] (Figure 3).

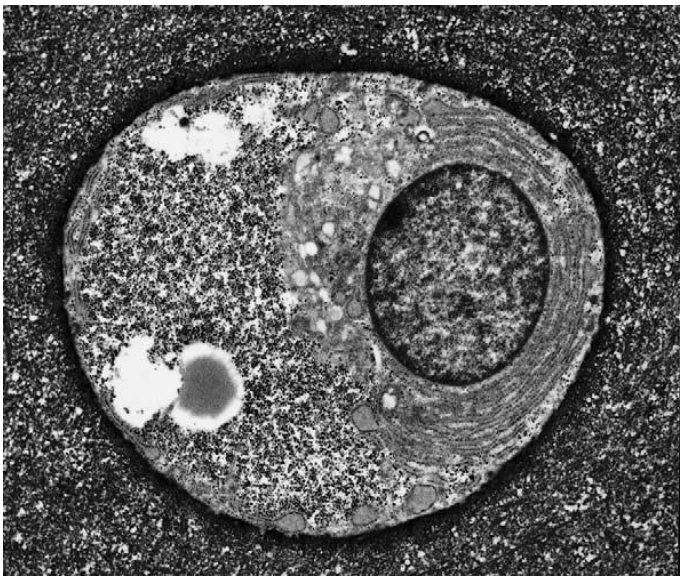

*Figure 3: Electron micrograph of a typical articular chondrocyte. The cell is typically rounded and contain ordered and rough endoplasmic reticulum, juxtanuclear Golgi apparatus and conspicuous deposits of glycogen including the remnants of lipid droplets. From Ref [20].*

Chondrocytes synthesize and provide the turnover of a huge volume of ECM components like collagens, glycoproteins, proteoglycans and hyaluronan and shown typical markers of metabolically active cells. The glycogen deposition inside cells and the expression of primary cilium[21] on the surface are some of these features. Chondrocytes are susceptible to

compressional, tensile and shear forces applied across the AC by mechanosensors and modify their molecular pathways, and their ECM synthesis or turnover in response to them[22].

### 1.2 Synovial membrane

The articular cartilage is wetted by the synovial fluid, contained within the joint cavity. The synovial fluid is produced by the synovial membrane (or synovium) that internally covers the joint capsule, a fibrous layer that surrounding the synovial joint (Figure 4A).

It is possible to distinguish two layers that compose the synovial membrane: the lining (or intima) layer, and the sub-intimal. Synoviocytes type A (macrophages-like cells) and type B (fibroblasts-like cells) are organized to form two or three layers that constitute the intima while, highly vascularised fibrous loose connective tissue, low in content of immune cells, composes the sub-intima[23] (Figure 4B). The vascular system provides nutrition factors that diffuse through the synovial fluid to reach AC. 75% of healthy synovium cells are type B synoviocytes that have the primary function to preserve joint health controlling the synovial tissue ECM and the synovial fluid[24]. A subclass of these cells (Synovium-Derived Stem Cells – SDSCs) express both markers of mesenchymal and fibroblasts lineage and they can be differentiated from other fibroblasts by high levels of UDP-glucose-6-dehydrogenase, cadherin 11, receptor-type protein tyrosine protein-phosphatase sigma and vascular cell adhesion protein 1[25–27]. Lubricin, the main lubricant of synovial fluid, hyaluronic and heparan sulfate-linked proteoglycans, the imperative components of synovial tissue ECM, are expressed by type B synoviocytes. An interesting ability of these cells, which has made them interesting for cartilage regeneration applications, is to differentiate *in-vitro* and *ex-vivo* into chondrocytes[28,29].

Type A synoviocytes have the functions of cleaning the bacterial infection and of remove debris from synovial fluid.

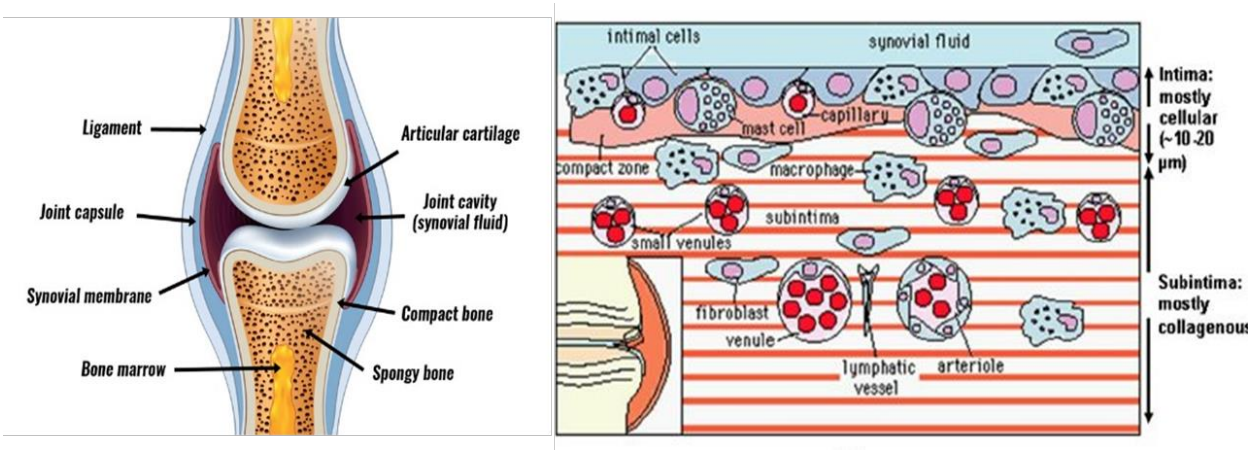


*Figure 4: Anatomical organisation of the synovial joint (A) and illustration describing the synovial membrane and synoviocytes (B). From Ref*[30]

### 1.3 Bone tissue

The fine architecture of the bone tissue allows it to fulfil its tasks without causing excessive overload. Eighty percent (80%) of the bone tissue is compact (or cortical) while the remainder is trabecular. Compact bone is extremely withstanding to daily physical strains, while spongy (or trabecular) bone supports the structure with interconnecting bony plates and rods called trabeculae and its cavities host bone marrow[31]. Compact and spongy are both composed of parallel sheet structures called lamellae formed by the alternate and regulated deposition of collagen fibers[32]. In compact bone, lamellae are organized concentrically to build up cylinders-structures that take the name of *Haversian Systems* or *Osteons*. They relate to each other thanks to branching through Havers and Volkmann channels. In spongy bone, the lamellae are parallel and organized to form the trabeculae (Figure 5).

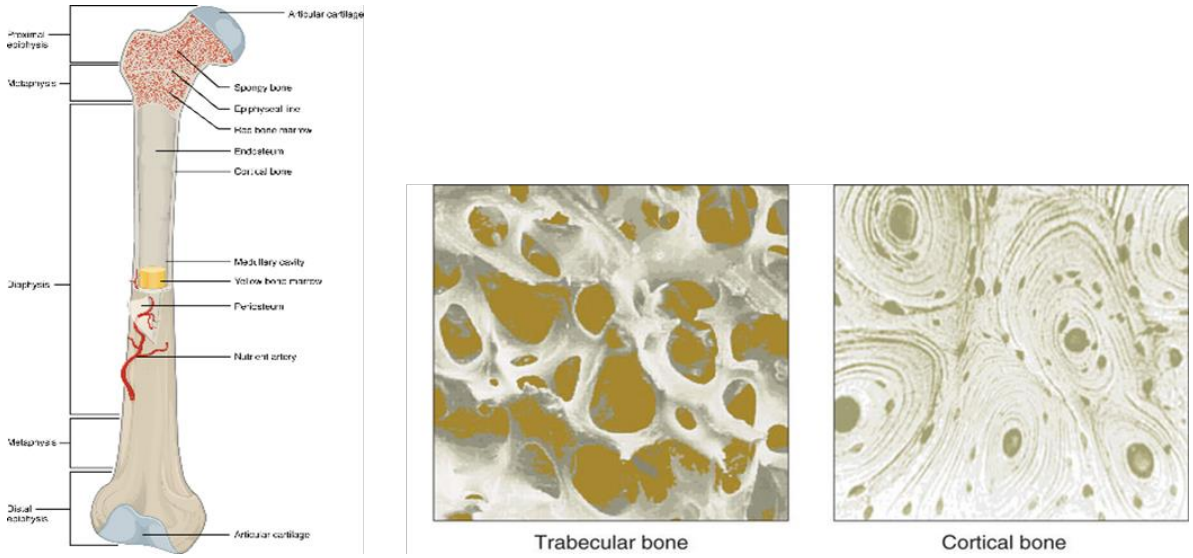


*Figure 5: On the left, illustration describing parts of long bone; on the right, trabecular and compact bone structural organisation.*

In long bones, two different regions can be identified: a long tubular cylinder, the diaphysis and a wider section at each end called epiphysis. The internal cavity of the diaphysis takes the name of the medullar cavity that is filled with red bone marrow in young people that goes to be replaced by yellow marrow in adults. The cylindrical wall of the diaphysis is composed of cortical bone. The epiphyses are occupied with spongy bone and red bone marrow that fill the holes between trabeculae. Metaphysis describes the region where each epiphysis meets the diaphysis.

Bone is covered, outside, by a double layer envelope called the periosteum and internally by endosteum. In the cortical close layer of the periosteum reside pluripotent periosteal stromal cells that are prompt to differentiate and assist the bone tissue repair[33] and remodelling. The outer fibrous layer is a dense irregular connective tissue. Periosteum lets the attachment of tendons and ligaments and covers the entire bone outer surface except where the epiphyses meet other bones to form joints. In joints, articular hyaline cartilage covers the epiphyses reducing friction and adsorbing the load stress. Endosteum is a membranous connective structure constitutes of lining cells[32] that participate in the growth, remodelling and repair throughout life. Periosteum and endosteum in addition to containing cells involved in tissue repair are

characterized by a high grade of vascularisation, innervation, and lymphatic vessels that preserved bone health and consequently its function.

### 1.3.1 Bone Extracellular Matrix

Bone ECM can greatly influence bone cell behaviours and, consequently, its composition and structure. It is made up of 40% organic and 60% inorganic components with differences based on sex, age, and health conditions[34]. 90% of the organic part is represented by collagen proteins, mainly Type I, while the remaining 10% contains non-collagenous proteins (NCPs).

Type I collagen provides the tensile strength[35] of bone and represents a platform for bone cells[36]. The base unit of Type I collagen is composed of two CollIα1 chains and a CollIα2 chain (post-translational modified) that are winded in triple helices in the cellular endoplasmic reticulum. When the polypeptide is secreted in the extracellular space the pro-peptides are removed from the N- and C-terminals and the processed collagen molecules form fibrils that are stabilized by crosslinks between collagen trimers[37]. The fibrils interact with collagenous and NCPs to form higher-order fibril bundles and fibers[38].

NCPs can exhibit several functions, such as cell adhesion, proliferation, differentiation, organization of the complex protein/growth factor interaction, and interaction with Type I collagen to regulate fibrinogenesis and promote or inhibit nucleation/mineralization. Five different types of NCPs are classified in bone ECM: proteoglycans/glycosaminoglycans (hyaluronan, decorin, biglycan, glypican, osteoglycin/mimecan, keratocan, osteoadherin, lumican, asporin, perlecan, and fibromodulin), γ-carboxyglutamic acid-containing proteins (osteocalcin and matrix Gla protein), glycoproteins (periostin, osteonectin/SPARC, tetranectin, tenascin C/X, secreted phosphoprotein 24), glycoproteins with RGD sequences (thrombospondins, fibronectin, vitronectin, fibrilins), and small integrin-binding ligand, N-

linked glycoproteins/SIBLINs [osteopontin, bone sialoprotein, MEPE, dentin sialophosphoprotein (DSS), dentin matrix protein-1 (DMP1), and Fam20c/DMP4][39].

Besides, bone ECM is also composed of cytokines [interleukins (IL-6/11)], colony-stimulating factors [granulocyte-macrophage colony-stimulating factor/GM-CSF and macrophage colony-stimulating factor (M-CSF)], growth factors [Transforming Growth Factor-Beta (TGF-β), Bone Morphogenetic Proteins (BMPs), Platelet-Derived Growth Factors (PDGFs), and Insulin-Like Growth Factors (IGFs)] and enzymes [Alkaline Phosphatase (ALP), Matrix Metalloproteases (MMPs), and cathepsins]. MMPs and Cathepsins are involved in matrix remodelling[40] while ALP bone isoform participates in the mineralization process allowing the conversion of pyrophosphate to phosphate[41].

During the bone mineralization process, the inorganic components precipitate throughout an organic background[42]. The main inorganic component is Hydroxyapatite (HA) that contains elements such as $Ca^{2+}$ and $PO_4^{3-}$ [43] and provides bone rigidity[35]. The mechanism of bone and cartilage mineralization is not fully understood and seems not only ascribable to extracellular elements, but also several intracellular enzymes as important regulators[44]. However, the essential factors that occur for mineralization are the deposition of a Collagen Type I template, the availability of phosphate and calcium, the pyrophosphate breakdown by ALP and the absence of mineralization inhibitors[39].

### 1.3.2 Bone vascularisation

High vascularisation characterizes bone tissue since it continuously delivers oxygen, nutrients and osteoprogenitor cells that are required for skeletal growth and remodelling[45] as well as removing metabolic waste products such as carbon dioxide and acid. Therefore, the skeleton needs a high grade of blood perfusion, which is satisfied by the reception of about 5.5-11% of cardiac output[46,47]. The principal arteries penetrate the cortex of long bones and perfuse the

medullary sinusoids, then exit via multiple small veins. The cortical bone is perfused by a mixture of arterial blood originating from the main nutrient arteries as well as from the separate, smaller periosteal arteries[48]. These arteries infiltrate through Volkmann's and Haversian channels and branch through the cortical tissue.

As widely known, embryonic bone development is carried out through two mechanisms: intramembranous and endochondral ossification. Intramembranous ossification allows the formation of facial and cranium flat bones, mandible, and clavicle[49], while endochondral happens during the development of long bones[50]. During both ossifications, vascularisation plays a pivotal role to induce osteogenesis. During intramembranous, the mesenchymal zone is invaded by capillaries inducing the mesenchymal stem cells (MSCs) to differentiate into osteoblasts[51]; the endochondral ossification uses a cartilaginous template which is invaded by blood vessels. The formation of such vessels allows the recruitment of osteogenic and vasculogenic cells while long bone expands both radially and longitudinally[52].

Moreover, vascularisation is also essential in adult bone repair. Bone damage is accompannied by vasculature disruption, acute necrosis, and hypoxia of the surrounding tissue[53]. The initial clot lets the invasion of the vascular network, then the clot matrix is replaced by fibrocartilage. Osteoclasts remove necrotic bone and remodel the damaged site while angiogenesis has the task to restore normal blood circulation[54].

Several cell signalling mechanisms cooperate to the couple induction of angiogenesis and osteogenesis to reach bone healing. Among these, it is interesting to note the role that vascular endothelial growth factor (VEGF) and bone morphogenetic protein-2 (BMP2) play. VEGF is secreted from MSCs and it can play a dual role depending on the cell target. If it is linked to endothelial cells, it has the role of inducing vascularization, while, if linked to osteoblasts, it has the task of inducing bone repair[55,56]. BMP-2 can induce osteoblasts differentiation; its

interaction with MSCs sets off a release of VEGF[57] that is proportional to BMP-2 exposure[58]. Hence BMP-2 and VEGF cooperate to induce osteogenesis and vasculogenesis.

### 1.3.3 Bone innervation

The innervation of the bone follows the pattern of vascularization. Fibers form specific meshwork within the periosteum that slopes through the external layer and internal layer into the bone itself[59], then penetrate the cortical bone alongside the Haversian systems[60]. In the marrow space, sensorial fibers branch and project endings mainly in the proximity of the epiphyseal area[61]. Sensory neurons terminate in bone with unmyelinated free endings (that can recognize and carry signals related to pain, temperature, and mechanical stimuli) or encapsulated nerve endings (that can detect low-frequency vibrations) enveloped in non-neural fibrous connective tissues that separate a single afferent nerve ending in the gelatinous material[62]. The sensory and sympathetic fibers are located predominantly in bone marrow, followed by the mineralized part of the bone and periosteum[63].

These innervations, in addition to carrying out their sensory activity, are also implicated in bone cell activation and differentiation through the release of neuropeptides that bind with specific receptors. It is also known that the denervation process decreases bone deposition by reducing the activity of osteoblasts while increasing osteoclasts' number and activity[62].

### 1.3.4 Bone cells

Bone lining cells, osteoblasts, osteocytes, and osteoclasts are the bone cells responsible for ECM modelling, but several types of other cells live and maturate in the bone compartment and participate/influence bone metabolism. These are mesenchymal stromal cells, endothelial cells, neurons, cells of the hematopoietic compartment, cells of inflammatory response and

adipocytes. The different cell types in bone could give a quick insight into the intricate mechanisms underlying the modulation of its ECM.

Bone lining cells, osteoblasts and osteocytes derived from the same progenitor cell but belong to different maturation steps (Figure 6) while osteoclasts derived from the hematopoietic compartment. Only bone lining cells and osteocytes are permanently localized in bone, osteoblasts and osteoclasts are recruited through several stimuli. Bone lining cells are flattened and elongated cells that cover the bone surface and show low synthetic activity. They are connected by gap junctions and send cell processes into surface canaliculi. Their function is still debated between those who argue that they represent a final stage of osteoblasts with the task of monitoring the ECM from the activity of osteoclasts[64], and those who consider them a source of precursors of osteoblasts implicated in the propagation of the signal that initiates bone resorption and remodelling[65].

Osteoblasts are derived from MSCs that can also differentiate in chondrocytes and adipocytes[66]. The MSCs mainly reside in the bone marrow and, to begin the osteogenesis, need to be recruited on the bone surface. The process of MSCs migration is essential to guarantee the active osteoblasts and, recently, has attracted huge interest[67]. MSCs migration cooperates with osteogenesis, and the expression of Runt-related transcription factor 2 (Runx2) and Osterix (Osx) are mandatory for the initial commitment[68–70]. Mature active osteoblasts in the bone formation areas display a cubical shape and forming a layer. They are interconnected with adherents and gap junctions, microfilaments and enzymes (such as protein kinases) associated with intracellular secondary messenger systems. This complex arrangement provides for intercellular adhesion and cell to cell communication to form a layer of cells[71]. Mature osteoblasts synthesize the components of ECM and produce a high amount of Collagen Type I, ALP, Osteocalcin, Bone Sialoproteins (BSP) and other matrix proteins[72–74]. Moreover, they are involved in ECM mineralization. The latter process is still debate but seems that the "*matrix*

*vesicle theory*"[75–79] offers an isolated microenvironment to facilitate the initial nucleation of apatite mineral. Briefly, matrix vesicles (MVs) containing ALP, adenosine triphosphatase (ATPase), inorganic pyrophosphatase as well as proteinases such as plasminogen activator, act as seeding sites for hydroxyapatite crystal formation through a localized enzymatic accumulation of calcium and phosphate. Mineral crystals formed inside the MVs grow progressively in size by the addition of $Ca^{2+}$ and $P_i$ ions and eventually rupture the MVs membrane to be deposited on the collagen scaffold. Collagen provides the orientation of proteins, like osteonectin, that nucleate hydroxyapatite.

Osteoblasts that remain entombed in their own ECM can take on two different fates: dead or reach the final differentiative stage represented by osteocytes. The osteocytes population is the most represented and the longest in the bone tissue. During the final step of osteogenic differentiation these cells change their morphology and protein expression, implement the synthesis of Dentin matrix protein-1 (Dmp1)[80], Matrix extracellular phosphoglycoprotein (Mepe)[81] and Sclerostin (Sost)[82]. Osteocytes are morphologically characterized by a cell body localized into bone holes called osteocytes' lacunas from which they spread several dendritic-type extensions. These cell extensions run through canaliculi excavated in the ECM by themselves and contact other osteocytes and cells of the more superficial layers. This peculiar morphology makes their functions extremely efficient. The osteocytes, branching within the ECM, act as sensors for the state of bone health and can exchange information with other osteocytes, as well as modulate the activity of osteoblasts and osteocytes. Their apoptosis, due to unloaded bones[83] or an excessive level of mechanical strain, promotes osteoclasts recruitment and the start of the remodelling process.

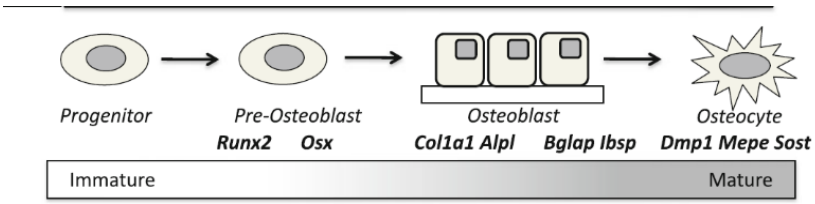


*Figure 6: Differentiating osteoblast lineage and genes expressed from the pre-osteoblast to the osteocytic stage. These include Runx2, osterix (Osx), collagen 1a1 (Col1a1), alkaline phosphatase (Alpl), osteocalcin (Bglap), bone sialoprotein (Ibsp), dentine–matrix protein-1 (Dmp1), matrix extracellular phosphoglycoprotein (Mepe) and sclerostin (Sost). From Ref 64.*

Osteoclasts derive from cells of the hematopoietic lineage that are recruited in bone compartments by the expression of a specific stimulus. In the site of interest, these cells fuse to form a giant multinucleated cell with a diameter varying from 50 to 200 µm and attach greatly to the surface to exercise their resorption function. Osteoclasts ultrastructure is characterized by well-developed Golgi apparatus, abundant pleomorphic mitochondria, vacuoles and lysosomes[51,84,85]. Osteoclasts integrin $\alpha_v\beta_3$ is involved in recognition and subsequent bonding to Arg-Gly-Asp (RGD)-containing molecules present in bone ECM like vitronectin, osteopontin, and BSP[86]. The RGD sequences are an essential but not enough element for osteoclast adhesion, and physical properties like hardness or roughness may be also necessary[87]. The bind provokes the osteoclast's cytoskeletal reorganization[88] with “podosomes” formations: columnar arrays of actin. The incessant podosomes assembly and disassembly let osteoclasts move along the bone surface also during the resorption.

Adhering to the bone ECM, osteoclasts become polarised with the formation of a ruffled border and sealing zone towards the bony side. The sealing zone, an exclusive band of actin[89], assists the attachment of osteoclasts to the bone surface and isolates the resorption area - called “Howship’s lacuna - from the surroundings. Into the sealed compartment generated between osteoclasts and bone ECM the pH is maintained low through the extracellular pumping of protons by the vacuolar $H^+$-ATPase pump localized in the ruffler border[90]; the acidification of the environment helps the dissolution of bone minerals. Moreover, lysosomal enzymes such as

tartrate-resistant acid phosphatase (TRAP) and cathepsin K (CATK) are actively secreted in Howship's lacunae to degrade ECM. Firstly, the hydroxyapatite is mobilized by the digestion of its links to collagen, then CATK or activated collagenases digest the collagen residues[91]. The degradation products are engulfed from osteoclasts ruffler border and incorporated in transcytotic vesicles[92–94] that are processed by the cells and the products are exocytosed through the functional secretory domain in the basolateral membrane facing bone marrow [95]. CATK and Matrix Metalloproteinase 9 (MMP-9) are then involved in Collagen Type I degradation in an acid environment[96].

### 1.3.5 Bone remodelling

Despite its static appearance, bone is continually renovated by continuous mechanisms of ECM resorption and new matrix deposition. In adults, the bone remodelling does not change bone size or shape, and each bone tissue resorption is followed by deposition of a comparable volume. Remodelling is essential to let microdamage repair, avoid old bone accumulation and for maintaining plasma/calcium homeostasis. A different mechanism, called modelling, appears during growth, where bone formation or resorption can occur independently of each other allowing adaptation of bone architecture and meet changing mechanical requirements. Modelling and remodelling act for bone health maintenance, preventing and repairing the damages[97]. The remodelling process occurs in the whole bone but, the remodelling rate of the trabecular part is higher than the cortical[98]. Bone cells are the main actors of this process, even if other cell types are involved, with several regulative mechanisms. The remodelling process asynchronously going along bone surfaces, reflecting the local final regulation of this process[97]. Remodelling can be schematized in four stages: Stage 1: the beginning of bone remodelling by the enrolment of osteoclast precursors into the "*bone remodelling compartment (BRC)*"; Stage 2: major bone resorption period, which includes osteoclast differentiation and function with

simultaneous recruitment of MSCs/osteoprogenitors; Stage 3: bone formation phase characterized by osteoblast differentiation and function (osteoid synthesis); and finally Stage 4: mineralization of osteoid and conclusion of bone remodelling[99] (Figure 7).

The unit in charge of bone remodelling is the basic multicellular unit (BMU) a temporary anatomical structure where osteoblasts and osteoclasts are the executive cells.

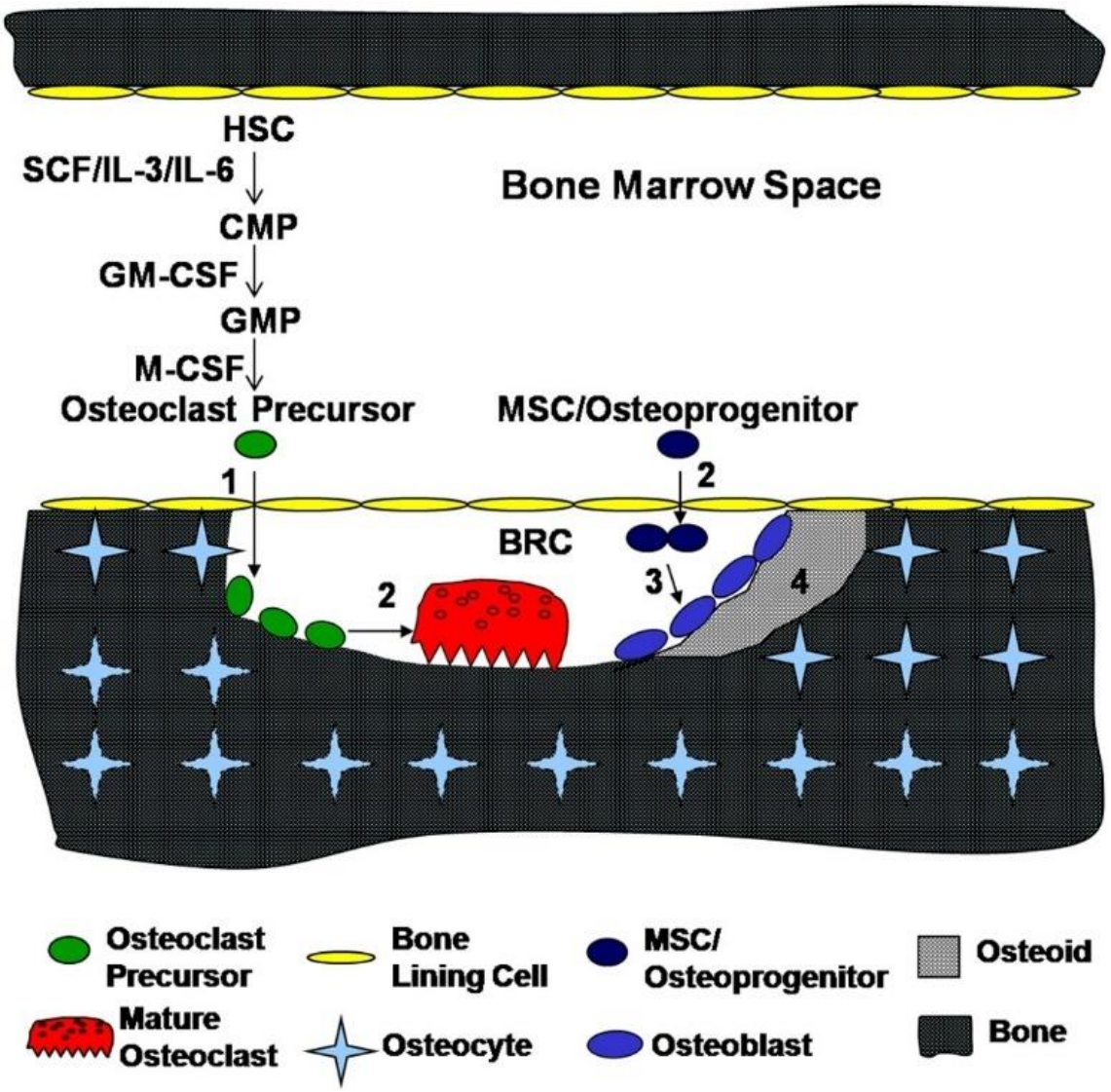


*Figure 7: Bone Remodelling stages. (1) stage 1; (2) stage 2; (3) stage 3; and (4) stage 4. HSC: hematopoietic stem cells; SCF: stem cell factor; CMP: common myeloid progenitor; GM-CSF: granulocyte-macrophage colony stimulating factor; GMP: granulocyte-macrophage progenitors; M-CSF: monocyte-macrophage colony stimulating factor; BRC: bone remodelling compartment; MSC: mesenchymal stem cells. From Ref*[100].

#### *1.3.5.1 Stage 1*

Osteocytes, by their bone surveillance activity, detect several environmental changes that can range from modification in the hormonal milieu (e.g., estrogen deficiency), to sense microcracks that affect the integrity of osteocytes processes inside the canaliculi[101] (which may lead to their apoptosis). By their intricate network, osteocytes transmit information to superficial bone lining cells[102,103] to, "trigger" bone remodelling with the formation of new BMU at cortical or trabecular surfaces[104]. Therefore, osteocytes are actively involved in the first step of bone remodelling preceding osteoclastogenesis[105], but can also provide topographical information about the localization and the dimension of the damage[106,107]. The superficial bone lining cells receive information and begin the BMU formation[108] in a high vascularised close space, the BRC, characterized by the presence of a canopy formed by bone lining cells to minimize the remotion of normal bone[109]. The expression of nuclear factor-κB ligand (RANKL) is essential for preosteoclasts activation. This expression is sustained by several cells like pre-osteoblasts, bone lining cells[110] but its main producers are osteocytes[104]. Macrophage Colony-Stimulating Factor (M-CSF) cooperates with RANKL for the stimulation of osteoclasts differentiation which is definitively initiated with adhesion to the reabsorption surface[100].

#### *1.3.5.2 Stage 2*

This stage is characterized by extensive resorption activity by osteoclasts that erode the bone ECM. The remodelling process has a different feature and activity in trabecular and cortical bone. In the trabecular surface, the erosion is along the main loading direction. By contrast, in the cortical bone, the BMUs proceed by osteonal tunnelling, during which osteoclasts excavate a canal that is refilled by osteoblasts (Figure 8). At the same time, the recruitment and migration of MSCs/osteoprogenitors appear.

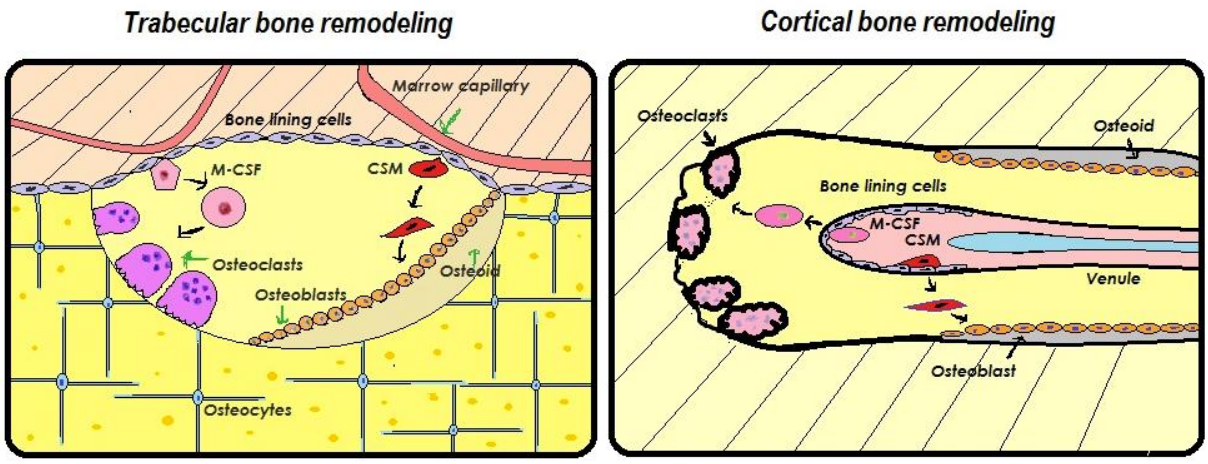


*Figure 8 Bone remodelling in trabecular and cortical bone. In cortical bone, the BMUs proceed by osteonal tunnelling, during which osteoclasts excavate a canal that is refilled by osteoblasts From Ref111 .*

#### *1.3.5.3 Stage 3*

The bone formation is slower than the resorption and includes both matrix deposition and mineralization. The recruitment of MSCs can be stimulated by molecules stored in the matrix and released during bone resorption, like TGF-β, and osteoclasts coupling factors called "clastokines"[112]. Once MSCs or early osteoblasts come in the resorption lacunae they differentiate and proliferate[113,114].

#### *1.3.5.4 Stage 4*

The ending signals are largely unknown and include the terminal differentiation of the osteoblast: osteoblasts become gradually flat and decrease their synthetic activity and, finally, become quiescent lining cells. Some osteoblasts differentiate into osteocytes that secrete inhibitory factors that slow the rate of bone formation as well as resorbed activity.

#### *1.3.5.5 Bone remodelling regulation*

Systemic and local regulation by several hormones and proteins can modulate the remodelling activity.

*Parathyroid hormone (PTH)* and *Calcitriol* (*i.e.,* 1,25-dihydroxycholecalciferol) are important regulators of calcium homeostasis. The first stimulates bone resorption and increase renal

tubular calcium reabsorption to rise the serum calcium concentration; concomitantly PTH stimulates renal calcitriol production that enhances intestinal calcium and phosphorus absorption promoting bone mineralization. Curious is the double effect of PTH: it stimulates bone formation when given intermittently and bone resorption when secreted continuously[115]. *Calcitonin* can inhibit osteoclasts' function but with a limited dose and low effects in the adult skeleton. *Glucocorticoids* are essential during osteoblasts maturation promoting the differentiation, but they decrease osteoblasts' activity leading to a high amount of unfunctional osteoblasts that do not produce osteoid but remain able to recruit osteoclasts[116]. *Estrogens* reduce the sensitivity of the osteoclast progenitor cells to RANKL, thereby preventing osteoclast formation[117] and stimulate osteoblast proliferation and decrease their apoptosis. Moreover, estrogens influence gene coding for enzymes, bone matrix proteins, hormone receptors, transcription factors, and they also upregulate the local production of OPG, IGF I, IGF II, and TGF-β[118].

The discovery of the OPG/RANKL/RANK system provided a clearer view of the local regulation of bone remodelling. RANKL is an homotrimeric protein produced by pre-osteoblasts, osteoblasts, osteocytes, periosteal cells[119–121], and other cells like activated-Tcells[122–124]. RANKL is a result of proteolytic division (by MMP3 or 7 and ADAM)[125,126] or alternative splicing on the membrane form[127]. RANKL binds with activated RANK, which is expressed by osteoclasts and its precursors[128]. RANKL has tasks for stimulating preosteoclasts' differentiation[129], adhesion[130], activation and maintenance[131].

RANK is a homotrimeric transmembrane receptor from the TNF family. Its expression is limited to osteoclasts progenitor cells (OPCs), dendritic cells, and mature osteoclasts[122].

Osteoprotegerin (OPG) is expressed from osteoblasts and plenty of other cells from heart, liver, spleen, and kidney. Moreover, a recent study suggested that B cells are in charge of 64% of the bone marrow OPG expression[132]. OPG plays an anti-osteoclastogenesis activity taking part as

a decoy receptor for RANKL[133] binding and inhibiting RANKL-RANK axis. Several agents that induce RANKL expression influence OPG regulation[134,135].

The RANKL/OPG ratio in bone marrow is a parameter for monitoring bone mass in normal and pathological states. Several factors like cytokines (TNF-α, IL-1, IL-6, IL-4, IL-11, and IL-17), hormones (vitamin D, estrogen, and glucocorticoids)[136,137], mesenchymal transcription factors (Wnt/b-catenin)[138–140] may affect the RANKL/RANK/OPG system control. Osteoclastogenesis may be enhanced via regulating RANKL expression by ROS (reactive oxygen species)[140,141] as well as by proinflammatory cytokines. The increase in inflammatory conditions leads to an overexpression of RANKL by T cells that correlates with lower bone mass density (BMD)[142,143]. In those pathological conditions like postmenopausal osteoporosis or rheumatoid arthritis, where hormone and cytokine levels are dysregulated, bone resorption might significantly increase mainly through RANKL and M-CSF expression enhancement[144,145].

### 1.4 Osteoarthritis

Osteoarthritis (OA) is an entire joint degenerative disease that affects AC, synovium, bone and subchondral bone[146]. The global prevalence of knee OA is 16% in individuals aged 15 years and over and increase up to 22,9% in individuals aged over 40 years, with an incidence of 203 per 10,000 person-year. The incidence grows with the increase of age, reaching a peak between 70-79 years old, thus dragging the peak of prevalence in old age[147]. The increase in life expectancy makes the OA the fourth leading cause of disability[148] globally, with a national medical expenditure that amounts to between 1% and 2.5% of the gross domestic product[149].

The main OA disabling symptom is pain that is typically intermittent and weight-bearing (mechanical) and, frequently, can lead to psychological stress[150]. Unfortunately, other

symptoms can occur like morning stiffness, reduced range of motion, crepitus, joint instability (buckling or giving-way), swelling, muscle weakness and fatigue.

As first-line treatments, education and self-management, exercise, weight loss if overweight or obese, and walking aids as indicated, are widely recommended[151,152]. For pain treatment, paracetamol and NSAIDs are often-recommended pharmacological methods[151]. New pain therapies such as nerve growth factor (NGF) antibody[153] and anti-IgE[154] appear to be promising. However, given the heterogeneity of the symptoms, personalized treatment is often necessary. The end-stage OA symptomatology is very severe with pain that can alter the normal sleep pattern, reduction of the walk capability and limitation of daily activities[155], making surgery the last chance.

### 1.4.1 Pathogenesis of osteoarthritis

OA is a degenerative disease that involves all joint tissues and, contrary to the common description of a wear-related pathology, it is the consequence of an active and unbalanced process of repair and destruction[156,157] (Figure 9). The actual causes of OA are not yet identified and there is still debating on the precise order of events that trigger its onset.

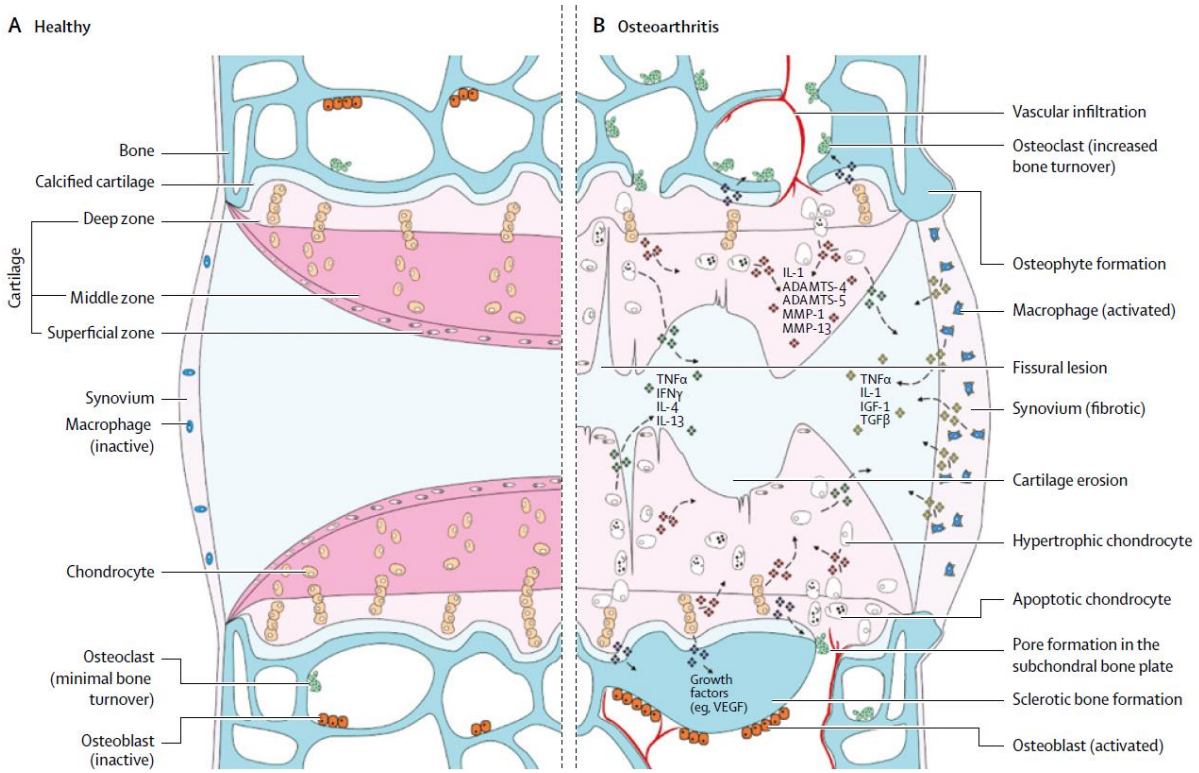


*Figure 9: Signalling pathways and structural changes in the development of osteoarthritis ADAMTS=a disintegrin and metalloproteinase with thrombospondin-like motifs. IL=interleukin. MMP=matrix metalloproteinase. TNF=tumour necrosis factor. IFN=interferon. IGF=insulin-like growth factor. TGF=transforming growth factor. VEGF=vascular endothelial growth factor. From Ref158.*

In articular cartilage, chondrocytes fail the synthesis and degradation homeostasis[159]. This dysregulation leads to variations in the ECM composition causing the loss of tissue integrity and the consequent increase of AC disruption susceptibility by physical forces[160]. The key promoter that compromises the balance between anabolic and catabolic processes is still unknown and the mechanisms that can influence chondrocytes behaviour can be multiple like growth factors, cytokines, ECM components as well as structural and physical stimuli[161].

One of the degenerative events that appear in early OA, is the production of "wear" particles that, overcoming the ability of resident macrophages to be engulfed, become mediators of the inflammation. The event that triggers the formation of these particles is still debated between their traumatic origin produced by microfractures or the onset of inflammation that generates an increase of the remodelling activity[162]. It can also be assumed that both mechanical and

inflammatory cues can lead to the same effects and that one can promote the inception of the other and vice versa. At present, there is not enough scientific evidence to understand which is the first and/or main activator.

The first response of joint cells to the early OA stage comprises the increase in the synthesis of the ECM components, and an intensive chondrocytes proliferation in the deep zone. Unfortunately, this first anabolic response is not able to stop chondrocytes apoptosis, as well as cartilage ECM variations, and favour the progression of OA. Pro-inflammatory cytokines TNF-α, IL-1β and IL-6 are produced by chondrocytes and type A synoviocytes after cell-contact with ECM breakdown components. Cytokines bind to chondrocytes receptors and stimulate the synthesis and the release of MMPs as well as inhibit the collagen II production[163]. The downregulation of collagen II synthesis and the increase of the degradation of pre-existing collagen weaken its network[164].

During early-stage OA, erosions appear on the AC surface, they deepen into the cartilage as the pathology progresses, opening cracks that are followed by the thickening of the calcified zone. Hypertrophic chondrocytes, in an attempt at tissue repair, increase their synthetic activity, generating matrix degradation products and pro-inflammatory mediators. These products lead to the decrease of the function of neighbouring chondrocytes and stimulate the proliferation and the production of pro-inflammatory molecules by synoviocytes.

Cartilage and subchondral bone changes are strictly connected, and it is not clear which tissue is modified earlier and affects the other. However, the high levels of cartilage oligomeric matrix protein (COMP) and BSP show that both are involved in the early stage of OA[165].

Several histological modifications appear at the subchondral bone level: immediately under the AC, the subchondral bone plate increases its thickness and beneath trabecular bone undergoes an intense remodelling activity associated with the increase in cross-linked N-telopeptide (NTx)

and C-telopeptide (CTx)[166] of type I collagen. The high turnover facilitates blood vessel invasion that penetrates through the tidemark and reaches the cartilage.

The OA subchondral bone is characterized by an abnormal deposition of the osteoid matrix that, due to an abnormal ratio between α1 and α2 collagen chains[167,168], is not able to convey correct mineralization with a consequent hypomineralisation of the tissue. Even if the apparent stiffness of the subchondral bone is maintained by the increase in trabecular number and volume[157], this area suffers from a reduction of its capability to absorb as well as dissipate energy and transmitting forces through the joint. This occurrence predisposes the articular surface to deformation[169]. The sclerotic bone changes lead to the development of bone marrow lesions that can be envisaged by magnetic resonance imaging (MRI) and the first bone cysts[170] appear. These lesions consisting of fibrosis, edema, bone marrow necrosis and trabecular abnormalities[171,172] and are marker of high metabolic activity.

At the joint's margins, pro-inflammatory pathways, overload, and abnormal joint kinematics lead to the reactivation of the endochondral ossification that culminates with the formation of osteophytes.

In the late stage of OA, the anatomy of the joint is fully altered, with the loss of the compartmental division between AC and subchondral bone. In areas where AC is destroyed, large bone sclerosis with osteoid deposition and bone necrosis appear[165]. The synovial fluid gets contact with the bone marrow and presumably leads to bone cysts formations[165,171].

It is not yet clear whether the involvement of the synovial membrane in the pathogenesis of OA is primary or secondary to the above-described variations[173]. Histological changes of OA synovium[174] are the hyperplasia of the intima, occasionally accompanied by lymphocytes and monocytes infiltration in sub-intima and increase in vascularisation.

Synovial cells produce molecules correlated with the OA progression, like MMP-1, 3, 9 and 13[175], proteolytic enzymes and cytokines like TNF-α, IL-1β and IL-6[176] that lead to AC

destruction. A vicious cycle of production of these degrading molecules is established by synoviocytes and chondrocytes that can influence both populations in an autocrine and paracrine manner[177].

Moreover, the cartilage breakdown products can stimulate synoviocytes to release collagenase and hydrolytic enzymes that lead to vascular hyperplasia inside the synovium[178].

The generated inflammatory status can drive to a neo-vascularisation, which is also sustained by cell-mediated inflammation, like macrophages secreting pro-angiogenic factors and stimulating endothelial cells to produce VEGF and basic fibroblast growth factor (bFGF)[178,179]; in turn, the angiogenesis perpetuates the inflammatory response[180]. Neo-vascularisation is meticulously associated with chronic synovitis and may occur in all stages of OA[181].

The progress of changes in the synovial membrane is related to the increase in the severity of the disease.

*TABLE1: JOINT TISSUES MODIFICATIONS IN OA*

| *Tissue* | Modifications |
|---|---|
| ***Articular cartilage*** | Wear particles |
| | Increased synthesis of ECM components |
| | Chondrocytes proliferation in the deep zone |
| | Chondrocytes apoptosis |
| | Chondrocytes hypertrophy |
| | Production of pro-inflammatory cytokines by chondrocytes |
| | Production of degradative enzymes by chondrocytes |
| | Type II of Collagen structural abnormalities |
| | Superficial deformation |
| | Cartilage cracks |
| | Thickening of calcified zone |
| ***Subchondral bone*** | Thickening of subchondral bone plate |
| | Intense bone remodelling activity |
| | Abnormal structural deposition Type I of Collagen |
| | Bone marrow lesions |
| | Bone cysts |
| | Osteophytes |
| | Bone necrosis |
| ***Synovial membrane*** | Production of pro-inflammatory cytokines by synoviocytes |
| | Production of degradative enzymes by synoviocytes |
| | Thickening |
| | Increase in vascularisation |
| | Increase of cell infiltration in the sub intima |

## 1.5 Models of osteoarthritis

Several animal models have been used to study the pathogenesis of OA, as well as to investigate new diagnostic tools or therapeutic interventions. Indeed, due to the heterogeneity of this pathology[182] no single animal model reflects the onset and the progression of human OA. For that reason, the selection of the appropriate animal model must be based on the aetiology under investigation and the intended purpose[183]. Studies for the development of therapeutic interventions or initial drug screening use small organisms like zebrafish, rodents (mice and rats), guinea pigs and rabbits for their relatively low cost, ease of handling and

maintenance[184,185]. Due to their anatomical similarities to the human joint, large model organisms are used to study the features of the pathological process of OA and efficacy of drugs before the clinical trials[186]. These models guarantee some advantages by merits of the naturally occurring primary and secondary OA, the possibility of arthroscopic intervention and diagnostic imaging[187]. Unfortunately, the use of large animal models is related to ethical considerations, cost, and slow disease progression[184].

Even if *in-vivo* models may represent most accurately the naturally occurring whole joint disease, *in-vitro* systems are widely used for their ease manipulation and, of great interest recently, for the shift towards the 3R experimentation philosophy of refining, reducing and replacing the use of animals in science[188]. However, the significance of *in-vitro* models to clinical diseases requires careful interpretations.

In the 2D models, primary cells or immortalised cell lines are cultured on a flat surface. These procedures offer systems for screening compounds capable to diminish the catabolic response involved in AC degradation, investigating signalling pathways and, thanks to their easy transfect manipulation, for the study of gene and protein expression. 2D cultures are inexpensive and let the setting of accurately controlled investigation conditions but, concomitantly, forces cells to grow in a planar environment where the oxygen and nutrient gradients do not represent their physiologic conditions[189]. Chondrocytes are susceptible to plastic polarisation, with alteration in cell mechanotransduction that impacts their signalling. In a 2D environment, chondrocytes undergo a process of de-differentiation with changes in their morphology from round to elongated fibroblasts-like cells and alterations in the genetic expression profile, by the reduction of aggrecan[190] and the increase of Type I Collagen production[191].

The 2D co-cultures let the investigation of multiple experimental parameters to understand cell-cell communication, with or without contact, in a shared environment. This technique is useful

to get insight into the mutual interaction of cell populations[191], but several limitations of this system still exist, including plastic polarisation and the failure in investigating cell-ECM interactions.

Considering that the environment of the total joint is essential in OA pathology, the 3D cell models represent an interesting alternative to 2D culture, because they provide a tool for the investigation of both cell-cell and cell-ECM interaction. A useful 3D model must be reproducible and not expensive. The currently existing 3D models include explants, and scaffold- based or scaffold-free systems.

Animal and human explants models are used within the OA field to explore the effect of cartilage loading during the evolution of the disease, studying the compressive overload on AC[192], as well as examine the relationship between the different tissues[193]. However, explants models retain shortcomings like cell death at the surgical edge, de-differentiation of outgrowths cells, finite source of the same biological sample[194] and, not least, the artificial environment produced could interfere with the investigations on mechanical loading and angiogenesis[195].

Cell culture pellets are used as scaffold-free systems. Cells are centrifuged to let them clamp together and assuming a 3D shape. The loss of plastic polarisation favours the increase in the expression of chondrocytes markers like Sox9, collagen II and aggrecan, and reduces the cell hypertrophy marker, such as collagen X, and calcification markers runx2 and ALP[196]. However, this system is not ideal to study the proliferation and cell death occurring in the centre of the pellet due to deprivation of nutrients and oxygen[197].

Scaffold-based systems provide a 3D platform for the study of cell behaviours as well as the surrounding environment and exploring the crosstalk between different cell types. Of importance during the development of these structures is the consideration of pore size and the interconnectivity, as they can alter cell fate and, consequently, their relationship with the ECM[198]. Hydrogels derived from chitosan, gelatin, alginate, and hyaluronan, which possess a

high-water component and biocompatibility, low immunogenicity, modifiability, porosity, bioactivity, and biodegradability are useful to mimic ECM. These hydrogels are suitable for chondrocytes viability and proliferation and promote the expression of collagen II, aggrecan and Sox9, molecules that normally decrease during 2D culture[199–201]. Synthetic hydrogels, compared to natural ones, offer greater reproducibility. Furthermore, 3D synthetic platforms can favour the expression of chondrocytes markers[202,203] and can be chemically modified with factors (e.g., TGF-β3) to promote chondrogenesis[204]. Remarkably, both natural and synthetic hydrogels can be manufactured through 3D printing, and this greatly increases their potential for applicability in 3D models.

## 2 Thesis aim

There is currently no predetermined *in-vitro* model (DM) of OA disease. This is essentially due to the defective knowledge on the onset of this pathology and to the numerous tissues' modification involved that make difficult to *in-vitro* reproduce OA.

A clear comprehension of the various mechanisms (e.g., mechanical, contact, paracrine) engaged in the pathology is necessary to understand its progression, as well as the targets to restore joint function.

The Ph.D. research activity was devoted to the development of two *in-vitro* culture models to study different aspects of OA.

The models were devoted to investigating:

1. The involvement of adult stem/stromal cells of the synovial membrane in bone remodelling, and to this purpose we used an indirect 2D co-culture approach;
2. The crosstalk between chondrocytes and subchondral bone in normal and pathological condition, developing an engineered 3D scaffold and simulating an inflamed microenvironment.

These two models allow the investigation of the cell behaviours from the three tissues involved in the pathogenesis of OA, and the development of a possible *in-vitro* platform for future studies encompassing the three components simultaneously.

## 3 2D model system: Synovium-Derived Stem Cells and osteoclasts activity.

Synovium-Derived Stem Cells (SDSCs) are Mesenchymal Stem/Stromal Cells (MSCs) resident in the Synovial Membrane (SM)[205,206]. SDSCs display the same BM-MSCs properties both in phenotypic and functional terms [207] but, comparing the two populations in terms of chondrogenic potential, SDSCs show a greater ability to differentiate making them attractive as a possible source for cartilage regeneration[208]. Both healthy (H) and OA synovium host SDSCs[208,209] that, unlike BM-MSCs, seems to preserve an effective proliferation rate and colony-forming potential despite the age of the patient[210].

The structural modification of subchondral bone during OA progression is an expected consequence of the alteration in the remodelling process. The signals induced by microdamage or by the increased of mechanical load, start bone resorption by the OCs at the inner bone surface[211]. The remodelling causes the release of TGF- β[212] and IGF-1[213] from bone ECM. The increase of these factor concentrations recruits MSCs to the remodelling site where they differentiate in OBs for new bone deposition, thus coupling bone remodelling spatially and temporally[214].

The remodelling process is not restricted to the bone compartment but active OCs are also involved in AC degradation during OA[215].

The capability of synovial cells to produce osteoclastogenic factors was intensively demonstrated but there is not enough evidence that supports the hypothesis of SDSCs could directly contribute to the pathogenesis or progression of OA.

To this aim, we isolated and cultured SDSCs from H and OA synovial membrane and compared *in-vitro* differences in terms of phenotype, morphology, differentiation potential, and capability to differentiate normal Peripheral Blood Mononuclear Cells (PBMCs) in mature and active OCs.

## 3.1 Draft of the study

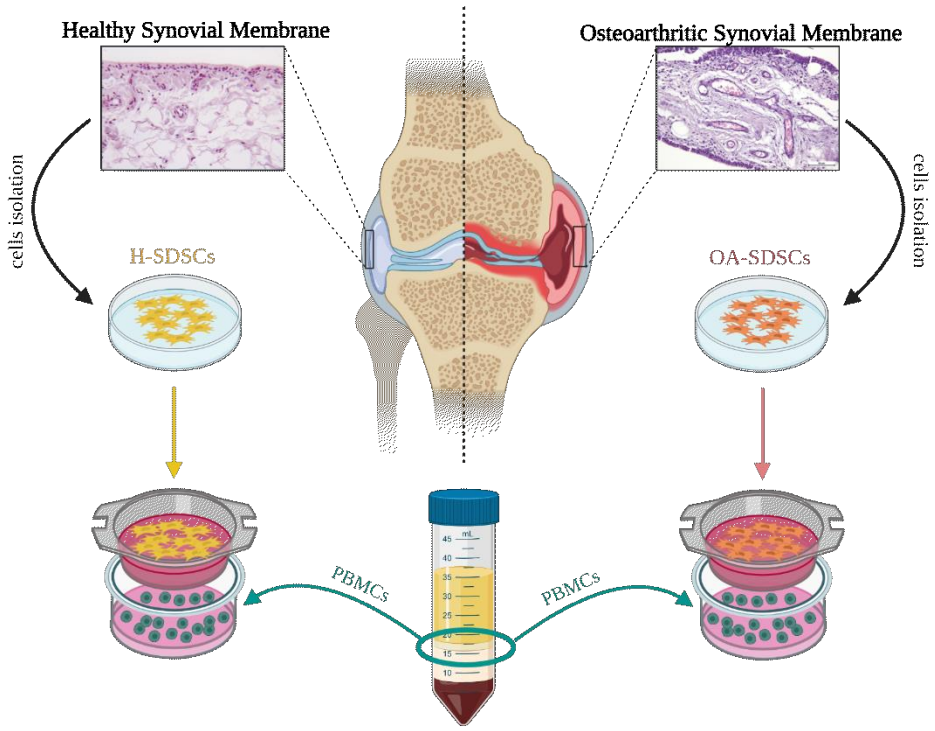


## 3.2 Materials and methods

### 3.2.1 SDSCs isolation

Synovial membranes were obtained during surgery for total knee arthroplasty in eight OA subjects (mean age 86 ± 3), treated in the Azienda Ospedaliera-Universitaria Ospedali Riuniti of Ancona (Italy). Control SM was obtained from two healthy subjects, gender matching, undergoing leg amputation. In accordance with the Local Ethical Committee guidelines and with the 1964 Helsinki Declaration, informed consent was obtained from all individual participants included in the study. Patients were aware that the tissue used for the study represented a discard of surgical procedures and the voluntariness of their participation to the study (freedom from coercion or undue influence, real or imagined). SDSCs were isolated according to De Bari et al. [205]: briefly, synovial tissues were rinsed with Dulbecco's Phosphate Buffered Saline (DPBS) (Sigma-Aldrich, Milan, Italy), minced into small pieces and then digested with 0.2% collagenase (Collagenase NB 4G Proved Grade, Serva Electrophoresis

Gmb H, Germany) in Dulbecco's Modified Eagle Medium/Nutrient Mixture F-12 (DMEM/F-12, Sigma–Aldrich), supplemented with 2% Fetal Bovine Serum (FBS) and 1% penicillin–streptomycin (100 U/ml) at 37◦C in a humified atmosphere, with 5% $CO_2$. FBS and antibiotics were both from GIBCO® (Thermo Fisher Scientific, Waltham, MA, U.S.A.). After an overnight incubation, samples were filtered through 40 μm nylon-mesh cell-strainers (BD Biosciences, San Jose, CA) to remove large debris. Single cell suspensions were cultured in DMEM/F-12 with 10% FBS and 1% antibiotics (from here on defined Complete Medium, CM) in tissue culture flasks, changing CM twice a week. Upon reaching 50% confluence, cells were carefully detached with 0.25% trypsin/1mM EDTA (Sigma–Aldrich). Non-adherent cells were gradually lost by medium changing. From each explant, we were able to obtain an adequate number of cells without excessive subculturing (i.e., within the fourth passage of subculture) allowing the setup of two different sets of experiments.

### 3.2.2 SDSCs characterization

The immunophenotype of synovial adherent cells was investigated by flow cytometry according to the minimal criteria of the International Society for Cellular Therapy (ISCT) [216]. The following fluorescein isothiocyanate (FITC)–conjugated mouse monoclonal antibodies (all by Immunotools, Friesoythe, Germany) were used: anti-CD14, CD34, CD45, CD73, CD90, CD105 and CD106 (StemCell Technologies, Milan, Italy). As isotype controls, FITC-coupled nonspecific mouse IgG replaced the primary antibodies. For each sample, at least 10000 events were acquired by FACSCalibur flow cytometry system (Becton Dickinson, CA, U.S.A.) and data were analysed using FCS Express 6 Plus. Software (De Novo Software, CA, U.S.A.). Forward (FSC)monitored the cell volume and Side scatter (SSC) evaluated the internal complexity.

### 3.2.3 SDSCs *in-vitro* differentiation

For in vitro chondrogenic, osteogenic and adipogenic differentiation, commercial kits from Life Technologies Corporation (Carlsbad, U.S.A.) were used according to the manufacturer's instructions. For *in-vitro*, chondrogenic, osteogenic and adipogenic differentiation commercial kits from Life Technologies Corporation (Carlsbad, U.S.A.) were used according to manufacturer's instructions.

The chondrogenic potential of adherent cells isolated from synovia was assessed using a pellet culture system. In brief, $5\times10^5$ cells were centrifuged for 10 min in 15 ml polypropylene tubes and then cultured for 14 days in 1 ml of STEMPRO® chondrogenic medium (Chondrogenesis Kit, Life Technologies Corporation, U.S.A.), replacing medium every 3 - 4 days. Cell pellets were paraffin-embedded, cut into 3 μm thick sections, and then stained with Alcian Blue solution pH 1 (Bio-Optica, Milan, Italy). For immunohistochemistry, deparaffinized sections were incubated with mouse anti aggrecan (Santa Cruz Biotechnology inc, Heidelberg, Germany) and anti-type II collagen (Merck Millipore, Darmstadt, Germany) antibodies. After overnight incubation at 4°C, the immune complex was evidenced by the streptavidin-biotin peroxidase technique (Envision peroxidase kit, Dako Cytomation, Milan, Italy). After the incubation with 0.05% of 3,3'-diaminobenzidine (Sigma–Aldrich) in 0.05 M Tris buffer, pH 7.6 with 0.01% hydrogen peroxide, samples were counterstained with Mayer's Hematoxylin (BioOptica) dehydrated in ethanol and coverslipped with Eukitt mounting medium (Electron Microscopy Sciences, PA, U.S.A.).

For osteogenesis, cells were seeded in chamber slides (Nunc™, Rochester, NY) at a density of $5\times10^3$ cells/cm$^2$ in appropriate induction medium (STEMPRO® Osteogenesis Kit, Life Technologies). After 21 days, Von Kossa staining evaluated matrix mineralization.

Adipogenic differentiation was performed by culturing $2\times10^4$ cells.cm$^2$ with STEMPRO® Adipogenesis Kit (Life Technologies) for 14 days and detected by Oil Red staining (Sigma–

Aldrich) according to manufacturer's instructions. The appearance of cytoplasmic lipid droplets was also identified by immunohistochemistry using a mouse antibody against perilipin 1 (dil. 1:100; Abcam, Cambridge, U.K.) and evidenced as described above. Cells maintained in CM represented the negative controls. Nikon DSVi1 digital camera and NIS Elements BR 3.22 imaging software (both from Nikon Instruments, Florence, Italy) were used for image acquisition.

### 3.2.4 Osteoclastogenesis assessment

In vitro osteoclastogenesis was induced in PBMCs by SDSCs through a Transwell (ThermoScientific™Nunc™Carrier Plate system, Milan, Italy) co-culture system. PBMCs were obtained from gender matching healthy donors using a density gradient Ficoll/Paque method. In brief, peripheral blood was diluted 1:1 in DPBS, layered on Histopaque®-1077 (Sigma–Aldrich) and centrifuged at 400×g for 30 min. PBMCs at the interface plasma/Ficoll were collected, washed in DPBS, suspended in α-MEM (Corning Inc., NY, U.S.A.) supplemented with 20% FBS, 1% antibiotics and 2ng/ml of M-CSF (PeproTech EC, London, U.K.).Cells were then seeded at a density of $2\times10^6$ cells/well on Aclar®Film 33C (EMS, Fort Washington, PA, U.S.A.) placed in 12-well tissue culture plates (TCPs). Cells were cultured for 6 days, removing non-adherent cells with media changes. SDSCs were then seeded in cell culture inserts (with pores 0.4μm) of the 12-well TCPs containing PBMCs, at a density of $2\times10^5$ cells/well (ratio 1:10). Co-cultures were maintained for 2 weeks. At each culture media refresh, adherent cells were observed by a light inverted microscope to assess multinucleated cell development. After 14 days, the inserts were removed, and cells in the wells analysed for cytoskeleton distribution and the IHC expression of Tartrate-Resistant Acid Phosphatase (TRAP) and cathepsin K (CATK). TRAP or CATK-positive multinuclear cells that contained more than three nuclei were identified as osteoclasts and counted. Nikon DSVi1 digital camera

and NIS Elements BR 3.22 imaging software were used for image acquisition. For the immunostaining evaluation of TRAP and CATK four images at 20× magnification from each sample were analysed in semi-quantitative manner. For each image, cells with more than three nuclei were examined for TRAP and CATK staining and ranked as: 0 (negative), 1 (weak staining), 2 (good staining), 3 (strong staining). The score was calculated considering the number of positive cells and the staining and analysed by GraphPad Prism 4 (https://www.graphpad.com/scientific-software/prism/). The resorptive ability of generated osteoclasts was assessed putting dentine discs (1 cm in diameter and 0.7 µm in thickness) at the bottom of the wells of the previously described co-culture systems and observed with a SEMPhilips XL 20.

### 3.2.5 qRT-PCR

The expression of genes involved in osteoclastogenesis (Interleukin 6, IL-6; RANKL and OPG) was assessed in SDSCs before and after co-culture with PBMCs. Total RNA was extracted from cell pellets using the PerfectPure RNA cultured cell kit (5-Prime GmbH, Hamburg, Germany) according to the manufacturer's instructions. RNA quantity and quality were evaluated by UV spectrophotometric analysis (bioPhotometer plus, Eppendorf GmbH, Germany). Standard reverse transcription was performed using the GoScript™ reverse transcription system (Promega Corporation, Italy) starting from 1.0 µg of total RNA. Each real-time quantitative PCR assay was executed in triplicate in white plastic ware using the Mastercycler Realplex2 (Eppendorf GmbH). A final volume of 10 µl with 1 µl of cDNA (corresponding to 50 ng of total RNA template), 1×SsoFast™ EvaGreen® Supermix (Bio-Rad), and 200 nM primers were used for PCR. The cycling conditions included an initial step at 95°C for 30 s, followed by 40 cycles at 95◦C for 5 s and at 60◦C for 20 s. Oligonucleotide sequences were designed with Primer 3 (v. 0.4.0) and showed in Table 2.

**TABLE 2: PRIMER SEQUENCES**

| GENES | Primer forward (5′→3′) | Primer reverse (3′→5′) |
|---|---|---|
| **GAPDH** | AGCCACATCGCTCAGACAC | GCCCAATACGACCAAATCC |
| **GUSB** | AAACGATTGCAGGGTTTCAC | TCTCGTCGGTGACTGTTCA |
| **IL-6** | CCAGAGCTGTGCAGATGAGT | CATTTGTGGTTGGGTCAGGG |
| **RANKL** | TAATGCCACCGACATCCCAT | ATGTTGGAGATCTTGGCCCA |
| **OPG** | TGATGGAAAGCTTACCGGGA | CAGGATCTGGTCACTGGGTT |

To avoid sequence homologies to pseudogenes or other undesired targets, primer specificity was checked by BLAST. Melt curve analysis confirmed PCR specificity. Reference genes and each gene of interest were amplified simultaneously under the same conditions in each PCR assay. Primers showed the same amplification efficiency. Glyceraldehyde 3-phosphate dehydrogenase, GAPDH and β-glucuronidase, GUSB were used to normalize cell mRNA data[217]. Normalization involved the ratio of mRNA concentrations of genes of interest (Ct values) to that of reference gene Ct medium values. Data were expressed as relative gene expression ($2^{-\Delta Ct}$). Each assay was performed in triplicate. To point out the effect of the different origin (OA vs H) or the co-culture system on SDSCs, ΔΔCt method for Fold-Change evaluation was used[218]. The qPCR efficiency in all our experiments was more than 90%.

### 3.2.6 Statistical analysis

Statistical analysis was performed by Prisma 4 Software (https://www.graphpad.com/scientific-software/prism/). The mean and standard deviation of two different experiments for cells obtained from each subject were analysed by Mann–Whitney U-test. Statistical significance was tested at $P<0.05$.

## 3.3 Results

### 3.3.1 SDSCs characterization

SDSCs isolated from synovial membranes of H and OA subjects showed no differences in term of phenotypic expression. Both populations were positive for CD73, CD90 and CD105 (>98% of positive cells), while they were negative for hemopoietic antigens CD14, CD34 and CD45 (positivity < 2%) (Figure 10). Conversely, the expression of CD106 showed significant differences between H and OA cells (42.75± 2.14 vs 49.02±2.45%; $P<0.05$).

The investigation of cell size (FSC) and inner granularity (SCC) revealed that SDSCs obtained from OA subjects were significantly greater than the H (250.49±6.89 vs 216.98±12.77, $P<0.01$) and showed an increased internal complexity (385.32±10.77 vs 339.20±8.13, $P<0.01$).

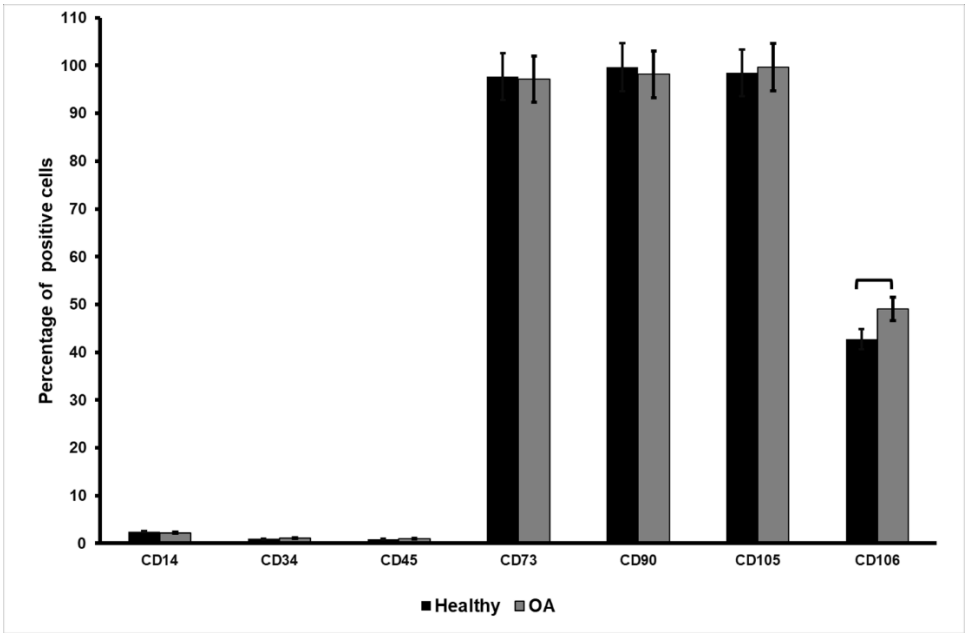


*Figure 10. SDSCs cytofluorimetric characterization. Cytofluorimetric analysis of MSC surface markers in SDSCs isolated from Healthy and Osteoarthritic synovial membrane (white plots indicate FITC negative controls), square brackets indicate significant (P<0.05) differences.*

### 3.3.2 SDSCs differentiation ability

The Alcian Blue staining as well as the immunohistochemical expression of aggrecan, Von Kossa and Alizarin Red mineralization assays, Oil Red O-staining and perilipin immunohistochemical expression (Figure 11) did not evidence changes in term of

differentiation potential into the three lineages (*i.e.,* chondrogenic, osteogenic and adipogenic) between SDSCs harvested from H and OA subjects.

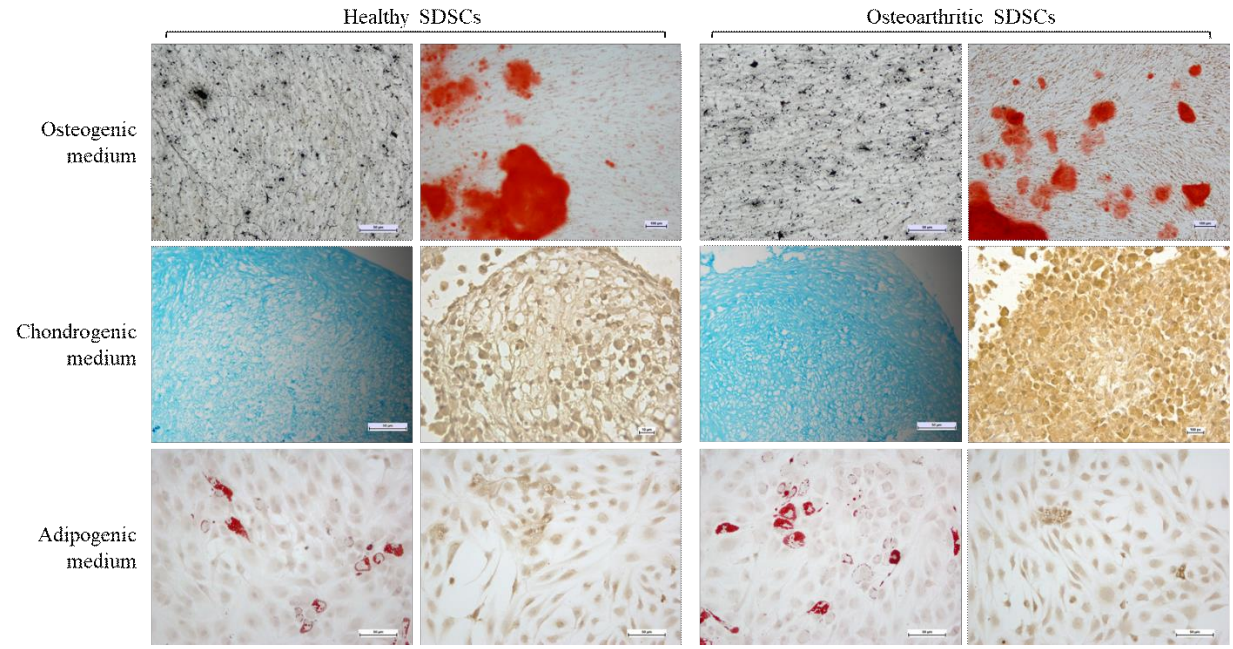


*Figure 11. SDSCs in-vitro differentiation potential assessment. Differentiation of SDSCs isolated from Healthy and Osteoarthritic synovial membrane toward osteoblasts (Von Kossa staining scale bars 50µm; Alizarin Red staining scale bar 100µm;), chondrocytes (Alcian Blue staining scale bar 50µm; IHC for aggrecan scale bar 10µm) and adipocytes (Oil Red staining and IHC for perilipin; scale bars: 50µm).*

### 3.3.3 Evaluation of Osteoclasts-like cells formation

After 8 days from the seeding, numerous multinucleated cells start to appear in both H-SDSCs/PBMCs and OA-SDSCs/PBMCs indirect co-culture systems. After 14 days, the differentiation of PBMCs (seeded in the bottom of the well) into OCs was evaluated. The presence of plentiful F-actin ring positive cells containing more than three nuclei and zipper-like structures were evidenced in both co-culture types through the detection of F-actin ring formation (Figure 12A). SEM observation confirmed the presence of multinucleated cells with resorbing pits only in osteoclast-like cells induced by OA-SDSCs (Figure 12A).

Multinucleated cells were positive for TRAP and CATK in both H and OA co-culture systems. Differentiated cells co-cultured with OA-SDSCs showed a slight albeit a not significantly

greater number of TRAP$^{+}$ cells and fewer CATK$^{+}$ cells in comparison to PBMCs co-cultured in presence of H-SDSCs (Figure 12B).

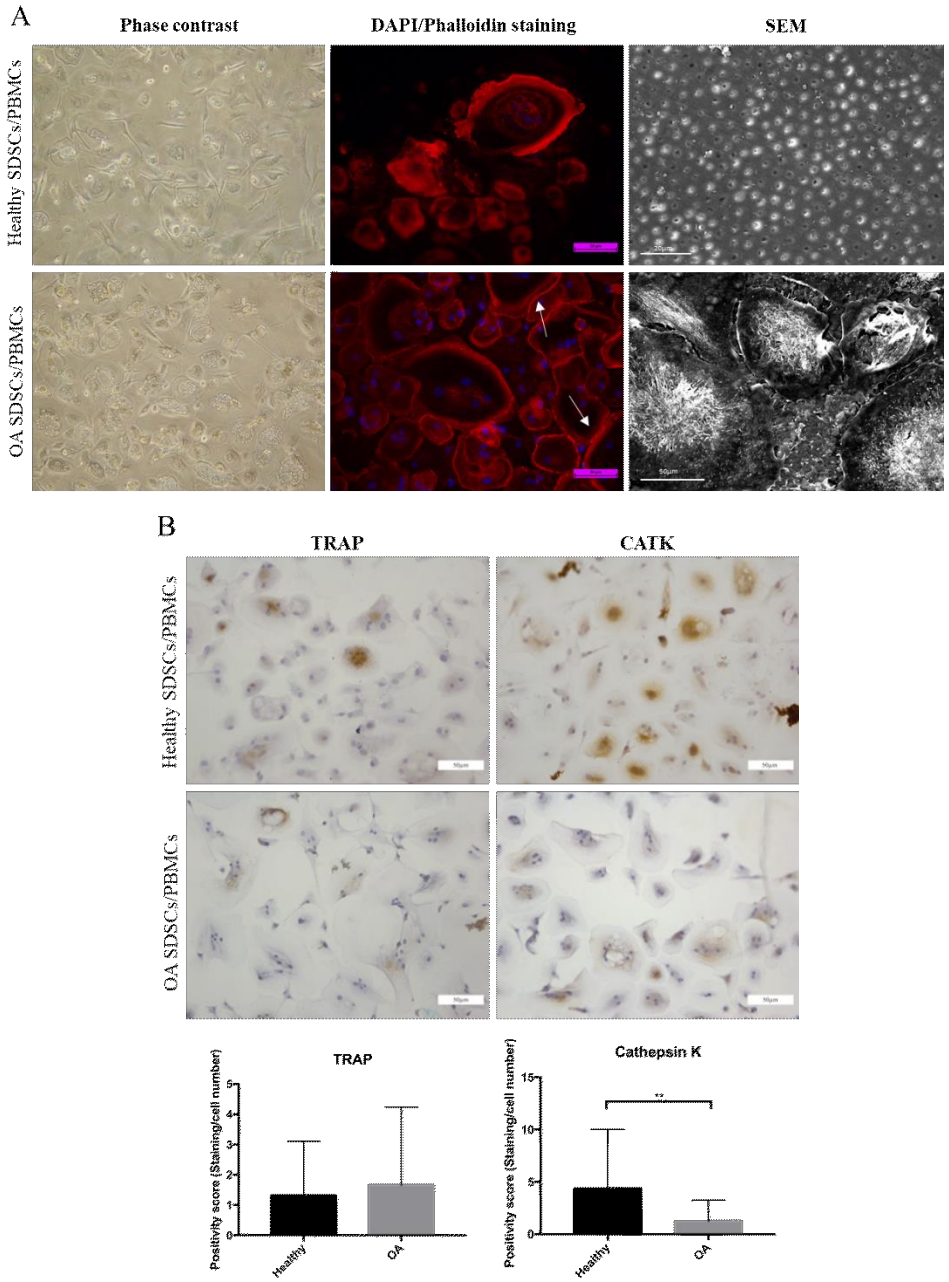


*Figure 12. Morphological evaluation of OCs like-cells formation. (A) Upper line: phase contrast, fluorescent DAPI/Phalloidin staining and SEM images displaying the generation of osteoclast-like cells formation after 14 days of co-culture of normal PBMCs with Healthy or Osteoarthritic SDSC. Phalloidin staining evidenced the appearance of the actin ring and of zipper-like structures (arrows). Bottom line shows SEM images of cells on dentin slices were active osteoclast-like are detected in OA-SDSCs/PBMCs co-culture. (B) IHC detection of CTSK and TRAP in Osteoclast-like cells after 14 days of co-culture with Health or Osteoarthritic-SDSCs, square brackets indicate significant (Scale bars: 50 µm; P<0.05) differences.*

### 3.3.4 qRT-PCR

OA-SDSCs gene expression for IL-6 and OPG were down regulated, four- and two-fold respectively, in comparison with H-SDSCs. In contrast, RANKL mRNA undergoes a significant increase responsible for the increase in RANKL/OPG ratio in OA-SDSCs.

RANKL and OPG were also evaluated in H and OA SDSCs after co-cultures. RANKL expression was up-regulated eight-fold in H SDSCs after 14 days of co-culture in comparison with H SDSCs cultured alone while its expression slightly, albeit significantly, decreased in post-co-culture OA SDSCs. Conversely, OPG mRNA was up regulated in both H and OA SDSCs after co-cultures. These changes caused a significant increase in the RANKL/OPG ratio in H SDSCs in comparison with OA cells (Figure 13).

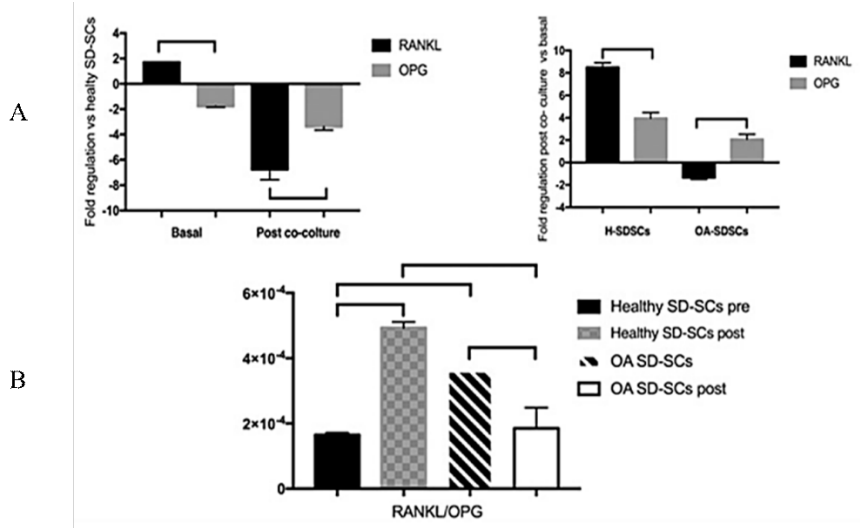


*Figure 13. Osteoclastogenic factors production by Healthy or Osteoarthritic SDSCs before and after co-cultures. (A) Histograms depict changes in mRNA expression of RANKL and OPG genes in Healthy or Osteoarthritic SDSCs, data are expressed as Fold-regulation ($2^{-\Delta\Delta Ct}$). (B) Histogram depicts changes in RANKL/OPG ratio in Healthy or Osteoarthritic SDSCs before and after co-culture. Square brackets indicate significant ($P<0.05$) differences.*

## 3.4 Discussion

The SM encapsulates the joint and through the production of synovial fluid, providing nutrients and proper lubrification essential for normal joint function[219]. The subchondral bone beneath calcified cartilage (subchondral plate) and the subchondral trabecular bone represent the

subchondral bone region (SB). SM and SB seem to play a pivotal role in OA progression, but their association triggering cartilage damage is still unclear.

The SB undergoes structural changes during the progression of OA passing from early Bone Marrow Lesions (BMLs), signs of biomechanical overload, up to osteosclerosis and osteophyte formation, considered features of advanced OA. These modifications are the consequences of cell-mediated bone remodelling process alterations[220].

The increase of remodelling activity is demonstrated by the high tendency of PBMCs isolated from OA patients to differentiate into OCs[221], as well as by the differentiation of Type A synoviocytes into OCs[222,223] under the M-CSF production by type B synoviocytes.

Age and chronic inflammation can modulate MSCs behaviour thus influencing the remodelling process, however, the mechanisms and the possible exchange between MSCs and other specialized cells remain undefined. MSCs can variate the expression of RANKL and OPG according to the inflammatory milieu, and support or inhibit osteoclastogenesis.

OA aetiology can affect MSCs behaviour[223] and, vice versa, their imbalance may encourage OA progression. However, the SDSCs involvement in OA pathophysiology is not supported by experimental pieces of evidence. Therefore, to investigate this aspect, SDSCs were isolated from healthy and osteoarthritic subjects and compared in terms of phenotype, morphology, gene expression and capability to induce OCs formation.

SDSCs were isolated following the protocol developed by De Bari et al[205]. The surface antigens pattern of both H and OA-SDSCs, evaluated by cytofluorimetry, was in line with previous studies[209]. Both H and OA populations showed similar and high positivity for CD90 and CD105, suggesting their remarkable and comparable chondrogenic differentiation capability[224,225]. This observation was also confirmed by in vitro chondrogenic differentiation. The only difference detected between the two populations was a rise of CD106 expression in OA-SDSCs. The expression of the CD106 marker should be enhanced by proinflammatory

cytokines[226] and its high positivity in OA-SDSCs could be a signal of cell response toward endogenous inflammatory environment. No differences in terms of adipogenic and osteogenic commitment were detected between H and OA-SDSCs, even if the previous study demonstrates that CD106 could be associated with changes in osteogenic and adipogenic potentials[227,228].

The gene expression analysis for bone remodelling genes RANKL and OPG, revealed that in OA-SDSCs the RANKL/OPG ratio was higher than H-SDSCs suggesting their potential involvement in the activation of multinucleated cells (chondroclasts and/or osteoclasts), accountable of cartilage and bone degradation during age-related diseases, such as OA.

No studies in literature evaluated the OA-SDSCs potential to stimulate PBMCs differentiation in active OCs. To go in-depth in this gap, SDSCs were isolated from H and OA SMs and each population was co-cultured with healthy PBMCs by transwell approach to evaluate their paracrine effect on osteoclastogenesis.

To assess OCs formation, phalloidin, SEM analysis on dentin slices and IHC for CATK and TRAP were performed on PBMCs after 14 days of co-culture with H or OA-SDSCs. Phalloidin immunofluorescence staining evidenced the presence of abundant cells showing F-actin ring organisation containing more than three nuclei in both co-cultures. Interestingly, only PBMCs cultured under OA-SDSCs stimulation were able to determine the formation of resorption pits on dentin slices.

The immunohistochemical detection of the specific OCs markers CATK and TRAP confirmed the achievement of mature OCs phenotype in both co-cultures and reinforced SEM observations. Both proteins investigated express their activity out of cells. No significant differences in TRAP expression were found between differently stimulated populations. TRAP is constantly released as an inactive monomeric form, and it is activated in the ruffle border of OCs by CATK cleavage[229]. CATK expression is higher in H-SDSCs stimulated co-culture.

The CATK form accumulation into the cell cytoplasm associated with the lack of resorption pits confirms the not resorptive nature of OCs generated during the co-culture with H SDSCs.

## 3.5 Conclusion

The 2D-model used in this study assesses for the first time the ability of SDSCs to induce osteoclastogenesis via paracrine factors. Moreover, it allowed comparing H and OA-SDSCs highlighting that cells isolated from the osteoarthritic patients have much greater osteoclastogenic potential than the healthy ones. Based on these results, it could be hypothesized that the inflammatory osteoarthritic microenvironment to which the SDSCs are subjected *in-vivo*, has still effects on cell behaviour *ex-vivo*.

Overall, these results highlight how the inflammatory microenvironment could be the target of OA therapies not only for the immediate response of the affected cells but also for the modulation of the cell memory that is established.

# 4 3D model system: An engineered *in-vitro* model to reproduce OA.

To date, the main treatments of OA focus on symptoms management. Systemic drugs are used to treat pain and inflammation, including oral analgesics and non-steroidal anti-inflammatory drugs[151,230] (FANS). The use of drugs at local level, through intra-articular injection, is a valid alternative to systemic administration. This approach entails the targeting of the only interested joint and let the use of more concentrated drug doses and/or a prolonged time of its release[231]. Multiple systems such as hydrogels, microparticles, nanoparticles, and micelles have been developed to improve drug delivery into the joints[232–234]. In order to evaluate the effectiveness of these systems, it is important to monitor both the drug release and the effective target selectivity. In this regard, the design of *in-vitro* models of OA is fundamental for: (i) studying and understanding the disease progression and (ii) to have reliable platforms to test novel drug delivery systems for the treatment of OA in a predictive way.

The development of 3D biomimetic models has made possible the study of cell interactions in relation to the surrounding ECM, overcoming the limitation of 2D models.

In the diarthrodial joint, load transfer is made possible by the functional osteochondral unit consisting of articular cartilage and subchondral bone. The molecular crosstalk that are established between these two neighbouring tissues can influence their physical as structural characteristic and it can be mediated by the presence of blood vessels and innervations that penetrate from the subchondral bone into the cartilage, as well as by the formation of microcracks and fissures[235]. The homeostasis of both tissues is therefore influenced by biological factors and signalling molecules able to cross the demarcation zone between one tissue and another. These two tissues are actively involved in the on-set and progression of the OA and, the alterations that affect them are closely related to the pain and to the amplification of inflammation[236]. For this reason, several *in-vitro* OA models reproducing the cartilage-

suchondral interface portion of the joint[237] have been set up with the aim of reproducing in a biomimetic manner the relative native tissue.

This part of the Ph.D. project aims to provide a highly reproducible, easy to manipulate and low-cost 3D model *in-vitro* mimicking the deep layer cartilage/subchondral bone interface. The developed model provides an efficient tool for testing new therapeutic options for the medical management of OA disease.

For this purpose, using tissue bio-engineered strategies, a three-dimensional structure respecting the histological characteristics of this region in terms of load capacity, ECM composition and organisation, and the cell arrangement was designed.

First, the materials, previously characterised in other studies[238,239], were selected: two natural hydrogels formulation based on gellan gum (GG) and chondroitin sulfate (CS) for the deep layer and a poly-lactic acid (PLA) thermoplastic polymer for the subchondral bone. Following, some physicochemical analyses were performed on the chosen concentrations of the materials. Then, the viability of chondrocyte-derived from immortalised MSCs and MSCs (respectively for the cartilage or the subchondral bone side) seeded within the model was evaluated. Also, the model biomimetic capacity was investigated through the examination of specific tissue-related markers. Finally, the ability to reproduce *in-vitro* the main alterations from the OA pathology was assessed by exposing cells in the 3D model to an inflamed microenvironment.

## 4.1 Draft of the study

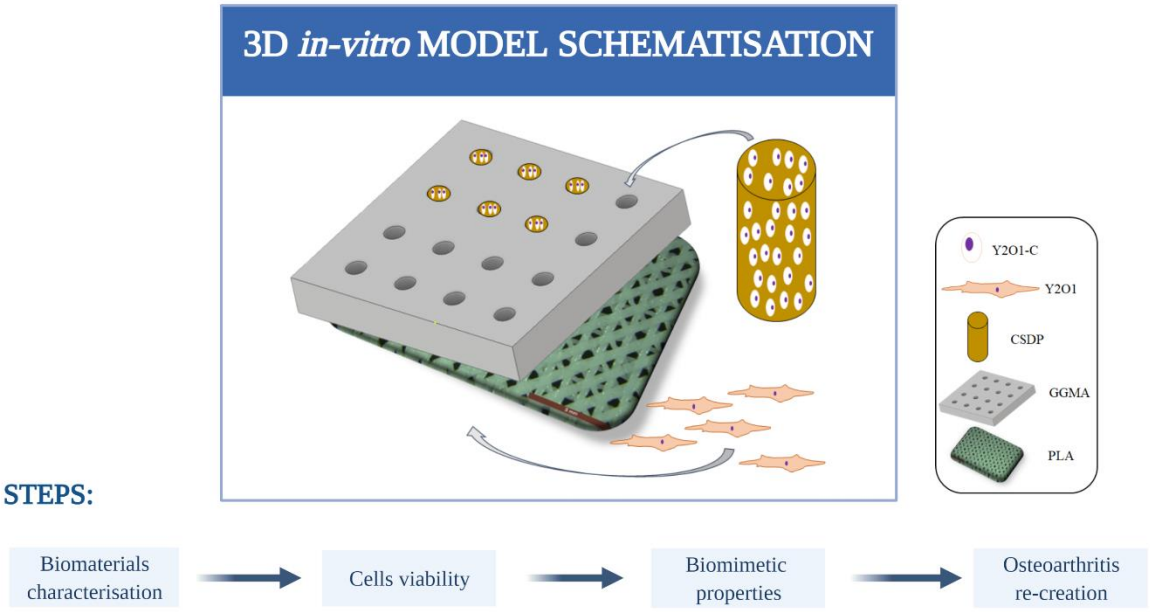


## 4.2 Materials and methods

All the reagents were bought from Sigma Aldrich, unless otherwise stated.

### 4.2.1 Gellan Gum Methacrylate synthesis (GGMA)

Highly methacrylated GGMA was synthesized by a reaction between Gellan Gum (Gelrite®, Molecular weight (MW) = 1.000.000) and methacrylic anhydride (MA)[239]. To summarise, GG (1%w/v) was dissolved at 90 °C in TRIS 1M (Trizma® base) pH 8.5-9.0, for 30 minutes. Then, MA (8% w/v) was added to the GG solution. The reaction was performed at 50 °C for 5 hours. The obtained GGMA solution was purified for 3 days by dialysis, using cellulose membrane (MW cut-off of 11-14 kD), against distilled water to remove the un-reacted materials. Then, the dialysed GGMA was lyophilised for 48 h in a freeze-dryer (Alpha 1–2 LDplus, CHRIST, Germany) and ready for the hydrogel manufacturing. The successful of the synthesis process was evaluated chemically via Attenuated total Reflection-Fourier transform infra-red (ATR-

FTIR), X-ray photoelectron spectroscopy (XPS) and 1H and 13C nuclear magnetic resonance (NMR) spectroscopy.

### 4.2.2 Chondroitin sulfate (CSDP) synthesis.

CSDP was synthetised as previously reported by Scalzone at al. [238]. Briefly, chondroitin 4-sulfate sodium salt from bovine trachea (CS; MW = 515.376 g/mol) (10% w/v) was dissolved in a buffer solution composed of 2-(N-Morpholino) ethane sulfonic acid (MES; MW = 195.24 g/mol) 0.1 M, and sodium chloride (NaCl; MW = 58.44 g/mol) 0.5 M, at pH 6.0. The, it was obtained a combination of CS,1-ethyl-3-(3-dimethylaminopropyl)-carbodiimide hydrochloride (EDC; MW = 191.70 g/mol) and N-hydroxy succinimide (NHS; MW = 115.09 g/mol) at a molar ration of 1:1:1, and let under stirring for 30 minutes. Dopamine hydrochloride (MW = 189.64 g/mol) was added to the CS/EDC/NHS solution, and let under stirring at pH 6.0 for 4 h. Then, the dialysis and lyophilisation were performed as previously reported for the GGMA (section 4.2.1), but the last day of dialysis was performed in acidified distilled water (pH < 2). The successful of the synthesis process was evaluated even in this case through ATR-FTIR, XPS and NMR spectroscopy.

### 4.2.3 GG hydrogel preparation

GG hydrogels (3% w/v) was prepared from freeze-dried GGMA, which was pre-sterilised under UV (254 nm) then dissolved in $dH_2O$ under constant stirring at 50°C covered from light with the addition of the lithium phenyl2,4,6-trimethylbenzoyl-phosphinate (LAP) photoinitiator (0.1% w/v) overnight. The hydrogel solution was poured in 48-well plate (500 mL per well) and left to crosslink under UV at 254 nm for 5 minutes to perform the subsequent physical and mechanical analysis.

#### *4.2.3.1 Morphological analysis*

The morphology of the freeze-dried gels (after-gelation) was assessed using JEOL JSM-5600LV Scanning Electron Microscope. Samples were gold coated using a BIO-RAD Sputter Coater machine. Their morphology was visualised and recorded at 6 mm working distance, 20 kV operation voltage and two different magnifications (35 x,100 x). The obtained images were analysed with ImageJ software, to calculate the porosity distribution of each sample (40 pores for each image and three images in total).

#### *4.2.3.2 Mechanical test*

To assess the mechanical properties of the obtained hydrogels, unconfined compression test was performed with a mechanical testing machine (EZ-SX, 20 N load cell, Shimadzu, Japan). Three samples were tested for compression at a rate of 1 mm/min-until the breaking of the hydrogel. Stress/strain (σ/ ε) graph was plotted and from that, the Young's modulus (E) calculated (slope of the linear-elastic region of the σ/ε curve (0-10 % strain)).

#### *4.2.3.3 Water uptake*

To analyse the water uptake kinetics of GG 3%, three freeze-dried samples (post-gelation, in a 48 well plate) were considered. GG lyophilised gels were singularly weighted, put in a 5mL vial with 3 mL of Dulbecco's phosphate buffered saline (PBS) and stored at 37 °C. The hydrogels were dried on filter paper and weighted at each time point (30 min, 1, 3, 5, 8, 24 and 48 h of incubation). The wet weight was measured (Wt) and compared to the initial wet weight (W0). The water uptake (WU) was defined according to Eq. (1):

$$WU\ (\%) = (W_t - W_i)/W_i \ \ x\ 100 \qquad \text{Eq.1}$$

### 4.2.4 CSDP hydrogel preparation

CSDP hydrogels were formed by the crosslinking of Catechol groups. Freeze dried CS/DP was dissolved at 15% w/v in cell media (DMEM/F12). The pH of the solution was adjusted to 7-8

by adding NaOH. When $NaIO_4$ was added, the sol/gel transition happened, and it was obtained the hydrogel in 30 seconds.

### 4.2.5 PLA 3D printing and functionalisation

A PLA (Ingeo™ Biopolymer, NatureWorks) grid to simulate the subchondral bone was extruded with the Rokit Invivo 3D bioprinter (RokitHealthcare) Fusion deposition modelling (FDM) head (nozzle size 0.4mm). The extrusion temperature was set to 215°C, the print and travel speed 2 mm/s: the infill pattern was a grid and the rotate angle was set to 45° between successive layers. Each printed scaffold had a dimension of 13x13 mm. PLA scaffolds were functionalised with nanohydroxyapatite (nHA) and gelatine (Gel) via polydopamine coating. Briefly, the scaffolds were incubated in polydopamine solution (DP dissolved in TRIS buffer 0.1M pH 8.5) overnight and then washed in $dH_2O$ and incubated for 7 hours in Gel (1.5% w/v) and nHA (5%w/w). The assessment of the morphology of the obtained scaffolds was performed with SEM.

### 4.2.6 Cell culture

Human TERT immortalised bone marrow stromal cell line (Y201)[240] was cultured at 37°C, 5% $CO_2$, in DMEM with low glucose content, with the addition of 10% foetal bovine serum (FBS), 2 mM L-glutamine, and a 1% penicillin–streptomycin (P/S) mixture (100 U/mL). To differentiate the Y201 in chondrocytes (Y201-C), cells were grown at 37°C, 5% CO2 in DMEM with P/S supplemented with 1%ITS+1, 10 ng/mL TGF-β3, 40 µg/mL L-Proline, 100 nM Dexamethasone, 50 µg/mL L-Ascorbic acid-2-phosphate) for 21 days. Differentiated cells (Y201-C) were cultured in DMEM/F12 supplemented with 10% FBS and 1% P/S and used at passage 14 after differentiation.

### 4.2.7 Manufacturing of the PLA/GG/CSDP

For the manufacturing of the osteochondral unit *in vitro*, it was followed a multi-step approach (Figure 15).

- A soft lithography technique was implemented for the obtainment of a multi-channelled gellan gum construct. As a first step, it was manufactured a PLA structure (14x14x2mm) (Ultimaker2, Netherland) provided with 16 channels (1mm diameter each). This structure was used as a positive for the formation of a negative Polydimethylsiloxane (PDMS)-based mould, composed of multiple pins obtained with a concentration of syligard and curing agent 10:1. The PDMS was let react at Room Temperature for 24 h and after that, the mould was detached from the PLA and ready for the manufacturing of the deep layer multi-channelled construct.
- For the osteochondral unit set-up, first of all the PDMS mould was sterilised under UV (254 nm), put in a 12 well plate and the GG 3% (2mL) poured on the top of each mould. The multi-well was exposed for 5 minutes to UV light (254nm), the PLA scaffolds were added on the top of each mould, let other 10 minutes under UV for the chemical photocrosslink and following, 500 mL of DMEM/F12 were added to complete the physical crosslinking.
- The, PDMS mould was removed, and a multi-channelled GG was obtained, adherent to the PLA scaffold. At this point, in each channel of the GG structure was added the pre-crosslinked CS (≈ 20uL) embedded with Y201-C ($3.5x10^6$cells/mL). The construct was let few minutes under the fume hood to complete the crosslinking and after that, the PLA was seeded with Y201 (at a concentration 1:4 compared to the Y201-C).
- The constructs were incubated at 37°C, 5% $CO_2$ with the addition of DMEM/F12 and the analyses performed over 21 days of culture.

- The pathological condition was set-up considering a cocktail of cytokines to chemically induce the OA inflammation environment (IL-1ß and TNF-α (1ng/mL), IL-6 (10 ng/mL), added from day 1 of culture.

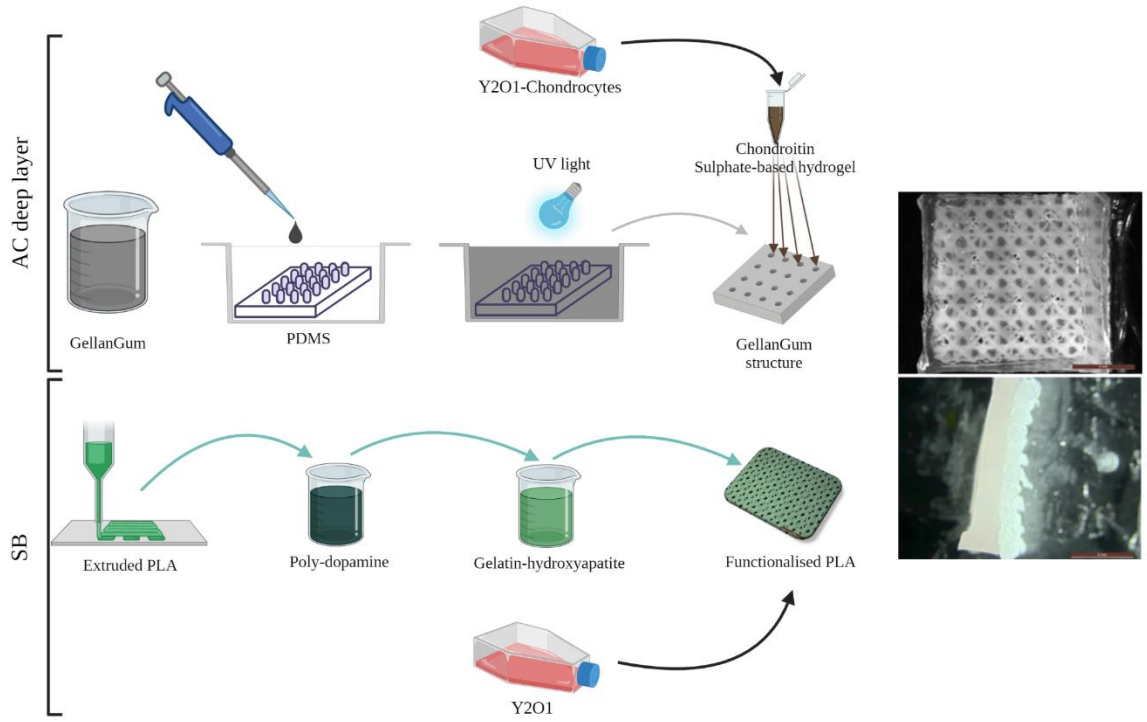


*Figure 14: Scheme of the manufacturing process.*

#### *4.2.7.1 Cells viability assessment*

To evaluate the viability of cells both in the GG/CSDP gels and on the PLA, a qualitative fluorescence-based kit (LIVE/DEAD® Cell Imaging Kit, Life Technologies, UK) was used, combining calcein-AM and ethidium bromide to produce two-color discrimination of the population of live cells (green) from the dead cells (red). Images were collected at 1,3 and 7 days using a Nikon A1R inverted confocal microscope for the GG/CSDP and using a EVOS M5000 microscope for the PLA and analysed with NIS-Elements Microscope Imaging Software.

#### *4.2.7.2 Cell morphology and distribution*

For fluorescent staining, samples were fixed in 4% w/v paraformaldehyde (PFA) for 30 minutes at 4°C. Then, cells were permeabilised with 0.1% v/v Tween20® in PBS and samples were incubated with phalloidin-tetramethylrhodamine B isothiocyanate (Phalloidin-Rhodamine) solution (1:1000 in 0.1% PBS/Tween20®) for 30 minutes at RT. Following, samples were washed with 0.1% PBS/Tween20® solution and immersed in 4′,6-diamidino-2-phenylindole (DAPI) solution (Vector Laboratories,UK) (1:2500 in 0.1% PBS/Tween20®) for 10 min at RT. Images were collected at 1,3 and 7 days using a Nikon A1R inverted confocal microscope for the GG/CSDP and using a EVOS M5000 microscope for the PLA and Nikon A1R inverted confocal microscope and analysed with NIS-Elements Microscope Imaging Software.

SEM (Tescan Vega LMU SEM (Tescan) images were performed after 24 hours of culture, samples were fixed in 2% Glutaraldehyde 1 h at 4°C, rinsed in 0.5 M cacodylic acid buffer and dehydrated in ethanol grades: 30 min in each 25%, 50%, 70%, 80%, twice in 95% and four times in 100% EtOH. Samples were stored at 4 °C in 100% EtOH until critical point dried. Finally, gels were mounted on carbon discs, gold-coated using a Polaron E5000 SEM Coating unit (Quorum Technologies Ltd, UK) and imaged.

#### *4.2.7.3 Cells metabolic activity*

To evaluate Y201-C metabolic activity CellTiter 96® AQueous MTS Reagent (Promega) was used according to manufacturer instruction at 1,3,7 days of culture. To evaluate the metabolic activity of Y201, it was used MTT (Thiazolyl Blue Tetrazolium Bromide) assay. The MTT solution was prepared following the supplier instructions, using serum-free DMEM without phenol red. Samples were incubated for 4 h at room temperature protected from light. Then, MTT solution was removed, replaced by 400 µL of dimethyl sulfoxide (DMSO) and the plates was under shaking for 30 min (Stuart Mini Microtitre Plate Shaker), to dissolve the formazan crystals. Then, 200 µl of each well solution (in duplicate) was transferred to a clear bottom 96-

well plate and a Filter-based multi-mode microplate reader (Biotek UK) was used to measure the absorbance at 570 nm. Analyses were performed at 1, 7, 14 and 21 days on PLA functionalised with polydopamine-gelatine (PLA/Gel) and polydopamine-gelatine-nanohydroxyapatite (PLA/Gel/nHA). The estimation of the cell number was performed based on a standard curve, generated by seeding Y201 at different densities (0, 5 000, 10 000, 30 000, 50 000, 100 000 and from there on up to 500 000 with a 50 000 increase).

#### *4.2.7.4 Alizarin Red staining*

To detect the calcium deposits in healthy and pathological models, samples were fixed in 4% PFA and washed in PBS twice and stained with 1 mL of Alizarin Red solution for 30 min at RT. Then, samples were washed with deionised water multiple times and dried overnight at 50°C in a 5% $CO_2$ atmosphere. Imaging of the samples was performed with stereomicroscope (Leica Microsystems). The experiment was performed at day 1,7, 14 and 21. To quantify the Alizarin Red, 10% acetic acid was added to each stained sample and let under shaking for 30 min, the acetic acid solution was transferred to 1.5mL Eppendorf tube, heated to 85°C for 10 min and then place in ice for 5 minutes. Then the solutions were treated with 10% ammonium hydroxide to neutralize the acetic pH to 4.1-4.5 and the reading was performed in duplicated at 405 nm absorbance with a Filter-based multi-mode microplate reader (Biotek UK). The standard curve was obtained in the range 0-2 mM Alizarin Red.

#### *4.2.7.5 Western Blot Analysis*

Total proteins were extracted from Y2O1 after 1, 7, 14 and 21 days of culture in healthy and pathological conditions using the RIPA Lysis Buffer System (sc-24948, Santa Cruz Biotechnology inc, Heidelberg, Germany) supplemented with protease inhibitors (S8820, Sigma-Aldrich, St. Louis, MO, USA). Protein concentration was measured by DC protein assay (LIT448D, Bio-Rad, CA, USA). Total protein extracts (20µg) were incubated with Tris-Glycine SDS Sample Buffer (2X) (Novex) according to the manufacturer's instructions,

fractionated in 4-15% SDS-PAGE gel. Gels (HC1000 Surecast, Thermo Fisher Scientific) were electrophoretically transferred to 0.2µm Nitrocellulose membranes (Bio-rad). Membranes were incubated with 5% milk in Tris-buffered saline with 0.1% Tween 20 (TBS-T) to block non-specific sites and then with rabbit anti-RANKL (45KDa; PA5-110268, Invitrogen) antibody at 4°C. Mouse anti-GAPDH (36KDa; 60004-1-Ig, Proteintech) was used as an endogenous control. After overnight incubation, the membrane was washed with TBS-T and then incubated with anti-rabbit and anti-mouse secondary antibodies conjugated to horseradish peroxidase for 1.30 h at room temperature. The detection of antibody binding was performed with Pierce ECL Western Blotting Substrate (Thermo Scientific) and images were acquired with an Alliance Mini HD9 (Uvitec, Cambridge, UK). Densitometric analysis was performed with ImageJ software (https://imagej.nih.gov/ij/download.html).

#### *4.2.7.6 GAGs quantification*

Quantitative assessment of GAGs production was performed with Alcian Blue (pH 2.5) staining at day1, day 14 and day 21 of culture. At each time point, samples were fixed with 4% PFA. Following, 500 µL of AlcianBlue solution was added to each sample for 30 minutes and then, samples were washed with $dH_2O$ until the blue disappeared. After, 28.66 g of guanidine hydrochloride was dissolved in 50 mL of $dH_2O$ and 500 µL of the obtained Guanidine solution was added to each sample and let for 3 hours under shaking. 100 µL were taken in triplicate from each well and reading was performed in absorbance at 630 nm with a Filter-based multi-mode microplate reader in a 96-clear bottom well plate. Results were reported considering a calibration curve obtained from the bare Chondroitin 4-sulfate sodium salt from bovine trachea in a range of 0-1µg.

#### *4.2.7.7 Stress-relaxation analysis*

Stress-relaxation tests were performed as proposed by Scalzone et al[241], using a single compression ramp at a speed of 10% $min^{-1}$ until reaching 10% strain. The strain was held

constant for 800 s, while the load was recorded as a function of time. The peak Young's modulus ($E_p$) was determined at 10% strain. The data obtained were analysed using MATLAB R2017 software. By fitting a third order exponential decay to the relaxation curves, obeying the generalized Maxwell model, two relaxation times were acquired: $\tau_1$ and $\tau_3$ which gave us information on the poroviscoelastic behaviour of healthy and pathological models after 14 days of culture compared to day 1.

#### 4.2.8 Statistical analysis

The results statistical significance was evaluated by GraphPad Prism Software (v. 8.4.1), using One-way ANOVA with repeated measurements. Then, Tukey's post hoc test was carried out to highlight the main factors determining data variability. Statistical significance was set at *p<0.05, ** p<0.01, *** p<0.001 and **** p<0.0001.

## 4.3 Results

### 4.3.1 Hydrogels characterisation

The characterisation of CSDP was extensively assessed by Scalzone et al.[238], therefore GGMA 3% physical and mechanical propertied were analysed.

Freeze-dried GGMA transverse cross-sections images (at high magnification) showed a spongy morphology with open macropores, elevated interconnectivity, and anisotropic porosity (Figure 15A). The 30% of pores diameter is between 100-150 µm, only 5% of pores showed less than 100 µm while the percentage remained constant at approximately 15% in 150-200, 200-250, 250-300 and > of 300 µm (Figure 15B).

The GGMA showed a very fast tendency to water uptake (WU), in fact, it reached 1016±170% in the first 30 minutes, then it increased gradually to 1433±57% in 3 hours and persisted at this value up to 48 hours (Figure 15D).

From the unconfined compression test was obtained a typical stress-strain curve and the Young's modulus calculated as the slope of the linear region of the curve (0-10%) is 31.4 ± 4.2 kPa.

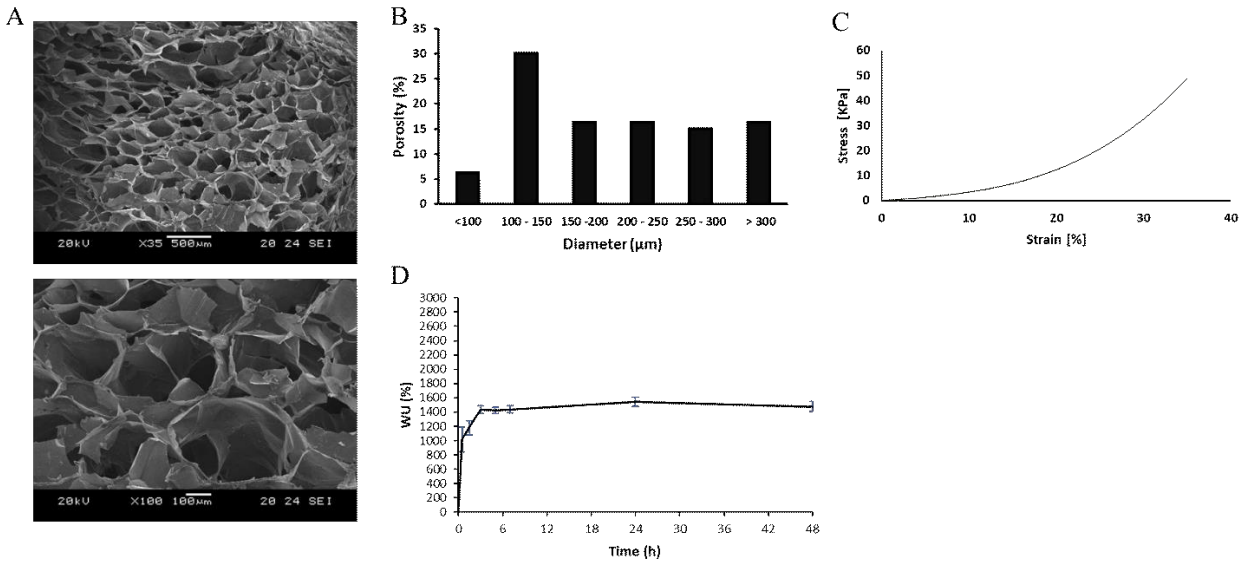


*Figure 15: GGMA3% characterisation. (A) SEM Images; (B) Histogram of pores dimension distribution, (C) Stress-strain curve obtained from unconfined compression test and (D) Water uptake. (Scale bar: up 500µm, down 100µm).*

### 4.3.2 PLA/GEL/nHA characterization

PLA filament was extruded in order to obtain a network with high interconnected porosity. PLA grid was then functionalised with Gel and nHA via DP coating. SEM analysis was done on bare PLA, PLA functionalised with Gel, and PLA functionalised with Gel and nHA to evaluate the morphology of the 3D printed scaffold and the effect of the functionalisation on it.

PLA filament surface was smooth and uniform (Figure 16A and E). After immersion in DP, lumps on the surface were observed (Figure 16B and F) without macrostructural variation. The formation of crest-like structures on the filaments were observed after DP/gel coating (Figure 16C and G). Not significant differences in the diameter of fibers were detected between DP/gel coated (332.4±56.3µm) and not-coated scaffold (378.5±46.2µm). The addiction of nHA to DP/gel grafting lead to uniform roughness formation (Figure 16D and H).

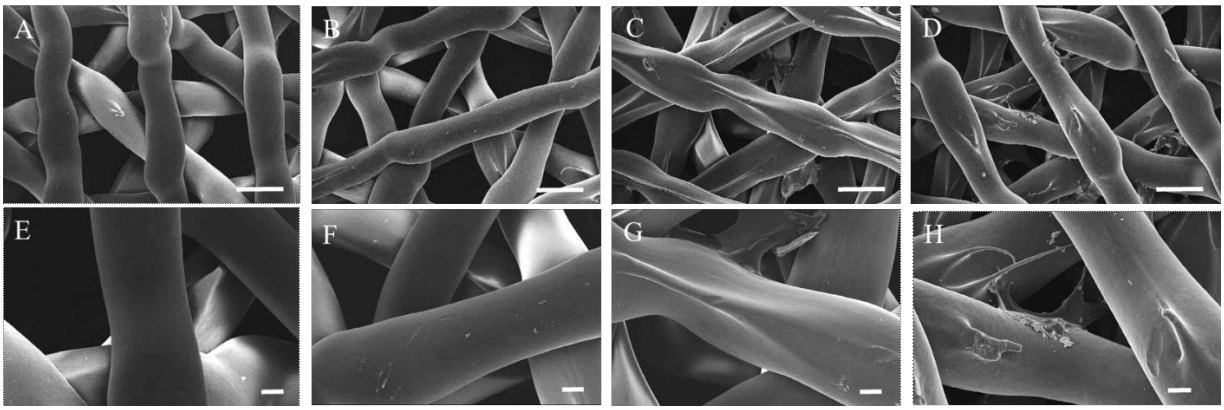


*Figure 16: PLA characterisation by SEM. (A, E) PLA; (B, F) PLA poly-dopamine; (C, G) PLA poly-dopamine 1,5%w/v gelatine and (D, H) PLA poly-dopamine 1,5%w/v gelatine 5%w/w nano-hydroxyapatite. (Scale bar: A-D 500µm; E-H 100µm)*

### 4.3.3 Cell viability

#### *4.3.3.1 Y2O1-C viability in GGMA CSDP hydrogels*

The viability of Y2O1-C embedded in CSDP and poured in GGMA hydrogels channels was assessed at day 1,3 and 7 of culture. Live and dead was performed at day 1 (Figure 17A and B) and 7 (Figure 17D and E) showed that most of the chondrocytes were alive and only a small number of dead cells was present. Also, DAPI and Phalloidin staining (Figure 17C and F) revealed that cells were homogeneously distributed into the channels of GGMA stacked one on top of each other on day 1, while a few of them start to move away from the inoculation site and diffuse into the GGMA from day 7.

The SEM analysis confirmed the presence of round-shaped chondrocytes also on the surface of the CSDP (poured in GGMA channels). At high magnification (Figure 17H) it was possible to see the surface of the CSDP which embedded the chondrocytes.

The quantitative measurement of the metabolic activity of chondrocytes has been carried out by MTS assay on days 1, 3 and 7. A slight significant decrease ($p<0.0001$) in this activity was detected on day 3 ($0.062\pm0.007$) compared to day 1 ($0.082 \pm 0.008$), then it remained stable up to 7 days (Figure 17I).

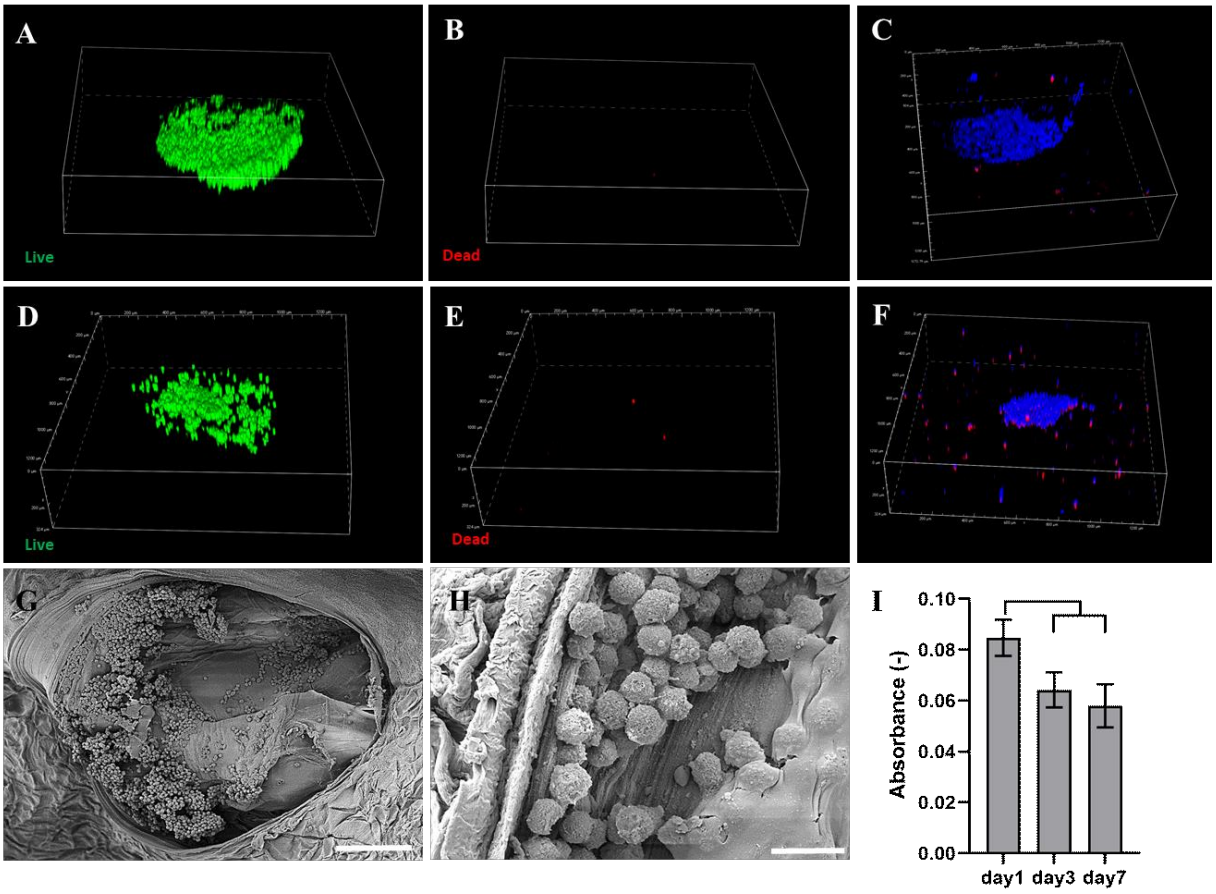


*Figure17: Y2O1-C viability. (A, B, D and E) Live and dead assay; (C and F) DAPI and phalloidin; (G and H) SEM. (A, B, C, G and H) Cells at 24h of culture; (D, E and F) cells at 7 days of culture. (I) MTS assay of chondrocytes at days 1, 3 and 7 of culture. (Scale bar: G 200µm; H 20µm. $p<0.0001$).*

#### *4.3.3.2 Y2O1 viability in functionalized PLA*

The viability of Y2O1 seeded on PLA/Gel and PLA/Gel/nHA was evaluated at day 1 and 7 with Live and dead assay. Cells were mainly viable at day 1 (green staining: calcein) and just few dead cells (red staining: ethidium bromide) could be found in Figure 18A. Cell viability was sustained at day 7 with colonisation of spaces between the filaments (Figure 18B). To assess the metabolic activity, MTT assay was performed at day 1, 7, 14 and 21 days of culture. The number of cells increased with time for both functionalisations (Figure 18G).

Y2O1 morphology and distribution were detected with DAPI and phalloidin staining at day 1 (Figure 18C) and 7 (Figure 18D). Cells appeared stretched and homogeneously distributed on PLA surface from day 1 and actin staining revealed the formation of focal adhesion anchoring

cells to the surface of the material. Cells completely wrapped the fibers at day 7 and numerous mitosis were detected (white arrow in Figure 18D).

SEM images confirmed the spread morphology of Y2O1 at day 1 (Figure 18E) and the presence of ECM that links cells to PLA filaments, at day 7 (Figure 18F).

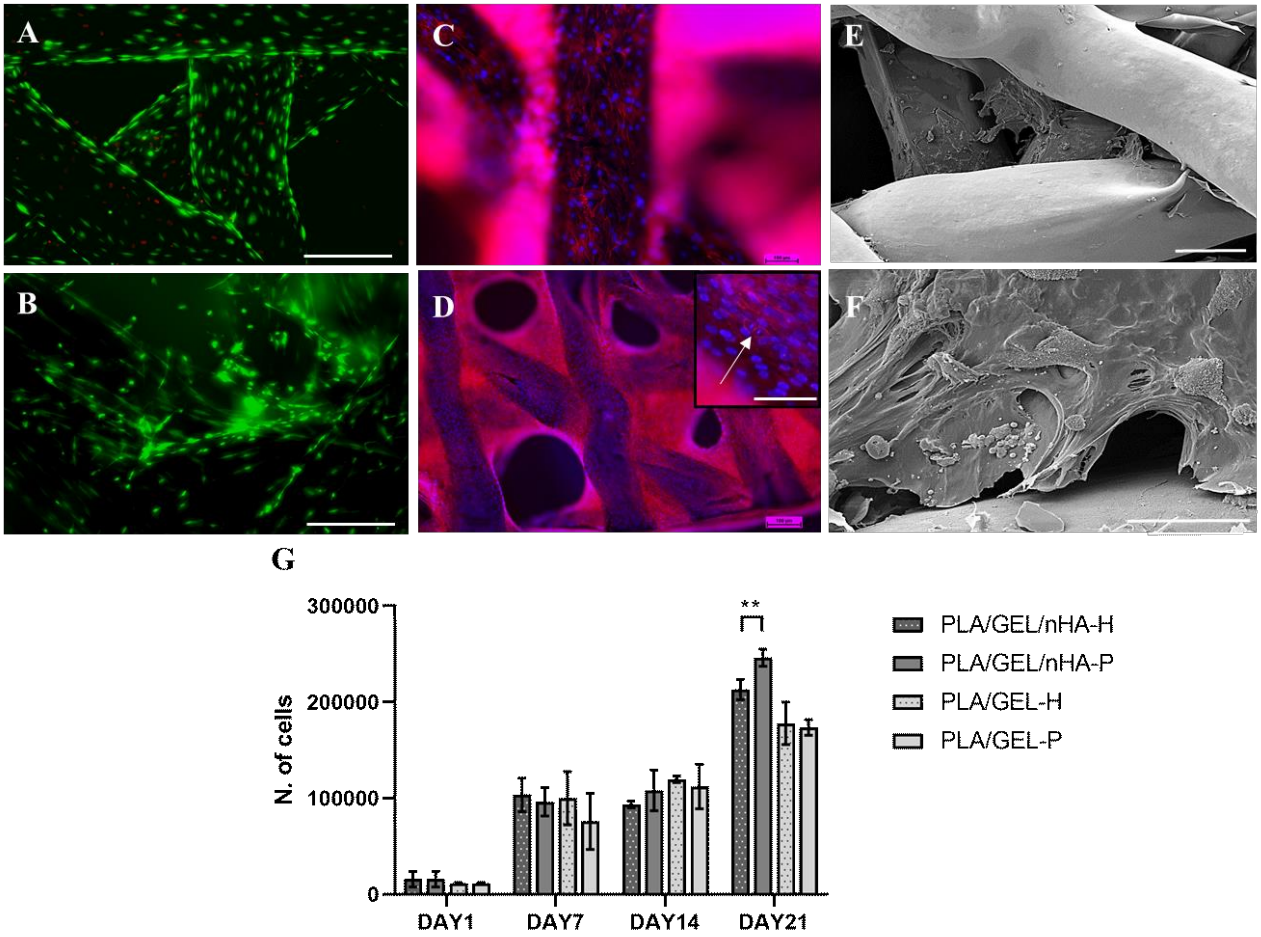


*Figure18: Y2O1 viability. (A and B) Live and dead assay; (C and D) DAPI and phalloidin; (E and F) SEM. (A, C, E and F) Cells at 24h of culture; (B and D) cells at 7 days of culture. (G) MTT assay at day 1, 7, 14 and 21 of culture of Y2O1 on PLA/Gel and PLA/Gel/nHA (Scale bar: A and B 500µm; C and D 100µm; E 200µm and F 50µm. $p<0.0001$).*

### 4.3.4 Assessment of healthy and OA conditions

The model was maintained in culture for 21 days in DMEM/F12 (Healthy model) and in DMEM/F12 with the addition of 10 ng/ml IL-6, 1 ng/ml TNF-α and 1 ng/ml IL-1β (Pathological model) to evaluate the expression of specific markers of articular cartilage and bone, both in healthy and pathological conditions.

#### *4.3.4.1 Mechanical modifications*

Stress-relaxation analyses demonstrated the change in behaviour of the deep-layer emulating hydrogel over 14 days of culture. Both at day 1 and day 14 Healthy stress vs time graphs show typical curves of a viscoelastic material. At day 1 (Figure 19A) the Peak Young's Modulus ($E_P$) obtained was 9.8±0.1kPa, which decreased to 1.1±0.2 kPa at equilibrium ($E_Y$); the relaxation times obtained were: viscoelastic relaxation time (τ1) 12.8±1.3 s and poroelastic relaxation time (τ3) 2698.8±727.6. At day 14, the $E_P$ did not change much in the Healthy model (Figure 19B), reaching the value of 10.7±0.0 s, while the $E_Y$ increased up to 4.1±0.2 kPa; the values of τ1 and τ3 respectively decreased to 7.7±2.0 s and 1471.0±191.6. The pathological model tested at 14 days (Figure 20C) showed an atypical stress vs time curve, in fact the sample never reached the equilibrium and the curve suddenly fell after 400 s. In this case, the calculated $E_P$ was of 12.1±0.1 kPa, τ1 8.8±2.4 s and τ3 1693.5±634.3 s. The value of τ3 calculated does not take in consideration the breaking of the sample and, at this regard, it was not possible to calculate $E_Y$, as the sample never reached the equilibrium.

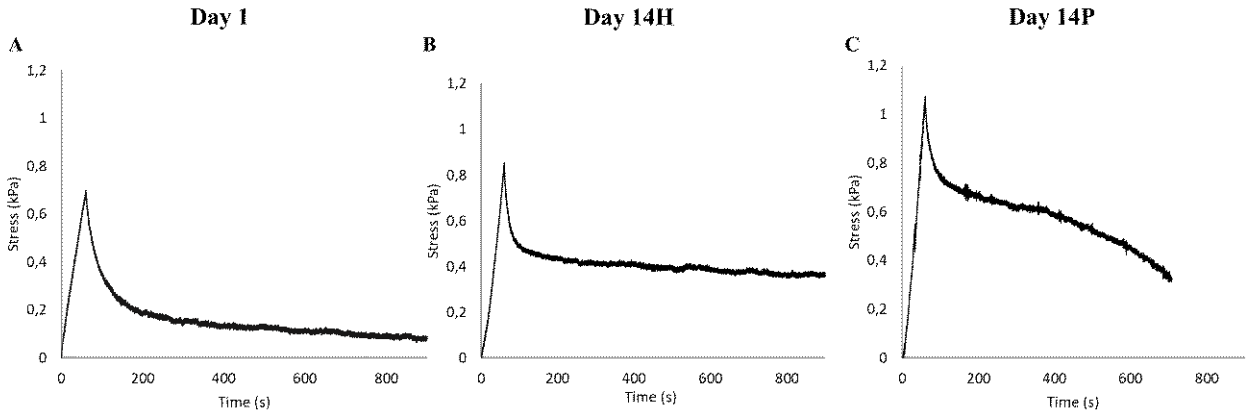


| Day1 | | | | Day14H | | | | Day14P | | | |
|---|---|---|---|---|---|---|---|---|---|---|---|
| $E_p$ (kPa) | $\tau_1$(s) | $\tau_3$(s) | $E_Y$ (kPa) | $E_p$ (kPa) | $\tau_1$(s) | $\tau_3$(s) | $E_Y$ (kPa) | $E_p$ (kPa) | $\tau_1$(s) | $\tau_3$(s) | $E_Y$ (kPa) |
| 9.8± 0.1 | 12.8±1.3s | 2698.5±727.6s | 1.1±0.2 | 10.7±0.0 | 7.7±2.0 | 1471.0±191.6 | 4.1±0.2 | 12.1±0.1 | 8.8±2.4 | 1693.5±634.3 | - |

*Figure 19 Stress relaxation curves of hydrogels with Y2O1-C at day 1 and 14 in healthy and pathological conditions.*

#### *4.3.4.2 Tissue-specific AC markers*

From GAGs quantification with Alcian blue, the healthy model showed a continuous increase in GAGs content over time, from 0.22±0.02µg at day 1 to 0.35±0.01µg at day 21. On the other side, the pathological model showed an increase of GAGs from day 1 (0.22±0.02µg) to day 7 (0.31±0.01µg), followed by a decrease on day 21 until almost reaching the values of day 1 (0.24±0.01µg) (Figure 20).

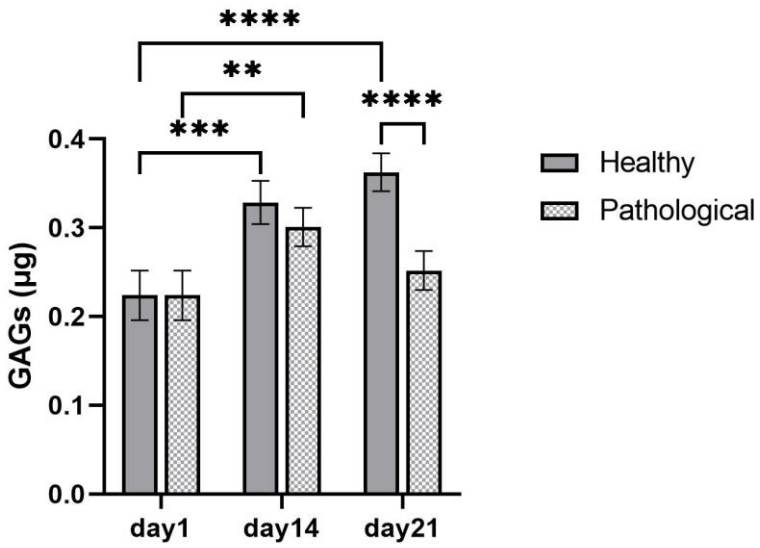


*Figure 20. GAGs quantification of the healthy and pathological model at days 7, 14 and 21 of cells culture (Statistics: ** p<0.01, *** p<0.001 and **** p<0.0001)*

#### *4.3.4.3 Tissue-specific bone markers*

The Y2O1 calcium deposition was evaluated in functionalised PLA/Gel/nHA using alizarin red staining and quantification at day 1, 7, 14, 21 in healthy and pathological conditions (Figure 21). The staining revealed zones of mineralisation on PLA surface up to day 21, mainly in the areas of intersecting fibers, both in healthy and pathological conditions (Figure 21D and G). The quantification demonstrated a slight increase of mineralisation in the heathy model on days 7 and 14 with a remarkedly increase at day 21. The pathological model showed an increase of

mineralisation that follow the trend of healthy samples but expressed a higher value at day 21 (Figure 21H). Western blot analysis for Y2O1 cultured on PLA/gel/nHA for 21 days in healthy and pathological conditions showed an increase of RANKL protein expression with time in inflamed environment.

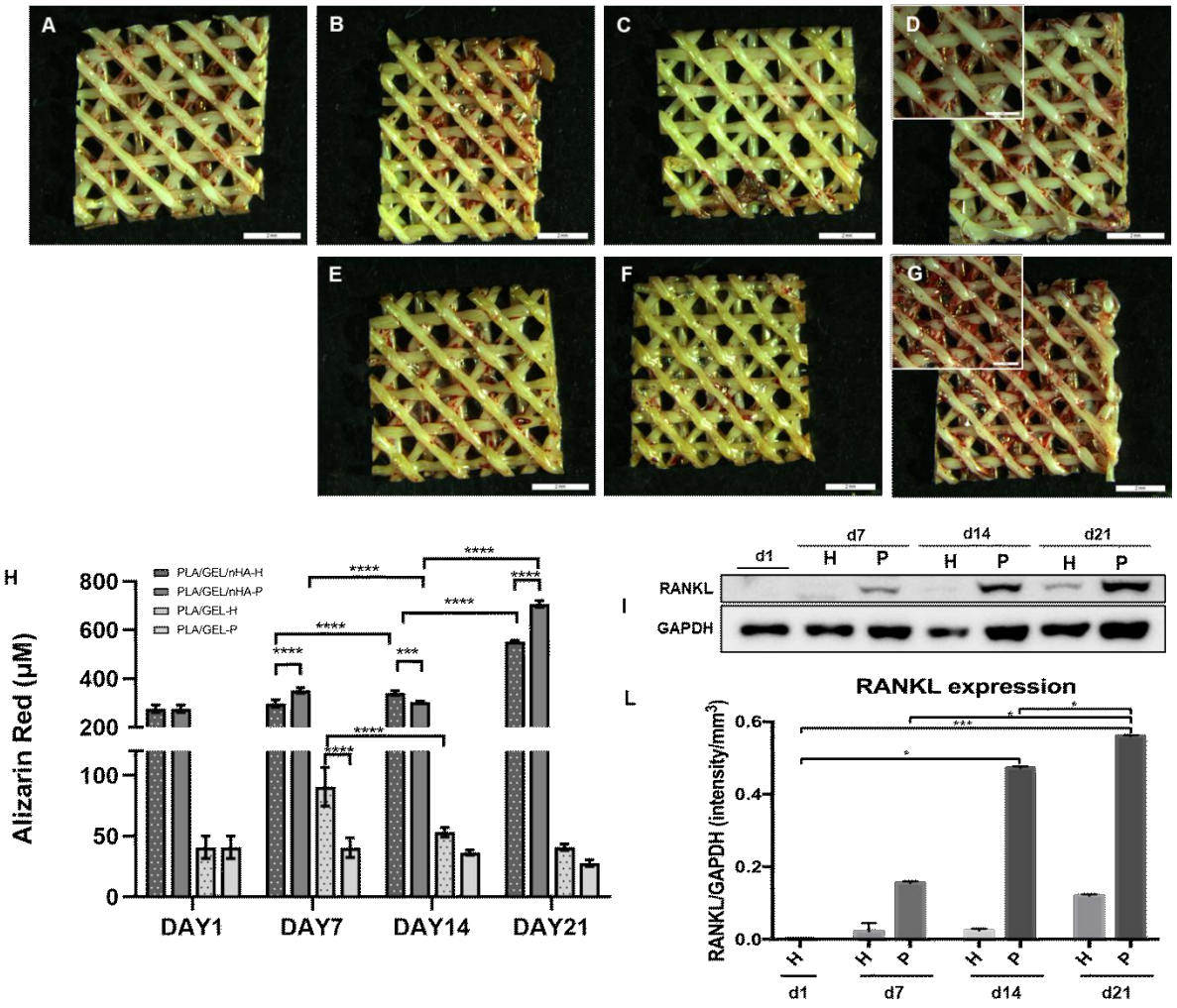


*Figure 21: (A-G) Alizarin Red staining and (H) quantification of PLA/Gel/nHA and PLA/Gel in healthy and pathological conditions. (A) day 1; (B and E) day 7; (C and F) day 14: (D and G) day 21. (A, B, C and D) healthy conditions; (E, F and G) OA conditions. (Scale bars 2mm; zoom window 1mm). (I) Western blotting for RANKL and GAPDH at day1, 7, 14 and 21 in healthy and pathological conditions; (l) Histograms depicting densitometric quantitation of western blotting, results are expressed as intensity normalized to GAPDH. (*p<0.05 ** p<0.01, *** p<0.001 and **** p<0.0001)*

## 4.4 Discussion

This study allowed us to develop a biomimetic model as reliable as possible for the mimicking of the osteochondral zone *in-vitro*.

The design of the model was developed trying to reproduce the histological characteristics of the osteochondral region. As far as the deep layer of cartilage is concerned, it was developed a construct with good load resistance property, porosity and able to host chondrocytes to form the classic palisade regions[2]. For the subchondral bone, the characteristic organization of the trabecular bone was replicated.

The choice of materials was guided by their biomimetic ability. For the deep layer of the cartilage, two hydrogels were chosen: chondroitin sulfate dopamine (CSDP) and GellanGum (GGMA). The chondroitin sulfate is an important glycosaminoglycans present in the native articular cartilage tissue and as the main compositional elements of the cartilage deep layer are proteoglycans, a chondroitin sulfate-based hydrogel was chosen for this study[242]. CSDP at 10% w/v and 20% w/v was extensively characterised in a previous work; both formulation showed good properties suitable for soft tissue engineering applications, such as good porosity, hydrophilicity and cell affinity[238]. As a drawback, this hydrogel formulation showed low mechanical property with a Young's modulus <10kPa for both formulations. In this work we decided to use a 15% w/v CSDP hydrogel and to combine it with GGMA in order to obtain good mechanical properties (*i.e.* stiffness), which is a fundamental characteristic of the deep layer of articular cartilage[243]. Gellan gum is another natural polymer, which has recently gained attention in tissue engineering thanks to its temperature-responsive gelation property, biocompatibility, and low toxicity[244–248]. Thus, in this work it was used a ionic- and photo-crosslinked methacrylated gellan gum (GGMA) hydrogels, partially characterised in a previous work (co-author)[239], where it showed good mechanical properties and suitability for cartilage tissue engineering application. In particular for this study it was chosen a 3%w/v concentration of GGMA, to be combined in the deep layer with CSDP. GGMA 3% possesses a Young's modulus of 31.4 ± 4.2 kPa, which falls within the range of hydrogels used for articular cartilage[249] (Figure 15C). Also, it is characterized by a high and well-distributed porosity that

facilitates the exchange of nutrients, which makes it particularly suitable for approaches that involve cell inclusion[250] (Figure 15 A and B). GGMA showed high hydrophilicity with a fast WU increase in the first hour and the reaching of plateau at 3 hours, demonstrating the high ability of the gel to flow and retent the water.

PLA is a synthetic polymer widely used for bone repair[251–253] approaches. PLA is a highly hydrophobic material and, for this reason, here has been functionalized with gelatin (Gel) to promote cell adhesion and nano-hydroxyapatite (nHA) to provide biomimetic[254] aptitude.

The model was set up by crosslinking the GGMA on a PDMS mould (previously obtained as reported in the methods section), in order to obtain a multi-channels structure in which the Y2O1-C embedded within the CSDP 15% w/v were seeded with a concentration of $0.6x10^6$ per construct[255]. During GGMA crosslinking the functionalized PLA was made to adhere to the GGMA opposite side of PDMS. MSCs (Y2O1) were seeded on PLA with a 4-fold lower ratio than chondrocytes.

Surface images of PLA demonstrated successful dopamine, gelatin and nHA coating on PLA. No modifications of the structure were found except for the homogeneous spreading of nanostructures desirable for anchoring, adhesion, and cell proliferation[256].

The live and dead assay on Y2O1-C demonstrates the non-toxicity of CSDP and GGMA construct. In fact, these cells remain viable even after 7 days of culture (Figure 17 A, B, C and D) confirming the property of diffusion of nutrients and elimination of waste metabolites within the hydrogel, thus providing a suitable environment for chondrocytes[257]. Morphological observation by confocal microscopy of cells stained with DAPI and phalloidin showed that cells incorporated in the gel assumed the round shape typical of chondrocytes[258] and that they tend to stack on top of each other, sinking into the depth of the canal (Figure 17C). At 7 days of culture the cells tend to migrate slightly in the porosities of the GGMA (Figure 17 D), this shift is maybe due to the production of ECM. The metabolic activity of these cells decreases on day

3 but remains stable until day 7 indicating an initial metabolic change, which is then sustained[259] (Figure 17I).

The investigation of cell viability on PLA was carried out first to evaluate the possible cytotoxicity of the material and secondly to understand if the nHA deposition could influence cells adhesion and proliferation. The live and dead assay on Y2O1 seeded onto the functionalized PLA shows that the material was not cytotoxic. DAPI and phalloidin staining showed how Y2O1 were able to fully adhere to the material and to spread by establishing focal contacts with the material surface[260]. Furthermore, it was evident that the cells uniformly colonized PLA fibers, tending to envelop the construct at day 7. SEM images confirmed the spread and elongated Y2O1 morphology as the ECM production at day 7 assuming an initial cell differentiation in an osteoblastic sense (Figure 18F).

The proliferation of Y2O1 on PLA/Gel/nHA and PLA/Gel was demonstrated by MTT assay. The increase in cellularity confirms the cytocompatibility of the materials.

Alizarin Red staining showed a high matrix calcification especially in PLA functionalised with nHA at day 21. The nHA particles show high bioactivity due to the higher solubility which increases the concentration of calcium ions in the surrounding microenvironment[261,262], increasing the osteoinductivity of the material[263,264].

Different methods have been adopted to develop OA in *in-vitro* culture models. Among these the most promising seems to be mechanically-induced OA models via load systems or chemically-induced OA with cytokines-based models[237]. The cytokines approach is certainly the simplest to use, the most standardizable and it is based on the addition of a cytokine or a cytokine cocktail directly to the culture medium. Different models used this type of OA induction by varying cytokine types, their concentrations or the ratio between cytokines. In this study, the concentration chosen for OA induction was based on a cocktail composed of 10ng/ml of IL-6, 1ng/ml of TNF-α, and 1ng/ml of IL-1β, which are the ones more involved in the OA

pathogenesis. Their ratio was based on the cytokines' prevalence in the synovial fluid isolated from OA patients[265] while their concentration was derived from the literature.

Stress relaxation analyses demonstrated that after 14 days of culture, the healthy samples showed a decreased relaxation time compared to day 1, probably due to an increased permeability, which allows fluid to flow in-out of the cartilage matrix more easily and rapidly, resulting in a lower-stress relaxation time[266]. Also, equilibrium modulus, defined as the stiffness of the gel as all the fluids flows out, underwent a 4-fold increase compared to day 1[241]. Following the addition of the cytokines to the culture medium, the mechanical properties of the AC portion showed a total modification of the stress relaxation curve at 14 days, comparing it to 14 days of culture in non-pathological conditions and day 1. The modification of the curve included a sudden collapse of the viscoelastic properties of the hydrogel. This behaviour could be due to the degradation of the structure following the increase in the catabolic activity of the cells[267]. The modification of the curve included an increase in the value of $E_P$ compared to the Healthy model and a collapse of the curve over the relaxation time. This result suggests that viscoelastic properties of the hydrogel are highly affected by the OA-induced environment, due to the breakage of the internal network: in fact, the pathological constructs never reached the equilibrium (as showed in the graph). This behaviour could be related to the increase in the catabolic activity of the cells[267], in fact an increased activity of enzymes such as, e.g., matrix metalloproteinases contribute to ECM breakdown which, in turn, deteriorates the mechanical properties of the tissue[268].

The glycosaminoglycan content increases at day 14 and 21 in the healthy model while it undergoes an initial increase at day 14 to return to the starting level at day 21 in the pathological ones. This trend is due to the initial response of the chondrocytes to the inflamed microenvironment with an increase biosynthetic activity, thus ECM production. This

production fails to meet the needs of the tissue causing an increase in matrix degradation products that amplify the inflammatory signal and the activity of proteolytic enzymes[165].

The deposition of calcium deposit increased at day 21 on PLA/GEL/nHA in healthy and pathological conditions with a greater expression in the OA milieu. The high mineralisation in pathological samples could be related to the increase of subchondral bone plate thickness in OA but more investigation is still necessary to confirm this theory. The increase of RANKL protein expression by Y2O1 with time in inflammatory conditions confirmed the RANK/RANKL/OPG pathway activation and, therefore, bone remodelling. The proposed pathological model being to induce changes in RANKL production may be suitable to mimic the subchondral cell-crosstalk (*e.g.,* recruitment of osteoclasts) and the consequent tissue modifications typical of OA.

## 4.5 Conclusions

In this work, it was developed a suitable approach to obtain an *in* vitro reproduction of the osteochondral portion of the joint. For this purpose, materials able to interface with this environment were used and their biomimetic capability was confirmed. These properties provided a suitable environment for cell adaptation limiting the development of artifacts.

Once the ability of the model to faithfully reproduce the characteristics of the subchondral portion was confirmed, an inflammatory microenvironment was used to reliably simulate OA *in-vitro*.

Cell behaviour, ECM production and the mechanical properties of the model subjected to an inflamed microenvironment were compared with the healthy counterpart, confirming the obtainment of an appropriate model. The proposed 3D-model provides a new *in-vitro* tool for the study of OA pathology, of the molecular patterns involved, as well as for the testing and development of new clinical treatments.

## 4.6 Limitation and perspectives

Considering the complex structural and functional organisation of the osteochondral tissue, the proposed 3D *in vitro* model was ambitious. Unfortunately, the Covid-19 world pandemic affects lab attendance and practice, thus delaying research activities. The work carried out provided promising data that will need further investigations. Anyway, the achievement of the following pre-established objectives represents an advancement of the research:

- Objective 1: Design a model that architecturally respected the area of interest by a careful analysis of the histological and structural characteristics of tissues.
- Objective 2: Identification of biomaterials capable of interfacing both with the characteristics of the designed model and the biological and structural parameters of the tissues.
- Objective 3: Practical application of biomaterials for the designed model.
- Objective 4: Assessment of biocompatibility of the biomaterials.
- Objective 5: Analysis of physiological tissue-related cell behaviour within the model.

An objective that needs further experiment to be completed is:

- Objective 6: Assessment of pathological model mimicking OA.

The obtained data confirmed that the proposed model was able to re-create an ideal environment for physiological cell behaviour, avoiding cell dedifferentiation and the appropriate expression of tissue-related markers. The proposed model is therefore an optimal tool for studying for the variation of cell activities due to specific stimulation.

Further in-depth analysis of specific tissue-related markers in pathological conditions as well as of the possibility to reverse pathological cell features and restore physiological behaviour, are forecasetd.

**References**


1. Juneja, P. & Hubbard, J. B. *Anatomy, Joints*. *StatPearls* (2018).
2. Sophia Fox, A. J., Bedi, A. & Rodeo, S. A. The basic science of articular cartilage: Structure, composition, and function. *Sports Health* **1**, 461–468 (2009).
3. Bhosale, A. M. & Richardson, J. B. Articular cartilage: Structure, injuries and review of management. *British Medical Bulletin* vol. 87 77–95 (2008).
4. Buckwalter, J. A. & Mankin, H. J. Articular cartilage: tissue design and chondrocyte-matrix interactions. *Instructional course lectures* vol. 47 477–486 (1998).
5. Buckwalter, J. A., Mow, V. C. & Ratcliffe, A. Restoration of Injured or Degenerated Articular Cartilage. *J. Am. Acad. Orthop. Surg.* **2**, 192–201 (1994).
6. Imhof, H. *et al.* Subchondral bone and cartilage disease: A rediscovered functional unit. *Investigative Radiology* vol. 35 581–588 (2000).
7. Eggli, P. S., Herrmann, W., Hunziker, E. B. & Schenk, R. K. Matrix compartments in the growth plate of the proximal tibia of rats. *Anat. Rec.* **211**, 246–257 (1985).
8. Guilak, F. & Mow, V. C. The mechanical environment of the chondrocyte: A biphasic finite element model of cell-matrix interactions in articular cartilage. *J. Biomech.* **33**, 1663–1673 (2000).
9. Muir, H. The chondrocyte, architect of cartilage. Biomechanics, structure, function and molecular biology of cartilage matrix macromolecules. *BioEssays* vol. 17 1039–1048 (1995).
10. Mow, V. C. & Guo, X. E. Mechano-electrochemical properties of articular cartilage: Their inhomogeneities and anisotropies. *Annual Review of Biomedical Engineering* vol. 4 175–209 (2002).
11. Martin, J. A. & Buckwalter, J. A. Telomere erosion and senescence in human articular cartilage chondrocytes. *Journals Gerontol. - Ser. A Biol. Sci. Med. Sci.* **56**, (2001).

12. Torzilli, P. A. Influence of cartilage conformation on its equilibrium water partition. *J. Orthop. Res.* **3**, 473–483 (1985).

13. Mow, V. C., Kuei, S. C., Lai, W. M. & Armstrong, C. G. Biphasic creep and stress relaxation of articular cartilage in compression: Theory and experiments. *J. Biomech. Eng.* **102**, 73–84 (1980).

14. Mow, V. C., Ratcliffe, A. & Robin Poole, A. Cartilage and diarthrodial joints as paradigms for hierarchical materials and structures. *Biomaterials* vol. 13 67–97 (1992).

15. Lai, W. M., Hou, J. S. & Mow, V. C. A triphasic theory for the swelling and deformation behaviors of articular cartilage. *J. Biomech. Eng.* **113**, 245–258 (1991).

16. Linn, F. C. & Sokoloff, L. Movement and composition of interstitial fluid of cartilage. *Arthritis Rheum.* **8**, 481–494 (1965).

17. Maroudas, A. Physicochemical Properties of Cartilage in the Light of Ion Exchange Theory. *Biophys. J.* **8**, 575–595 (1968).

18. Xia, B. *et al.* Osteoarthritis Pathogenesis: A Review of Molecular Mechanisms. *Calcified Tissue International* vol. 95 495–505 (2014).

19. POOLE, C. A. Review. Articular cartilage chondrons: form, function and failure. *J. Anat.* **191**, 1–13 (1997).

20. Archer, C. W. & Francis-West, P. The chondrocyte. *International Journal of Biochemistry and Cell Biology* vol. 35 401–404 (2003).

21. Ruhlen, R. & Marberry, K. The chondrocyte primary cilium. *Osteoarthritis and Cartilage* vol. 22 1071–1076 (2014).

22. Zhao, Z. *et al.* Mechanotransduction pathways in the regulation of cartilage chondrocyte homoeostasis. *J. Cell. Mol. Med.* **24**, 5408–5419 (2020).

23. Iwanaga, T., Shikichi, M., Kitamura, H., Yanase, H. & Nozawa-Inoue, K. Morphology and functional roles of synoviocytes in the joint. *Archives of Histology and Cytology* vol.

63 17–31 (2000).

24. Bhattaram, P. & Chandrasekharan, U. The joint synovium: A critical determinant of articular cartilage fate in inflammatory joint diseases. *Seminars in Cell and Developmental Biology* vol. 62 86–93 (2017).

25. De Bari, C. Are mesenchymal stem cells in rheumatoid arthritis the good or bad guys? *Arthritis Research and Therapy* vol. 17 113 (2015).

26. Bartok, B. & Firestein, G. S. Fibroblast-like synoviocytes: Key effector cells in rheumatoid arthritis. *Immunological Reviews* vol. 233 233–255 (2010).

27. Doody, K. M. *et al.* Targeting phosphatase-dependent proteoglycan switch for rheumatoid arthritis therapy. *Sci. Transl. Med.* **7**, 288ra76-288ra76 (2015).

28. Karystinou, A. *et al.* Distinct mesenchymal progenitor cell subsets in the adult human synovium. *Rheumatology* **48**, 1057–1064 (2009).

29. Shirasawa, S. *et al.* In vitro chondrogenesis of human synovium-derived mesenchymal stem cells: Optimal condition and comparison with bone marrow-derived cells. *J. Cell. Biochem.* **97**, 84–97 (2006).

30. Tiwari, N. *et al.* Imaging of normal and pathologic joint synovium using nonlinear optical microscopy as a potential diagnostic tool. *J. Biomed. Opt.* **15**, 056001 (2010).

31. Bone structure. (2014).

32. Clarke, B. Normal bone anatomy and physiology. *Clinical journal of the American Society of Nephrology : CJASN* vol. 3 Suppl 3 S131 (2008).

33. Ferretti, C. Periosteum derived stem cells for regenerative medicine proposals: Boosting current knowledge. *World J. Stem Cells* **6**, 266 (2014).

34. Lin, X., Patil, S., Gao, Y. G. & Qian, A. The Bone Extracellular Matrix in Bone Formation and Regeneration. *Frontiers in Pharmacology* vol. 11 757 (2020).

35. Kolb, A. D. & Bussard, K. M. The Bone Extracellular Matrix as an Ideal Milieu for

Cancer Cell Metastases. *Cancers (Basel)*. **11**, 1020 (2019).

36. Saito, M. & Marumo, K. Effects of Collagen Crosslinking on Bone Material Properties in Health and Disease. *Calcified Tissue International* vol. 97 242–261 (2015).

37. Fedarko, N. S. Osteoblast/Osteoclast Development and Function in Osteogenesis Imperfecta. in *Osteogenesis Imperfecta: A Translational Approach to Brittle Bone Disease* 45–56 (Elsevier Inc., 2013). doi:10.1016/B978-0-12-397165-4.00005-8.

38. Varma, S., Orgel, J. P. R. O. & Schieber, J. D. Nanomechanics of Type I Collagen. *Biophys. J.* **111**, 50–56 (2016).

39. Paiva, K. B. S. & Granjeiro, J. M. Matrix Metalloproteinases in Bone Resorption, Remodeling, and Repair. in *Progress in Molecular Biology and Translational Science* vol. 148 203–303 (Elsevier B.V., 2017).

40. Allori, A. C., Sailon, A. M. & Warren, S. M. Biological basis of bone formation, remodeling, and repair - Part II: Extracellular matrix. *Tissue Engineering - Part B: Reviews* vol. 14 275–283 (2008).

41. Allori, A. C., Sailon, A. M. & Warren, S. M. Biological basis of bone formation, remodeling, and repair - Part I: Biochemical signaling molecules. *Tissue Engineering - Part B: Reviews* vol. 14 259–273 (2008).

42. Dey, P. Bone Mineralisation. in *Contemporary Topics about Phosphorus in Biology and Materials* (IntechOpen, 2020). doi:10.5772/intechopen.92065.

43. Licini, C., Vitale-Brovarone, C. & Mattioli-Belmonte, M. Collagen and non-collagenous proteins molecular crosstalk in the pathophysiology of osteoporosis. *Cytokine and Growth Factor Reviews* vol. 49 59–69 (2019).

44. Murshed, M. Mechanism of Bone Mineralization. *Cold Spring Harbor perspectives in medicine* vol. 8 (2018).

45. Schmid, J., Wallkamm, B., Hämmerle, C. H. F., Gogolewski, S. & Lang, N. P. The

significance of angiogenesis in guided bone regeneration. A case report of a rabbit experiment. *Clin. Oral Implants Res.* **8**, 244–248 (1997).

46. Cumming, J. D. & Nutt, M. E. Bone-marrow blood flow and cardiac output in the rabbit. *J. Physiol.* **162**, 30–34 (1962).

47. Gross, P. M., Heistad, D. D. & Marcus, M. L. Neurohumoral regulation of blood flow to bones and marrow. *Am. J. Physiol. - Hear. Circ. Physiol.* **6**, (1979).

48. Marenzana, M. & Arnett, T. R. The Key Role of the Blood Supply to Bone. *Bone Research* vol. 1 203–215 (2013).

49. Takarada, T. *et al.* Genetic analysis of Runx2 function during intramembranous ossification. *Dev.* **143**, 211–218 (2016).

50. Ortega, N., Behonick, D. J. & Werb, Z. Matrix remodeling during endochondral ossification. *Trends in Cell Biology* vol. 14 86–93 (2004).

51. Hall, B. K. & Miyake, T. The membranous skeleton: the role of cell condensations in vertebrate skeletogenesis. *Anatomy and Embryology* vol. 186 107–124 (1992).

52. Langen, U. H. *et al.* Cell-matrix signals specify bone endothelial cells during developmental osteogenesis. *Nat. Cell Biol.* **19**, 189–201 (2017).

53. Glowacki, J. Angiogenesis in fracture repair. in *Clinical Orthopaedics and Related Research* (Lippincott Williams and Wilkins, 1998). doi:10.1097/00003086-199810001-00010.

54. Hankenson, K. D., Dishowitz, M., Gray, C. & Schenker, M. Angiogenesis in bone regeneration. *Injury* **42**, 556–561 (2011).

55. Tammela, T., Enholm, B., Alitalo, K. & Paavonen, K. The biology of vascular endothelial growth factors. *Cardiovascular Research* vol. 65 550–563 (2005).

56. Street, J. *et al.* Vascular endothelial growth factor stimulates bone repair by promoting angiogenesis and bone turnover. *Proc. Natl. Acad. Sci. U. S. A.* **99**, 9656–9661 (2002).

57. Deckers, M. M. L. *et al.* Bone Morphogenetic Proteins Stimulate Angiogenesis through Osteoblast-Derived Vascular Endothelial Growth Factor A. *Endocrinology* **143**, 1545–1553 (2002).

58. Raida, M., Heymann, A. C., Güther, C. & Niederwieser, D. Role of bone morphogenetic protein 2 in the crosstalk between endothelial progenitor cells and mesenchymal stem cells. *Int. J. Mol. Med.* **18**, 735–739 (2006).

59. Brazill, J. M., Beeve, A. T., Craft, C. S., Ivanusic, J. J. & Scheller, E. L. Nerves in Bone: Evolving Concepts in Pain and Anabolism. *J. Bone Miner. Res.* **34**, 1393–1406 (2019).

60. Huang, Y. *et al.* Sensory innervation around immediately vs. delayed loaded implants: A pilot study. *Int. J. Oral Sci.* **7**, 49–55 (2015).

61. Imai, S., Tokunaga, Y., Maeda, T., Kikkawa, M. & Hukuda, S. Calcitonin gene-related peptide, substance P, and tyrosine hydroxylase-immunoreactive innervation of rat bone marrows: An immunohistochemical and ultrastructural investigation on possible efferent and afferent mechanisms. *J. Orthop. Res.* **15**, 133–140 (1997).

62. Marrella, A. *et al.* Engineering vascularized and innervated bone biomaterials for improved skeletal tissue regeneration. *Materials Today* vol. 21 362–376 (2018).

63. Mach, D. B. *et al.* Origins of skeletal pain: Sensory and sympathetic innervation of the mouse femur. *Neuroscience* **113**, 155–166 (2002).

64. Tonna, S. & Sims, N. A. Talking among ourselves: Paracrine control of bone formation within the osteoblast lineage. *Calcified Tissue International* vol. 94 35–45 (2014).

65. Miller, S. C., de Saint-Georges, L., Bowman, B. M. & Jee, W. S. Bone lining cells: structure and function. *Scanning Microsc.* **3**, 951–953 (1989).

66. Bianco, P., Robey, P. G. & Simmons, P. J. Mesenchymal Stem Cells: Revisiting History, Concepts, and Assays. *Cell Stem Cell* vol. 2 313–319 (2008).

67. Su, P. *et al.* Mesenchymal Stem Cell Migration during Bone Formation and Bone

Diseases Therapy. *Int. J. Mol. Sci.* **19**, 2343 (2018).

68. Komori, T. *et al.* Targeted disruption of Cbfa1 results in a complete lack of bone formation owing to maturational arrest of osteoblasts. *Cell* **89**, 755–764 (1997).

69. Ducy, P. *et al.* A Cbfa1-dependent genetic pathway controls bone formation beyond embryonic development. *Genes Dev.* **13**, 1025–1036 (1999).

70. Nakashima, K. *et al.* The novel zinc finger-containing transcription factor Osterix is required for osteoblast differentiation and bone formation. *Cell* **108**, 17–29 (2002).

71. Mohamed, A. M. F. S. An overview of bone cells and their regulating factors of differentiation. *Malaysian Journal of Medical Sciences* vol. 15 4–12 (2008).

72. Aubin, J. E. Regulation of Osteoblast Formation and Function. *Rev. Endocr. Metab. Disord.* **2**, 81–94 (2001).

73. Aubin, J. E., Liu, F., Malaval, L. & Gupta, A. K. Osteoblast and chondroblast differentiation. *Bone* **17**, (1995).

74. Sims, N. A. *et al.* Human and murine osteocalcin gene expression: Conserved tissue restricted expression and divergent responses to 1,25- dihydroxyvitamin D3 in vivo. *Mol. Endocrinol.* **11**, 1695–1708 (1997).

75. Anderson, H. C. *et al.* Impaired calcification around matrix vesicles of growth plate and bone in alkaline phosphatase-deficient mice. *Am. J. Pathol.* **164**, 841–847 (2004).

76. Anderson, H. C. Mineralization by matrix vesicles. *Scan. Electron Microsc.* 953–964 (1984).

77. Anderson, H. C., Garimella, R. & Tague, S. E. The role of matrix vesicles in growth plate development and biomineralization. *Front. Biosci.* **10**, 822–837 (2005).

78. Golub, E. E. Role of matrix vesicles in biomineralization. *Biochimica et Biophysica Acta - General Subjects* vol. 1790 1592–1598 (2009).

79. Wu, L. N. Y., Genge, B. R., Kang, M. W., Arsenault, A. L. & Wuthier, R. E. Changes in

phospholipid extractability and composition accompany mineralization of chicken growth plate cartilage matrix vesicles. *J. Biol. Chem.* **277**, 5126–5133 (2002).

80. Toyosawa, S. *et al.* Dentin matrix protein 1 is predominantly expressed in chicken and rat osteocytes but not in osteoblasts. *J. Bone Miner. Res.* **16**, 2017–2026 (2001).

81. Gowen, L. C. *et al.* Targeted disruption of the osteoblast/osteocyte factor 45 gene (Of45) results in increased bone formation and bone mass. *J. Biol. Chem.* **278**, 1998–2007 (2003).

82. Van Bezooijen, R. L. *et al.* Sclerostin Is an Osteocyte-expressed Negative Regulator of Bone Formation, but Not a Classical BMP Antagonist. *J. Exp. Med.* **199**, 805–814 (2004).

83. Aguirre, J. I. *et al.* Osteocyte apoptosis is induced by weightlessness in mice and precedes osteoclast recruitment and bone loss. *J. Bone Miner. Res.* **21**, 605–615 (2006).

84. Suda, T., Nakamura, I., Jimi, E. & Takahashi, N. Regulation of osteoclast function. *Journal of Bone and Mineral Research* vol. 12 869–879 (1997).

85. Väänänen, H. K., Zhao, H., Mulari, M. & Halleen, J. M. The cell biology of osteoclast function. *J. Cell Sci.* **113 ( Pt 3**, 377–381 (2000).

86. Nakamura, I., Duong, L. T., Rodan, S. B. & Rodan, G. A. Involvement of αvβ3 integrins in osteoclast function. *Journal of Bone and Mineral Metabolism* vol. 25 337–344 (2007).

87. Takahashi, N., Ejiri, S., Yanagisawa, S. & Ozawa, H. Regulation of osteoclast polarization. *Odontology* vol. 95 1–9 (2007).

88. Reinholt, F. P., Hultenby, K., Oldberg, A. & Heinegard, D. Osteopontin - A possible anchor of osteoclasts to bone. *Proc. Natl. Acad. Sci. U. S. A.* **87**, 4473–4475 (1990).

89. Luxenburg, C. *et al.* The architecture of the adhesive apparatus of cultured osteoclasts: From podosome formation to sealing zone assembly. *PLoS One* **2**, 179 (2007).

90. Blair, H. C., Teitelbaum, S. L., Ghiselli, R. & Gluck, S. Osteoclastic bone resorption by

a polarized vacuolar proton pump. *Science (80-. ).* **245**, 855–857 (1989).

91. HADJIDAKIS, D. J. & ANDROULAKIS, I. I. Bone Remodeling. *Ann. N. Y. Acad. Sci.* **1092**, 385–396 (2006).

92. Nesbitt, S. A. & Horton, M. A. Trafficking of matrix collagens through bone-resorbing osteoclasts. *Science (80-. ).* **276**, 266–269 (1997).

93. Yamaki, M., Nakamura, H., Takahashi, N., Udagawa, N. & Ozawa, H. Transcytosis of calcium from bone by osteoclast-like cells evidenced by direct visualization of calcium in cells. *Arch. Biochem. Biophys.* **440**, 10–17 (2005).

94. Salo, J., Lehenkari, P., Mulari, M., Metsikkö, K. & Väänänen, H. K. Removal of osteoclast bone resorption products by transcytosis. *Science (80-. ).* **276**, 270–273 (1997).

95. Destaing, O., Saltel, F., Géminard, J. C., Jurdic, P. & Bard, F. Podosomes display actin turnover and dynamic self-organization in osteoclasts expressing actin-green fluorescent protein. *Mol. Biol. Cell* **14**, 407–416 (2003).

96. Tezuka, K. *et al.* Identification of matrix metalloproteinase 9 in rabbit osteoclasts. *J. Biol. Chem.* **269**, 15006–15009 (1994).

97. Seeman, E. Bone modeling and remodeling. *Critical Reviews in Eukaryotic Gene Expression* vol. 19 219–233 (2009).

98. Li, J. *et al.* Different bone remodeling levels of trabecular and cortical bone in response to changes in Wnt/β-catenin signaling in mice. *J. Orthop. Res.* **35**, 812–819 (2017).

99. Martin, T. J. & Seeman, E. New mechanisms and targets in the treatment of bone fragility. *Clin. Sci.* **112**, 77–91 (2007).

100. Xu, F. & Teitelbaum, S. L. Osteoclasts: New Insights. *Bone Research* vol. 1 11–26 (2013).

101. Hazenberg, J. G., Freeley, M., Foran, E., Lee, T. C. & Taylor, D. Microdamage: A cell

transducing mechanism based on ruptured osteocyte processes. *J. Biomech.* **39**, 2096–2103 (2006).

102. Everts, V. *et al.* The bone lining cell: Its role in cleaning Howship's lacunae and initiating bone formation. *J. Bone Miner. Res.* **17**, 77–90 (2002).

103. Bonewald, L. F. Osteocyte Messages from a Bony Tomb. *Cell Metabolism* vol. 5 410–411 (2007).

104. Bonewald, L. F. The amazing osteocyte. *J. Bone Miner. Res.* **26**, 229–238 (2011).

105. Clark, W. D. *et al.* Osteocyte apoptosis and osteoclast presence in chicken radii 0-4 days following osteotomy. *Calcif. Tissue Int.* **77**, 327–336 (2005).

106. Verborgt, O., Gibson, G. J. & Schaffler, M. B. Loss of osteocyte integrity in association with microdamage and bone remodeling after fatigue in vivo. *J. Bone Miner. Res.* **15**, 60–67 (2000).

107. Taylor, D. Bone maintenance and remodeling: A control system based on fatigue damage. *J. Orthop. Res.* **15**, 601–606 (1997).

108. Parfitt, A. M. The bone remodeling compartment: A circulatory function for bone lining cells. *Journal of Bone and Mineral Research* vol. 16 1583–1585 (2001).

109. Hauge, E. M., Qvesel, D., Eriksen, E. F., Mosekilde, L. & Melsen, F. Cancellous bone remodeling occurs in specialized compartments lined by cells expressing osteoblastic markers. *J. Bone Miner. Res.* **16**, 1575–1582 (2001).

110. Eriksen, E. F., Eghbali-Fatourechi, G. Z. & Khosla, S. Remodeling and vascular spaces in bone. *Journal of Bone and Mineral Research* vol. 22 1–6 (2007).

111. Y., A., Valds-Flores, M., Orozco, L. & Velzquez-Cruz, R. Molecular Aspects of Bone Remodeling. in *Topics in Osteoporosis* (InTech, 2013). doi:10.5772/54905.

112. Tang, Y. *et al.* TGF-B1-induced migration of bone mesenchymal stem cells couples bone resorption with formation. *Nat. Med.* **15**, 757–765 (2009).

113. Eriksen, E. F. Cellular mechanisms of bone remodeling. *Reviews in Endocrine and Metabolic Disorders* vol. 11 219–227 (2010).

114. Teti, A. Bone development: Overview of bone cells and signaling. *Current Osteoporosis Reports* vol. 9 264–273 (2011).

115. Kim, C. H. *et al.* Trabecular Bone Response to Mechanical and Parathyroid Hormone Stimulation: The Role of Mechanical Microenvironment. *J. Bone Miner. Res.* **18**, 2116–2125 (2003).

116. Weinstein, R. S., Jilka, R. L., Michael Parfitt, A. & Manolagas, S. C. Inhibition of osteoblastogenesis and promotion of apoptosis of osteoblasts end osteocytes by glucocorticoids potential mechanisms of their deleterious effects on bone. *J. Clin. Invest.* **102**, 274–282 (1998).

117. Srivastava, S. *et al.* Estrogen Decreases Osteoclast Formation by Down-regulating Receptor Activator of NF-κB Ligand (RANKL)-induced JNK Activation. *J. Biol. Chem.* **276**, 8836–8840 (2001).

118. Manolagas, S. C. Birth and Death of Bone Cells: Basic Regulatory Mechanisms and Implications for the Pathogenesis and Treatment of Osteoporosis*. *Endocr. Rev.* **21**, 115–137 (2000).

119. Collin-Osdoby, P. Regulation of vascular calcification by osteoclast regulatory factors RANKL and osteoprotegerin. *Circulation Research* vol. 95 1046–1057 (2004).

120. Silvestrini, G. *et al.* Detection of osteoprotegerin (OPG) and its ligand (RANKL) mRNA and protein in femur and tibia of the rat. *J. Mol. Histol.* **36**, 59–67 (2005).

121. Nakashima, T. *et al.* Evidence for osteocyte regulation of bone homeostasis through RANKL expression. *Nat. Med.* **17**, 1231–1234 (2011).

122. Wada, T., Nakashima, T., Hiroshi, N. & Penninger, J. M. RANKL-RANK signaling in osteoclastogenesis and bone disease. *Trends in Molecular Medicine* vol. 12 17–25

(2006).

123. Kearns, A. E., Khosla, S. & Kostenuik, P. J. Receptor activator of nuclear factor κB ligand and osteoprotegerin regulation of bone remodeling in health and disease. *Endocrine Reviews* vol. 29 155–192 (2008).

124. Takayanagi, H. Osteoimmunology: Shared mechanisms and crosstalk between the immune and bone systems. *Nature Reviews Immunology* vol. 7 292–304 (2007).

125. Hikita, A. *et al.* Negative regulation of osteoclastogenesis by ectodomain shedding of receptor activator of NF-κB ligand. *J. Biol. Chem.* **281**, 36846–36855 (2006).

126. Lynch, C. C. *et al.* MMP-7 promotes prostate cancer-induced osteolysis via the solubilization of RANKL. *Cancer Cell* **7**, 485–496 (2005).

127. Ikeda, T., Kasai, M., Utsuyama, M. & Hirokawa, K. Determination of Three Isoforms of the Receptor Activator of Nuclear Factor-κB Ligand and Their Differential Expression in Bone and Thymus*. *Endocrinology* **142**, 1419–1426 (2001).

128. Hsu, H. *et al.* Tumor necrosis factor receptor family member RANK mediates osteoclast differentiation and activation induced by osteoprotegerin ligand. *Proc. Natl. Acad. Sci. U. S. A.* **96**, 3540–3545 (1999).

129. Lacey, D. L. *et al.* Osteoprotegerin ligand is a cytokine that regulates osteoclast differentiation and activation. *Cell* **93**, 165–176 (1998).

130. Bucay, N. *et al.* Osteoprotegerin-deficient mice develop early onset osteoporosis and arterial calcification. *Genes Dev.* **12**, 1260–1268 (1998).

131. Li, J. *et al.* RANK is the intrinsic hematopoietic cell surface receptor that controls osteoclastogenesis and regulation of bone mass and calcium metabolism. *Proc. Natl. Acad. Sci. U. S. A.* **97**, 1566–1571 (2000).

132. Li, Y. *et al.* B cells and T cells are critical for the preservation of bone homeostasis and attainment of peak bone mass in vivo. *Blood* **109**, 3839–3848 (2007).

133. Tobeiha, M., Moghadasian, M. H., Amin, N. & Jafarnejad, S. RANKL/RANK/OPG Pathway: A Mechanism Involved in Exercise-Induced Bone Remodeling. *BioMed Research International* vol. 2020 6910312–6910312 (2020).

134. Boyle, W. J., Simonet, W. S. & Lacey, D. L. Osteoclast differentiation and activation. *Nature* vol. 423 337–342 (2003).

135. Hofbauer, L. C. & Schoppet, M. Clinical implications of the osteoprotegerin/RANKL/RANK system for bone and vascular diseases. *Journal of the American Medical Association* vol. 292 490–495 (2004).

136. Nardone, V., D'Asta, F. & Brandi, M. L. Pharmacological management of osteogenesis. *Clinics* vol. 69 438–446 (2014).

137. Ominsky, M. S. *et al.* RANKL Inhibition with Osteoprotegerin Increases Bone Strength by Improving Cortical and Trabecular bone Architecture in Ovariectomized Rats. *J. Bone Miner. Res.* **23**, 672–682 (2008).

138. Theoleyre, S. *et al.* The molecular triad OPG/RANK/RANKL: Involvement in the orchestration of pathophysiological bone remodeling. *Cytokine and Growth Factor Reviews* vol. 15 457–475 (2004).

139. Cundy, T. *et al.* A mutation in the gene TNFRSF11B encoding osteoprotegerin causes an idiopathic hyperphosphatasia phenotype. *Hum. Mol. Genet.* **11**, 2119–2127 (2002).

140. Glass, D. A. *et al.* Canonical Wnt signaling in differentiated osteoblasts controls osteoclast differentiation. *Dev. Cell* **8**, 751–764 (2005).

141. Muhammad, N., Luke, D. A., Shuid, A. N., Mohamed, N. & Soelaiman, I. N. Tocotrienol supplementation in postmenopausal osteoporosis: evidence from a laboratory study. *Clinics* **68**, 1338–1343 (2013).

142. Turk, N., Cukovic-Cavka, S., Korsic, M., Turk, Z. & Vucelic, B. Proinflammatory cytokines and receptor activator of nuclear factor κB-ligand/osteoprotegerin associated

with bone deterioration in patients with Crohn's disease. *Eur. J. Gastroenterol. Hepatol.* **21**, 159–166 (2009).

143. Sylvester, F. A. *et al.* Natural history of bone metabolism and bone mineral density in children with inflammatory bowel disease. *Inflamm. Bowel Dis.* **13**, 42–50 (2007).

144. Boyce, B. F. & Xing, L. Biology of RANK, RANKL, and osteoprotegerin. *Arthritis Research and Therapy* vol. 9 S1 (2007).

145. D'Haese, P. C. *et al.* A multicenter study on the effects of lanthanum carbonate (Fosrenol™) and calcium carbonate on renal bone disease in dialysis patients. in *Kidney International, Supplement* vol. 63 S73–S78 (Blackwell Publishing Inc., 2003).

146. Yuan, X. L. *et al.* Bone-cartilage interface crosstalk in osteoarthritis: Potential pathways and future therapeutic strategies. *Osteoarthritis and Cartilage* vol. 22 1077–1089 (2014).

147. Cui, A. *et al.* Global, regional prevalence, incidence and risk factors of knee osteoarthritis in population-based studies. *EClinicalMedicine* **29**–**30**, 100587 (2020).

148. Woolf, A. D. & Pfleger, B. Burden of major musculoskeletal conditions. *Bull. World Health Organ.* **81**, 646–656 (2003).

149. Hunter, D. J., Schofield, D. & Callander, E. The individual and socioeconomic impact of osteoarthritis. *Nature Reviews Rheumatology* vol. 10 437–441 (2014).

150. Hunter, D. J., McDougall, J. J. & Keefe, F. J. The Symptoms of Osteoarthritis and the Genesis of Pain. *Medical Clinics of North America* vol. 93 83–100 (2009).

151. Nelson, A. E., Allen, K. D., Golightly, Y. M., Goode, A. P. & Jordan, J. M. A systematic review of recommendations and guidelines for the management of osteoarthritis: The Chronic Osteoarthritis Management Initiative of the U.S. Bone and Joint Initiative. *Semin. Arthritis Rheum.* **43**, 701–712 (2014).

152. Block, J. A. Osteoarthritis: OA guidelines: Improving care or merely codifying practice? *Nature Reviews Rheumatology* vol. 10 324–326 (2014).

153. Chen, J. *et al.* Efficacy and safety of tanezumab on osteoarthritis knee and hip pains: A meta-analysis of randomized controlled trials. *Pain Med. (United States)* **18**, 374–385 (2017).

154. Aquili, A., Farinelli, L., Bottegoni, C., Antonicelli, L. & Gigante, A. The effect of anti-IgE therapy in knee osteoarthritis: a pilot observational study. *J. Biol. Regul. Homeost. Agents* **31**, 1–5 (2017).

155. Culliford, D. J. *et al.* The lifetime risk of total hip and knee arthroplasty: Results from the UK general practice research database. *Osteoarthr. Cartil.* **20**, 519–524 (2012).

156. Dieppe, P. Developments in osteoarthritis. *Rheumatology* **50**, 245–247 (2011).

157. Martel-Pelletier, J. & Pelletier, J. P. Is osteoarthritis a disease involving only cartilage or other articular tissues? *Eklem Hastalik. Cerrahisi* **21**, 2–14 (2010).

158. Glyn-Jones, S. *et al.* Osteoarthritis. in *The Lancet* vol. 386 376–387 (Lancet Publishing Group, 2015).

159. Heijink, A. *et al.* Biomechanical considerations in the pathogenesis of osteoarthritis of the knee. *Knee Surgery, Sports Traumatology, Arthroscopy* vol. 20 423–435 (2012).

160. Loeser, R. F., Collins, J. A. & Diekman, B. O. Ageing and the pathogenesis of osteoarthritis. *Nature Reviews Rheumatology* vol. 12 412–420 (2016).

161. Man, G. S. & Mologhianu, G. Osteoarthritis pathogenesis - a complex process that involves the entire joint. *Journal of medicine and life* vol. 7 37–41 (2014).

162. Wang, M., Peng, Z., Vasilev, K. & Ketheesan, N. Investigation of wear particles generated in human knee joints using atomic force microscopy. *Tribol. Lett.* **51**, 161–170 (2013).

163. Stannus, O. *et al.* Circulating levels of IL-6 and TNF-α are associated with knee radiographic osteoarthritis and knee cartilage loss in older adults. *Osteoarthr. Cartil.* **18**, 1441–1447 (2010).

164. Buckwalter, J. A., Mankin, H. J. & Grodzinsky, A. J. Articular cartilage and osteoarthritis. *Instr. Course Lect.* **54**, 465–480 (2005).

165. Aigner, T. & McKenna, L. Molecular pathology and pathobiology of osteoarthritic cartilage. *Cellular and Molecular Life Sciences* vol. 59 5–18 (2002).

166. Davis, C. R. *et al.* Can biochemical markers serve as surrogates for imaging in knee osteoarthritis? *Arthritis Rheum.* **56**, 4038–4047 (2007).

167. Bailey, A. J., Sims, T. J. & Knott, L. Phenotypic expression of osteoblast collagen in osteoarthritic bone: Production of type I homotrimer. *Int. J. Biochem. Cell Biol.* **34**, 176–182 (2002).

168. Couchourel, D. *et al.* Altered mineralization of human osteoarthritic osteoblasts is attributable to abnormal type I collagen production. *Arthritis Rheum.* **60**, 1438–1450 (2009).

169. Neogi, T. Clinical significance of bone changes in osteoarthritis. *Ther. Adv. Musculoskelet. Dis.* **4**, 259–267 (2012).

170. Tanamas, S. K. *et al.* The association between subchondral bone cysts and tibial cartilage volume and risk of joint replacement in people with knee osteoarthritis: A longitudinal study. *Arthritis Res. Ther.* **12**, R58 (2010).

171. Braun, H. J. & Gold, G. E. Diagnosis of osteoarthritis: Imaging. *Bone* **51**, 278–288 (2012).

172. Taljanovic, M. S. *et al.* Bone marrow edema pattern in advanced hip osteoarthritis: Quantitative assessment with magnetic resonance imaging and correlation with clinical examination, radiographic findings, and histopathology. *Skeletal Radiol.* **37**, 423–431 (2008).

173. Sutton, S. *et al.* The contribution of the synovium, synovial derived inflammatory cytokines and neuropeptides to the pathogenesis of osteoarthritis. *Veterinary Journal*

vol. 179 10–24 (2009).

174. Brandt, K. D., Dieppe, P. & Radin, E. Etiopathogenesis of Osteoarthritis. *Medical Clinics of North America* vol. 93 1–24 (2009).

175. Yuan, G. H. *et al.* Characterization of cells from pannus-like tissue over articular cartilage of advanced osteoarthritis. *Osteoarthr. Cartil.* **12**, 38–45 (2004).

176. Sellam, J. & Berenbaum, F. The role of synovitis in pathophysiology and clinical symptoms of osteoarthritis. *Nature Reviews Rheumatology* vol. 6 625–635 (2010).

177. Krasnokutsky, S., Attur, M., Palmer, G., Samuels, J. & Abramson, S. B. Current concepts in the pathogenesis of osteoarthritis. *Osteoarthritis and Cartilage* vol. 16 (2008).

178. Ashraf, S. & Walsh, D. A. Angiogenesis in osteoarthritis. *Current Opinion in Rheumatology* vol. 20 573–580 (2008).

179. Bonnet, C. S. & Walsh, D. A. Osteoarthritis, angiogenesis and inflammation. *Rheumatology* vol. 44 7–16 (2005).

180. Hasegawa, M., Segawa, T., Maeda, M., Yoshida, T. & Sudo, A. Thrombin-cleaved osteopontin levels in synovial fluid correlate with disease severity of knee osteoarthritis. *J. Rheumatol.* **38**, 129–134 (2011).

181. Haywood, L. *et al.* Inflammation and angiogenesis in osteoarthritis. *Arthritis Rheum.* **48**, 2173–2177 (2003).

182. Lampropoulou-Adamidou, K. *et al.* Useful animal models for the research of osteoarthritis. *European Journal of Orthopaedic Surgery and Traumatology* vol. 24 263–271 (2014).

183. Samvelyan, H. J., Hughes, D., Stevens, C. & Staines, K. A. Models of Osteoarthritis: Relevance and New Insights. *Calcified Tissue International* vol. 1 3 (2020).

184. Teeple, E., Jay, G. D., Elsaid, K. A. & Fleming, B. C. Animal models of osteoarthritis: Challenges of model selection and analysis. *AAPS Journal* vol. 15 438–446 (2013).

185. Mitchell, R. E. *et al.* New tools for studying osteoarthritis genetics in zebrafish. *Osteoarthr. Cartil.* **21**, 269–278 (2013).

186. McCoy, A. M. Animal Models of Osteoarthritis: Comparisons and Key Considerations. *Vet. Pathol.* **52**, 803–818 (2015).

187. Gregory, M. H. *et al.* A Review of Translational Animal Models for Knee Osteoarthritis. *Arthritis* **2012**, 1–14 (2012).

188. Madden, J. C. *et al.* Strategies for the optimisation of in vivo experiments in accordance with the 3Rs philosophy. *Regul. Toxicol. Pharmacol.* **63**, 140–154 (2012).

189. Anton, D., Burckel, H., Josset, E. & Noel, G. Three-dimensional cell culture: A breakthrough in vivo. *International Journal of Molecular Sciences* vol. 16 5517–5527 (2015).

190. Stokes, D. G. *et al.* Assessment of the gene expression profile of differentiated and dedifferentiated human fetal chondrocytes by microarray analysis. *Arthritis Rheum.* **46**, 404–419 (2002).

191. Marlovits, S., Hombauer, M., Truppe, M., Vècsei, V. & Schlegel, W. Changes in the ratio of type-I and type-II collagen expression during monolayer culture of human chondrocytes. *J. Bone Jt. Surg. - Ser. B* **86**, 286–295 (2004).

192. Lee, C. M., Kisiday, J. D., McIlwraith, C. W., Grodzinsky, A. J. & Frisbie, D. D. Development of an in vitro model of injuryinduced osteoarthritis in cartilage explants from adult horses through application of single-impact compressive overload. *Am. J. Vet. Res.* **74**, 40–47 (2013).

193. Haltmayer, E. *et al.* Co-culture of osteochondral explants and synovial membrane as in vitro model for osteoarthritis. *PLoS One* **14**, (2019).

194. Byron, C. R. & Trahan, R. A. Comparison of the Effects of Interleukin-1 on Equine Articular Cartilage Explants and Cocultures of Osteochondral and Synovial Explants.

*Front. Vet. Sci.* **4**, 152 (2017).

195. Geurts, J., Jurić, D., Müller, M., Schären, S. & Netzer, C. Novel ex vivo human osteochondral explant model of knee and spine osteoarthritis enables assessment of inflammatory and drug treatment responses. *Int. J. Mol. Sci.* **19**, (2018).

196. Caron, M. M. J. *et al.* Redifferentiation of dedifferentiated human articular chondrocytes: Comparison of 2D and 3D cultures. *Osteoarthr. Cartil.* **20**, 1170–1178 (2012).

197. Hirao, M., Tamai, N., Tsumaki, N., Yoshikawa, H. & Myoui, A. Oxygen tension regulates chondrocyte differentiation and function during endochondral ossification. *J. Biol. Chem.* **281**, 31079–31092 (2006).

198. Duval, K. *et al.* Modeling physiological events in 2D vs. 3D cell culture. *Physiology* vol. 32 266–277 (2017).

199. Zeng, L., Yao, Y., Wang, D. A. & Chen, X. Effect of microcavitary alginate hydrogel with different pore sizes on chondrocyte culture for cartilage tissue engineering. *Mater. Sci. Eng. C* **34**, 168–175 (2014).

200. Remya, N. S. & Nair, P. D. Engineering cartilage tissue interfaces using a natural glycosaminoglycan hydrogel matrix - An in vitro study. *Mater. Sci. Eng. C* **33**, 575–582 (2013).

201. An, H. *et al.* Hyaluronate-alginate hybrid hydrogels modified with biomimetic peptides for controlling the chondrocyte phenotype. *Carbohydr. Polym.* **197**, 422–430 (2018).

202. Dey, P. *et al.* Mimicking of Chondrocyte Microenvironment Using In Situ Forming Dendritic Polyglycerol Sulfate-Based Synthetic Polyanionic Hydrogels. *Macromol. Biosci.* **16**, 580–590 (2016).

203. Inagaki, Y. *et al.* Effects of culture on PAMPS/PDMAAm double-network gel on chondrogenic differentiation of mouse C3H10T1/2 cells: In vitro experimental study. *BMC Musculoskelet. Disord.* **15**, 320 (2014).

204. Stüdle, C. *et al.* Spatially confined induction of endochondral ossification by functionalized hydrogels for ectopic engineering of osteochondral tissues. *Biomaterials* **171**, 219–229 (2018).

205. De Bari, C., Dell'Accio, F., Tylzanowski, P. & Luyten, F. P. Multipotent mesenchymal stem cells from adult human synovial membrane. *Arthritis Rheum.* **44**, 1928–1942 (2001).

206. Hermida-Gómez, T. *et al.* Quantification of cells expressing mesenchymal stem cell markers in healthy and osteoarthritic synovial membranes. *J. Rheumatol.* **38**, 339–349 (2011).

207. Djouad, F. *et al.* Transcriptional profiles discriminate bone marrow-derived and synovium-derived mesenchymal stem cells. *Arthritis Res. Ther.* **7**, R1304 (2005).

208. Kurth, T. *et al.* Chondrogenic potential of human synovial mesenchymal stem cells in alginate. *Osteoarthr. Cartil.* **15**, 1178–1189 (2007).

209. Sakaguchi, Y., Sekiya, I., Yagishita, K. & Muneta, T. Comparison of human stem cells derived from various mesenchymal tissues: Superiority of synovium as a cell source. *Arthritis Rheum.* **52**, 2521–2529 (2005).

210. Kim, M.-J. *et al.* Generation of human induced pluripotent stem cells from osteoarthritis patient-derived synovial cells. *Arthritis Rheum.* **63**, 3010–3021 (2011).

211. Ilas, D. C., Churchman, S. M., McGonagle, D. & Jones, E. Targeting subchondral bone mesenchymal stem cell activities for intrinsic joint repair in osteoarthritis. *Futur. Sci. OA* **3**, FSO228 (2017).

212. Crane, J. L. & Cao, X. Bone marrow mesenchymal stem cells and TGF-β signaling in bone remodeling. *Journal of Clinical Investigation* vol. 124 466–472 (2014).

213. Xian, L. *et al.* Matrix IGF-1 maintains bone mass by activation of mTOR in mesenchymal stem cells. *Nat. Med.* **18**, 1095–1101 (2012).

214. Crane, J. L. & Cao, X. Function of matrix IGF-1 in coupling bone resorption and formation. *Journal of Molecular Medicine* vol. 92 107–115 (2014).

215. Löfvall, H. *et al.* Osteoclasts degrade bone and cartilage knee joint compartments through different resorption processes. *Arthritis Res. Ther.* **20**, (2018).

216. Dominici, M. *et al.* Minimal criteria for defining multipotent mesenchymal stromal cells. The International Society for Cellular Therapy position statement. *Cytotherapy* **8**, 315–317 (2006).

217. Ragni, E., Viganò, M., Rebulla, P., Giordano, R. & Lazzari, L. What is beyond a qRT-PCR study on mesenchymal stem cell differentiation properties: how to choose the most reliable housekeeping genes. *J. Cell. Mol. Med.* **17**, 168–180 (2013).

218. Livak, K. J. & Schmittgen, T. D. Analysis of relative gene expression data using real-time quantitative PCR and the 2-ΔΔCT method. *Methods* **25**, 402–408 (2001).

219. D. Smith, M. The Normal Synovium. *Open Rheumatol. J.* **5**, 100–106 (2012).

220. Wong, S. H. J., Chiu, K. Y. & Yan, C. H. Osteophytes. *Journal of Orthopaedic Surgery* vol. 24 403–410 (2016).

221. Durand, M. *et al.* Monocytes from patients with osteoarthritis display increased osteoclastogenesis and bone resorption: The In Vitro Osteoclast Differentiation in Arthritis study. *Arthritis Rheum.* **65**, 148–158 (2013).

222. Danks, L., Sabokbar, A., Gundle, R. & Athanasou, N. A. Synovial macrophage-osteoclast differentiation in inflammatory arthritis. *Ann. Rheum. Dis.* **61**, 916–921 (2002).

223. Suzuki, Y. *et al.* Osteoclast-like cells in an in vitro model of bone destruction by rheumatoid synovium. *Rheumatology* **40**, 673–682 (2001).

224. Fickert, S., Fiedler, J. & Brenner, R. E. Identification, quantification and isolation of mesenchymal progenitor cell from osteoarthritic synovium by fluorescence automated

cell sorting. *Osteoarthr. Cartil.* **11**, 790–800 (2003).

225. Nagase, T. *et al.* Analysis of the chondrogenic potential of human synovial stem cells according to harvest site and culture parameters in knees with medial compartment osteoarthritis. *Arthritis Rheum.* **58**, 1389–1398 (2008).

226. Laschober, G. T. *et al.* Age-specific changes of mesenchymal stem cells are paralleled by upregulation of CD106 expression as a response to an inflammatory environment. *Rejuvenation Res.* **14**, 119–131 (2011).

227. Fukiage, K. *et al.* Expression of vascular cell adhesion molecule-1 indicates the differentiation potential of human bone marrow stromal cells. *Biochem. Biophys. Res. Commun.* **365**, 406–412 (2008).

228. Liu, F. *et al.* Changes in the expression of CD106, osteogenic genes, and transcription factors involved in the osteogenic differentiation of human bone marrow mesenchymal stem cells. *J. Bone Miner. Metab.* **26**, 312–320 (2008).

229. Ljusberg, J. *et al.* Proteolytic excision of a repressive loop domain in tartrate-resistant acid phosphatase by cathepsin K in osteoclasts. *J. Biol. Chem.* **280**, 28370–28381 (2005).

230. Kolasinski, S. L. *et al.* 2019 American College of Rheumatology/Arthritis Foundation Guideline for the Management of Osteoarthritis of the Hand, Hip, and Knee. *Arthritis Rheumatol.* **72**, 220–233 (2020).

231. Salgado, C., Jordan, O. & Allémann, E. Osteoarthritis In Vitro Models: Applications and Implications in Development of Intra-Articular Drug Delivery Systems. *Pharmaceutics* **13**, 60 (2021).

232. Gómez-Gaete, C. *et al.* Development, characterization and in vitro evaluation of biodegradable rhein-loaded microparticles for treatment of osteoarthritis. *Eur. J. Pharm. Sci.* **96**, 390–397 (2017).

233. Lin, J. B., Poh, S. & Panitch, A. Controlled release of anti-inflammatory peptides from

reducible thermosensitive nanoparticles suppresses cartilage inflammation. *Nanomedicine Nanotechnology, Biol. Med.* **12**, 2095–2100 (2016).

234. Dong, J. *et al.* Intra-articular delivery of liposomal celecoxib-hyaluronate combination for the treatment of osteoarthritis in rabbit model. *Int. J. Pharm.* **441**, 285–290 (2013).

235. Sharma, A. R., Jagga, S., Lee, S. S. & Nam, J. S. Interplay between cartilage and subchondral bone contributing to pathogenesis of osteoarthritis. *International Journal of Molecular Sciences* vol. 14 19805–19830 (2013).

236. Man, G. S. & Mologhianu, G. Osteoarthritis pathogenesis - a complex process that involves the entire joint. *Journal of medicine and life* vol. 7 37–41 (2014).

237. Johnson, C. I., Argyle, D. J. & Clements, D. N. In vitro models for the study of osteoarthritis. *Veterinary Journal* vol. 209 40–49 (2016).

238. Scalzone, A. *et al.* pH-Triggered Adhesiveness and Cohesiveness of Chondroitin Sulfate-Catechol Biopolymer for Biomedical Applications. *Front. Bioeng. Biotechnol.* **8**, (2020).

239. Scalzone, A. *et al.* Photocurable Manuka Honey-loaded gellan-gum bioinks for 3D-bioprinted engineered articular cartilage constructs.

240. James, S. *et al.* Multiparameter Analysis of Human Bone Marrow Stromal Cells Identifies Distinct Immunomodulatory and Differentiation-Competent Subtypes. *Stem Cell Reports* **4**, 1004–1015 (2015).

241. Scalzone, A. *et al.* The interplay between chondrocyte spheroids and mesenchymal stem cells boosts cartilage regeneration within a 3D natural-based hydrogel. *Sci. Rep.* **9**, 1–12 (2019).

242. Muir, H. Proteoglycans of cartilage. *J. clin. Path* **31**, 67–81.

243. Little, C. J., Bawolin, N. K. & Chen, X. Mechanical properties of natural cartilage and tissue-engineered constructs. *Tissue Eng. - Part B Rev.* **17**, 213–227 (2011).

244. Oliveira, J. T. *et al.* Gellan gum: A new biomaterial for cartilage tissue engineering applications. *J. Biomed. Mater. Res. - Part A* **93**, 852–863 (2010).

245. Kim, W. K. *et al.* Evaluation of cartilage regeneration of chondrocyte encapsulated gellan gum-based hyaluronic acid blended hydrogel. *Int. J. Biol. Macromol.* **141**, 51–59 (2019).

246. Oliveira, J. T. *et al.* Performance of new gellan gum hydrogels combined with human articular chondrocytes for cartilage regeneration when subcutaneously implanted in nude mice. *J. Tissue Eng. Regen. Med.* **3**, 493–500 (2009).

247. Oliveira, J. T. *et al.* Injectable gellan gum hydrogels with autologous cells for the treatment of rabbit articular cartilage defects. *J. Orthop. Res.* **28**, 1193–1199 (2010).

248. Silva-Correia, J. *et al.* Gellan gum-based hydrogels for intervertebral disc tissue-engineering applications. *J. Tissue Eng. Regen. Med.* **5**, (2011).

249. Kerin, A. J., Wisnom, M. R. & Adams, M. A. The compressive strength of articular cartilage. *Proc. Inst. Mech. Eng. Part H J. Eng. Med.* **212**, 273–280 (1998).

250. Annabi, N. *et al.* Controlling the porosity and microarchitecture of hydrogels for tissue engineering. *Tissue Engineering - Part B: Reviews* vol. 16 371–383 (2010).

251. Grémare, A. *et al.* Characterization of printed PLA scaffolds for bone tissue engineering. *J. Biomed. Mater. Res. - Part A* **106**, 887–894 (2018).

252. Gregor, A. *et al.* Designing of PLA scaffolds for bone tissue replacement fabricated by ordinary commercial 3D printer. *J. Biol. Eng.* **11**, (2017).

253. Additive manufacturing of PLA-based scaffolds intended for bone regeneration and strategies to improve their biological properties - Search Results - PubMed. https://pubmed.ncbi.nlm.nih.gov/?term=Additive+manufacturing+of+PLA-based+scaffolds+intended+for+bone+regeneration+and+strategies+to+improve+their+biological+properties.

254. Li, X. *et al.* Degradable Three Dimensional-Printed Polylactic Acid Scaffold with Long-Term Antibacterial Activity. *ACS Sustain. Chem. Eng.* **6**, 2047–2054 (2018).

255. Ren, X. *et al.* Engineering zonal cartilage through bioprinting collagen type II hydrogel constructs with biomimetic chondrocyte density gradient. *BMC Musculoskelet. Disord.* **17**, 301 (2016).

256. Shekaran, A. & García, A. J. Extracellular matrix-mimetic adhesive biomaterials for bone repair. *Journal of Biomedical Materials Research - Part A* vol. 96 A 261–272 (2011).

257. Lafont, J. E. Lack of oxygen in articular cartilage: Consequences for chondrocyte biology. *International Journal of Experimental Pathology* vol. 91 99–106 (2010).

258. Archer, C. W. & Francis-West, P. The chondrocyte. *International Journal of Biochemistry and Cell Biology* vol. 35 401–404 (2003).

259. Gibson, J. S., Milner, P. I., White, R., Fairfax, T. P. A. & Wilkins, R. J. Oxygen and reactive oxygen species in articular cartilage: Modulators of ionic homeostasis. *Pflugers Archiv European Journal of Physiology* vol. 455 563–573 (2008).

260. Mattila, P. K. & Lappalainen, P. Filopodia: Molecular architecture and cellular functions. *Nature Reviews Molecular Cell Biology* vol. 9 446–454 (2008).

261. Nosouhian, S., Razavi, M., Jafari-Pozve, N. & Rismanchian, M. Comparative evaluation of hydroxyapatite and nano-bioglass in two forms of conventional micro-and nano-particles in repairing bone defects (an animal study). *Indian J. Dent. Res.* **26**, 366–371 (2015).

262. Oberbek, P. *et al.* Characterization and influence of hydroxyapatite nanopowders on living cells. *Beilstein J. Nanotechnol.* **9**, 3079–3094 (2018).

263. Vaquette, C., Ivanovski, S., Hamlet, S. M. & Hutmacher, D. W. Effect of culture conditions and calcium phosphate coating on ectopic bone formation. *Biomaterials* **34**,

5538–5551 (2013).

264. Tian, B. *et al.* Fabrication of silver nanoparticle-doped hydroxyapatite coatings with oriented block arrays for enhancing bactericidal effect and osteoinductivity. *J. Mech. Behav. Biomed. Mater.* **61**, 345–359 (2016).

265. Sohn, D. H. *et al.* Plasma proteins present in osteoarthritic synovial fluid can stimulate cytokine production via Toll-like receptor 4. *Arthritis Res. Ther.* **14**, (2012).

266. Kumar, R. *et al.* Comparison of Compressive Stress-Relaxation Behavior in Osteoarthritic (ICRS Graded) Human Articular Cartilage. *Int. J. Mol. Sci.* **19**, 413 (2018).

267. Stannus, O. *et al.* Circulating levels of IL-6 and TNF-α are associated with knee radiographic osteoarthritis and knee cartilage loss in older adults. *Osteoarthr. Cartil.* **18**, 1441–1447 (2010).

268. Mieloch, Richter, Trzeciak, Giersig & Rybka. Osteoarthritis Severely Decreases the Elasticity and Hardness of Knee Joint Cartilage: A Nanoindentation Study. *J. Clin. Med.* **8**, 1865 (2019).